1972

Interdiffusion in the systems (Nickel(X)-Oxide) - (Cobalt(X)-Oxide) and (Manganese(X)-Oxide) - Magnesium-Oxide

Denis Albert Brosnan
Iowa State University

INFORMATION TO USERS

This dissertation was produced from a microfilm copy of the original document. While the most advanced technological means to photograph and reproduce this document have been used, the quality is heavily dependent upon the quality of the original submitted.

The following explanation of techniques is provided to help you understand markings or patterns which may appear on this reproduction.

1. The sign or "target" for pages apparently lacking from the document photographed is "Missing Page(s)". If it was possible to obtain the missing page(s) or section, they are spliced into the film along with adjacent pages. This may have necessitated cutting thru an image and duplicating adjacent pages to insure you complete continuity.

2. When an image on the film is obliterated with a large round black mark, it is an indication that the photographer suspected that the copy may have moved during exposure and thus cause a blurred image. You will find a good image of the page in the adjacent frame.

3. When a map, drawing or chart, etc., was part of the material being photographed the photographer followed a definite method in "sectioning" the material. It is customary to begin photoing at the upper left hand corner of a large sheet and to continue photoing from left to right in equal sections with a small overlap. If necessary, sectioning is continued again — beginning below the first row and continuing on until complete.

4. The majority of users indicate that the textual content is of greatest value, however, a somewhat higher quality reproduction could be made from "photographs" if essential to the understanding of the dissertation. Silver prints of "photographs" may be ordered at additional charge by writing the Order Department, giving the catalog number, title, author and specific pages you wish reproduced.

University Microfilms

300 North Zeeb Road
Ann Arbor, Michigan 48106

A Xerox Education Company

Interdiffusion in the systems Ni_xO-Co_xO and Mn_xO-MgO

by

Denis Albert Brosnan

A Dissertation Submitted to the

Graduate Faculty in Partial Fulfillment of

The Requirements for the Degree of

DOCTOR OF PHILOSOPHY

Major Subject: Ceramic Engineering

Approved:

Signature was redacted for privacy.

In Charge of Major Work

Signature was redacted for privacy.

For the Major Department

Signature was redacted for privacy.

For the Graduate College

Iowa State University
Ames, Iowa

1972

TABLE OF CONTENTS

INTRODUCTION

Interdiffusion measurements in solids are of importance in that information is revealed concerning mechanisms of atom movement which in turn influence the kinetics of many solid state processes. Knowledge of fundamental processes in solids can help the materials engineer produce materials of greater utility to society. Measurements of interdiffusion rates aid in the interpretation of phenomena such as sintering, oxidation, creep, and reaction kinetics. Discussions of the significance of interdiffusion experiments in solids are available in the literature (1, 2, 3).

Interdiffusion measurements in systems of transition metal oxides such as Ni_xO, Co_xO, and Mn_xO are of interest because the rate of interdiffusion can be interpreted with respect to knowledge of departures from stoichiometry and defect structures of these oxides. It is also interesting to study interdiffusion between a nonstoichiometric oxide such as Mn_xO and a nearly stoichiometric oxide such as MgO. In this case the interdiffusion rate can be interpreted on the basis of the effect of a nonstoichiometric addition to a nearly stoichiometric host. The simple structure of these oxides aids in the interpretation of experimental data.

In this thesis both of the cases mentioned in the above paragraph are considered. In the first case interdiffusion

between the two nonstoichiometric oxides Ni_xO and Co_xO are examined. In the second case interdiffusion between the nearly stoichiometric oxide MgO and the nonstoichiometric oxide Mn_xO is examined.

THEORETICAL CONSIDERATIONS

Mechanisms of Diffusion

Diffusion is the net displacement of atoms in solids resulting from the combined effects of individual atomic jumping events in the presence of a chemical potential gradient. The possible mechanisms of jumps in crystalline solids may be classed as either the direct exchange or ring mechanisms requiring the simultaneous movement of two or more atoms, or the point defect mechanisms which utilize jumps to unfilled allowable positions in crystals. There is no experimental evidence for the existence of the direct exchange or ring mechanisms. These mechanisms are considered unlikely due to a high energy of activation (3, 4). The point defect mechanisms include the vacancy mechanism, the interstitial mechanism, and the interstitialcy mechanism. Other mechanisms include translation along dislocations, through grain boundaries, or across surfaces.

The vacancy mechanism involves the jump of a diffusing atom from a normal lattice site to an adjacent vacant normal lattice site. The vacancy mechanism may be largely responsible for cation diffusion in oxides. Because cations and anions are located on interpenetrating sublattices in oxides, cations must move through the anion sublattice in order to accomplish a diffusional jump. It has been shown that the distortion of the anion sublattice in the process of diffusion is less

for the vacancy mechanism of cation diffusion than for a direct exchange mechanism (2, 3). From geometrical considerations of atom packing in crystals, Azâroff (5, 6) has considered the possible paths available for diffusion in cubic close packed crystals. There is the possibility of a continuous path for diffusion via the vacancy jump mechanism on alternating octahedral and tetrahedral sites. Another possible path for diffusion by the vacancy mechanism exists along a chain of adjacent octhedral sites.

The interstitial mechanism involves the jump of an atom from an interstitial site to an adjacent vacant interstitial site. This mechanism is likely for the diffusion of small impurity atoms which do not greatly displace atoms in the host crystal during individual jumps (3).

The interstitialcy mechanism involves the jump of a diffusing atom from an interstitial site to an adjacent normal site with the atom originally located on the normal site simultaneously jumping to a vacant interstitial site. There are several considerations which suggest that the interstitialcy mechanism may be operable in oxides. Considerations using a rigid sphere model for the anion sublattice in a NaCl type lattice reveal that if interstitial occupation is allowable, less distortion is required for an interstitialcy process than for a vacancy mechanism (for the same size of diffusing cation) (7). The recent discovery of tetrahedrally

coordinated cations in oxides with the NaCl structure (8, 9, 10) suggests that the interstitialcy mechanism may be important in oxide systems.

Phenomenological Description of Diffusion

If an initially inhomogeneous material is annealed, chemical species will move in such a manner as to eliminate all chemical potential gradients. Fick (11) has described the process for diffusion in one dimension stating that the quantity of material passing through a unit area of a plane perpendicular to the direction of diffusion per unit time is proportional to the negative of the concentration gradient in the direction of diffusion. Mathematically, Fick's equation is given by

$$J = - \tilde{D} \frac{\partial C}{\partial x} \tag{1a}$$

where J is the flux of one diffusing species, C is the concentration in particles per unit volume of that species, x is the spatial coordinate in the direction of the concentration gradient, and $\tilde{D}$ is a proportionality constant called the interdiffusion coefficient. The term "interdiffusion coefficient" is used because Equation 1a describes a bulk intermixing process and includes the effects of the fluxes of all mobile species present. The relation given in Equation 1a is referred to as Fick's First Law.

A more general form of Equation 1a which describes the

motion of k diffusing species, and which is not restricted to a single diffusional coordinate, is given by

$$J_i = - \sum_k D_{ik} \nabla C_k \qquad (1b)$$

where D_{ik} is a tensor quantity. Equation 1b is reduced to Equation 1a under the restrictions specified by Fick.

In the event that an unsteady state condition exists, i.e. the concentration of diffusant at some position is a function of time, Fick's First Law remains valid but is difficult to apply because of its mathematical form. A continuity equation may be combined with Equation 1a and the result, which is valid for diffusion in one dimension, is given by

$$\frac{\partial C}{\partial t} = \frac{\partial}{\partial x} \left(\tilde{D} \frac{\partial C}{\partial x} \right). \qquad (2)$$

This equation is referred to as Fick's Second Law. In the general case D is a function of concentration (and therefore of position), and Equation 2 becomes

$$\frac{\partial C}{\partial t} = \tilde{D} \frac{\partial^2 C}{\partial x^2} + \frac{\partial C}{\partial x} \frac{\partial \tilde{D}}{\partial x} . \qquad (3)$$

Techniques for the solution of Equation 3 are presented in a later section of this thesis.

Darken (12) has analyzed interdiffusion between pairs of metals in binary alloys relating the interdiffusion coef-

ficient to the self diffusion coefficients of the constituents. A self diffusion coefficient is defined as a diffusion coefficient measured in the absence of a chemical concentration gradient. The interdiffusion situation is considered in which one species moves in one direction faster than the other species moves in the opposite direction resulting in a net flow of matter. The phenomenon of a net flow of matter may be monitored through observation of the movement of inert markers relative to some fixed position during the diffusion process (Kirkendall effect).

Darken made the following assumptions:

(1) Two chemically distinct species are present with the same atomic volume.

(2) Marker motion is measured relative to the end of the semi-infinite experimental specimen.

(3) No charge effects are present.

(4) The mobility of each species is equivalent to its respective tracer mobility.

The velocity of the marker, V, is related to the intrinsic diffusion coefficients of species 1 and 2, i.e. D_1 and D_2 respectively, through

$$V = \frac{1}{C} \left(D_1 \frac{\partial C_1}{\partial x} + D_2 \frac{\partial C_2}{\partial x} \right) \qquad (4)$$

where C_1 is the concentration of component 1, C_2 is the concentration of component 2, and C is the total concentration.

The intrinsic diffusion coefficient describes the flux of one species in a chemical concentration gradient provided all other species are immobile. The interdiffusion coefficient, which includes the effect of all mobile species, is related to the intrinsic diffusion coefficients through

$$\tilde{D} = N_1 D_2 + N_2 D_1 \tag{5}$$

where N_1 and N_2 are the mole fractions of components 1 and 2, respectively. In general, the self diffusion coefficients and intrinsic diffusion coefficients are not equivalent, with the relationship between them being

$$D_1 = D_{1,\ self}\left(1 + N_1 \frac{\partial \ell n \gamma_1}{\partial N_1}\right) \tag{6}$$

where γ_1 is the activity coefficient of species 1 in the solid solution.

From assumption (4) above, the tracer self diffusion coefficient, D_1^*, is equal to the self diffusion coefficient, i.e.

$$D_1^* = D_{1,self} \tag{7}$$

if $\partial \ell n \gamma_1^* / \partial \ell n\ N_1^* = 0$--neglecting any relationship between the structure of crystals and the mechanism of diffusion. The interdiffusion coefficient may be related to D^* through a combination of Equations 5, 6, and 7 which yields the Darken equation.

$$\tilde{D} = (N_1 D_2^* + N_2 D_1^*)\left(1 + N_2 \frac{\partial \ell n \gamma_2}{\partial N_2}\right). \qquad (8)$$

Interdiffusion of binary ceramics containing a common anion may be examined in a treatment similar to that presented by Jost (13). The following assumptions are made:

(1) The system is binary in cations A and B of the same charge, i.e., $Z_A = Z_B$, with a common anion Y.

(2) Anions are stationary with respect to any axis with cation migration through the anion matrix.

(3) The solid solution is ideal, i.e. $\frac{\partial \ell n \gamma_i}{\partial N_i} = 0$.

(4) The ionic volumes of species A and B are the same.

(5) Diffusion is in one dimension in an unbounded system.

The flux of cation A, J_A, is proportional to the electrochemical potential gradient, i.e.

$$J_A = - b_A \left[kT \frac{dC_A}{dx} - C_A Ze \frac{d\phi}{dx}\right] \qquad (9)$$

where b_A = the mobility of species A
k = Boltzmann constant
x = spatial coordinate
Z = cation valence
C_i = concentration of species i
e = electronic charge
ϕ = electrical potential

Similarly, the flux of cations B, J_B, is given by

$$J_B = b_B\left[kT\frac{dC_A}{dx} + C_B Ze\frac{d\phi}{dx}\right] \tag{10}$$

In order for electrical neutrality to be maintained no net flux can exist, i.e.

$$J_A = J_B \tag{11}$$

combining Equations 9, 10, and 11 yields a solution for J_A, i.e.

$$J_A = -\frac{dC_A}{dx}\left[\frac{kTb_Ab_B(C_A + C_B)}{b_AC_A + b_BC_B}\right]. \tag{12}$$

By analogy of Equation 12 above to Fick's First Law the interdiffusion coefficient in the mixed crystal, $\tilde{D}_{(A+B)}$, may be defined as

$$\tilde{D}_{(A+B)} = \frac{kTb_Ab_B(C_B + C_B)}{b_AC_A + b_BC_B} \tag{13}$$

or

$$\tilde{D}_{(A+B)} = \frac{b_Ab_BkT}{N_Ab_A + N_Bb_B}. \tag{14}$$

An interesting case arises when the mobility of one species greatly exceeds that of the other, i.e. $b_A >> b_B$. If $N_A \simeq N_B$, then,

$$\tilde{D}_{(A+B)} = b_BkT. \tag{15}$$

In this case the interdiffusion process is limited by the species with lowest mobility.

Cooper and Heasley (14) have considered binary interdiffusion in ceramics in which case the common anion may or may not be mobile. This treatment was limited to ions of the same charge. Three specific cases were examined as follows:

(1) The first case concerns the situation in which the mobilities of both cations and anions are similar but the self diffusion coefficient of cation A in (AB)Y, D_{AA}, is greater than the self diffusion coefficient of cation B in (AB)Y, D_{BB}, i.e. $D_{AA} > D_{BB}$. In such a case a relaxation flux does exist resulting in inert marker movement.

(2) The mobility of one cation is much lower than that of the other cation, i.e. $D_{BB} << D_{AA}, D_{YY}$. In this case a relaxation flux also exists with final marker position at the AY and (AB)Y interface.

(3) The mobility of the anion is much lower than that of either cation, i.e. $D_{YY} << D_{AA}, D_{BB}$. Only in this case the relaxation flux does not exist with consequently no marker movement.

The case in which charge effects are present may be even more complicated because the mobility of electronic charge carriers must be considered. Additional considerations may

involve a binding energy between charge carriers and aliovalent cations. These binding energies and mobilities in effect limit the rate at which the diffusion potential is satisfied and thereby limit the overall rate of atom movement. A general treatment of the subject has been presented by Lindström (15).

Defect Structure of Oxides

Because of their powerful influence on the diffusion process, the study of defects is intimately related to any diffusion study in oxides. The discussion here will be limited to point defects, i.e. defects involving only a small number of atomic species. More complete reviews of the subject of defects are available in the literature (16).

The subject of point defects includes intrinsic or thermally-generated defects, defects caused by deviations from stoichiometry, defects induced by the incorporation of foreign atoms into the host material, and association of defects. The notation of Kröger and Vink (17) is used here, with symbols defined in Table 1.

In a pure stoichiometric oxide there are several types of thermally-generated defects possible. Schottky disorder in an oxide MO involves the creation of equal numbers of cation and anion vacancies. Frenkel disorder involves the formation of equal numbers of either cation vacancies or anion vacancies and interstitials. Antistructural disorder

Table 1. Summary of defect notation

Symbol	Definition
h	hole
e	electron
p	hole concentration
n	electron concentration
p_M	metal partial pressure
p_{O_2}	oxygen partial pressure
K_i	equilibrium constant (i = equation number)
ΔG_i	free energy change (i = equation number)
R	gas constant
T	temperature (°Kelvin)
V_S	vacancy (S = site either metal or nonmetal)
V_S', $V_S^{\cdot}$	singly charged vacancy (' = negative, $^{\cdot}$ = positive)
V_S'', $V_S^{\cdot\cdot}$	doubly charged vacancy
N	number of positive or negative ions in crystal
N_i	number of interstitial sites
N_ℓ	number of lattice sites of either cations or anions
Z	number of nearest neighbors to a vacancy
ϕ	energy of formation of vacancy pair
k	Boltzmann constant
$Al_{Mg}^{\cdot}$	positively charged aluminum ion on magnesium site
O_O	oxygen ion on oxygen site

Table 1 (Continued)

Symbol	Definition
N^*	number of vacancy pairs per unit volume
M_i	metal ion on interstitial site
σ	electrical conductivity
σ_p	electrical conductivity due to holes
σ_n	electrical conductivity due to electrons

consists of an interchange of cations and anions from their normal positions.

The formation of the Schottky defect has been discussed by Tallan et al. (18). The process for an oxide MO is given as

$$M_M + O_O = V_M + V_O + M(g) + \frac{1}{2} O_2(g) \qquad (16a)$$

or equivalently,

$$V_M + V_O = 0. \qquad (16b)$$

The defects may ionize according to the pseudo-reactions

$$V_O = V_O^{\bullet} + e \qquad (17)$$

$$V_O^{\bullet} = V_O^{\bullet\bullet} + e \qquad (18)$$

and

$$V_M = V_M^{'} + h \qquad (19)$$

$$V_M^{'} = V_M^{''} + h \qquad (20)$$

and so on to any degree of ionization which is physically possible.

Intrinsic processes in the material also lead to the generation of electrons and holes, i.e.

$$\text{nil} = h + e \ . \tag{21}$$

The law of mass action may be applied to Equations 16 through 21 with the assumption of unit activities for all species. For example, the equilibrium expression corresponding to Equations 16 are given by the following:

$$[V_M][V_O]p_M p_{O_2}^{1/2} = K_{16a} = \exp(-\Delta G_{16}/RT) \tag{22}$$

$$[V_M][V_O] = K_S = \exp(-\Delta G_S/RT) \ . \tag{23}$$

In ionic materials electrical neutrality must be maintained, i.e.

$$n + [V_M'] + 2[V_M''] = p + [V_O^{\cdot}] + 2[V_O^{\cdot\cdot}] \tag{24}$$

and, if stoichiometry is maintained,

$$[V_M] + [V_M'] + [V_M''] = [V_O] + [V_O^{\cdot}] + [V_O^{\cdot\cdot}] \ . \tag{25}$$

If the appropriate equilibrium constants are known, a solution may be obtained for the concentration of each defect.

The equilibrium concentration of Schottky defects may be calculated using statistical methods. Above absolute zero the equilibrium fraction of vacancy pairs has been given by

Dekker (19) for NaCl type crystals as

$$\frac{n}{N} = \left(\frac{\nu}{\nu'}\right)^{3z} \exp(-\phi/kT) \qquad (26)$$

where n is the number of Schottky defects per unit volume of crystal, N is the number of allowable ion pairs per unit volume in a perfect crystal, ν' is the vibrational frequency of atoms near the vacancy pair at temperature T, ν is the vibrational frequency of atoms in a perfect crystal at temperature T, and other symbols are defined in Table 1. An expression similar to Equation 26 has been formulated by Mott and Gurney (20) to describe the formation of Frenkel defects

$$\frac{n^*}{N_\ell N_i} = \left(\frac{\nu}{\nu'}\right)^{32} \exp(-\phi_F/kT) \qquad (27)$$

where n* is the number of Frenkel defects per unit volume of crystal, and N_ℓ and N_i are the numbers per unit volume of ions in normal positions and in interstitial positions respectively.

Modifications in the defect structure may arise from changes in stoichiometry of the oxide. For purposes of simplification the formation of only singly-ionized vacancies is considered. The oxidation of a metal ion in an oxide MO may be visualized as

$$2M_M = M_M^{\cdot} + V_M' + M(g). \qquad (28)$$

Alternatively, one may write

$$\frac{1}{2}O_2(g) = O_O + V'_M + h. \tag{29}$$

If the electrical neutrality condition is

$$[V'_M] = p \tag{30}$$

the equilibrium constant for Equation 29 is

$$K_{29} = \frac{[V'_M]^2}{p_{O_2}^{1/2}} = \frac{p^2}{p_{O_2}^{1/2}} \tag{31}$$

and

$$[V'_M] = K_{29}^{1/2} p_{O_2}^{1/4}. \tag{32}$$

The addition of foreign ions to the host may result in formation of defects. Consider the incorporation of trivalent aluminum in MgO given by

$$Al_2O_3 = 2Al_{Mg}^{\cdot} + V_{Mg}^{''} + 3O_O . \tag{33}$$

In the case in which only doubly ionized magnesium vacancies are allowed, the number of induced magnesium vacancies is one-half the aluminum ion concentration. In the case of incorporation of a variable valence impurity in an oxide, the number of cation vacancies is dependent on temperature and oxygen partial pressure as well as concentration of incorporated impurity.

Atomic Theory of Diffusion

A result of the three-dimensional random walk theory of diffusion in which individual jumps are not correlated with one another is given by Shewmon (2) as

$$D = \frac{1}{6} \Gamma \alpha^2 \tag{34}$$

where Γ is the total jump frequency of a diffusing atom, α is the jump distance, and D describes the random movement of atomic species. If all jumps are of the same length, as in a cubic crystal, and if all adjacent sites have an equal probability of being the next resident site for the jumping defect, then

$$\Gamma = k\omega \tag{35}$$

where k is the number of specific adjacent sites and ω is the jump frequency into a specific adjacent site. Then for the cubic system

$$D = \frac{k\alpha^2}{6} \omega = \gamma a_o \omega \tag{36}$$

where γ is a geometrical constant and a_o is the lattice parameter. The frequency of jumping into a specific adjacent site ω is taken as the frequency at which the jumping species acquires sufficient energy to overcome any barrier to a complete jump, ω_a, times the probability that the adjacent site is unoccupied, p_v, i.e.

$$\omega = \omega_a p_v. \tag{37}$$

Assuming the ensemble is governed by Boltzmann statistics

$$\omega_a = \nu \exp(-\Delta G_m/RT) \tag{38}$$

where ν is the frequency of vibration toward a specific site, ΔG_m is the free energy associated with one mole of jumping species in the saddle point configuration, R is the gas constant, and T is temperature. The exponential term actually represents the probability of any given vibration achieving sufficient energy for a successful jump. Substitution of Equations 37 and 38 into Equation 36 yields

$$D = \gamma a_o^2 \nu p_v \exp(-\Delta G_m/RT). \tag{39}$$

For a vacancy jump mechanism in a face centered cubic lattice, i.e. the cation sublattice in the NaCl structure, k = 12 and $\alpha = 0.707\ a_o$ so that

$$D = a_o^2 \nu p_v \exp(-\Delta G_m/RT). \tag{40}$$

If the crystal contains only Schottky defects

$$p_v = \exp(-\Delta G^f/2RT) \tag{41}$$

where ΔG^f is the free energy of formation of Schottky pair. Combination of Equations 40 and 41 yields

$$D = a_o^2 \nu \exp[-(\Delta G^f/2RT + \Delta G_m/RT)]. \tag{42}$$

If diffusion coefficients are characterized by tracer atom jumps, the correlated nature of such jumps can be reconciled with the random walk treatment by introducing a correlation coefficient

$$D = \frac{1}{6} f \Gamma \alpha^2. \tag{43}$$

Since $\Gamma = \Gamma_v p_v$, where $\Gamma_v = \omega_a k$ represents the jump frequency for a vacancy, Equations 39 and 43 combine to give

$$D^* = f a_o^2 \nu p_v \exp(-\Delta G_m / RT) \tag{44}$$

for a face centered cubic lattice. Values of the correlation coefficient f and further discussion of the correlation effect and its relation to impurity diffusion are available in the works of Friauf (4) and Bakker (21).

REVIEW OF EXPERIMENTAL LITERATURE

Stoichiometry of Oxides of Interest

Magnesium oxide is thought to exhibit only small deviations from stoichiometry (22). Magnesium oxide crystallizes in the NaCl structure and is highly ionic in character (23). Estimates of the energy of formation of Schottky defects in MgO range from 90 to 130 kcal/mole (22, 24). The lack of higher oxidation states for magnesium other than plus two eliminates the possibility of metal deficit due to additional oxidation of cations. The possibility of metal excess through formation of magnesium interstitials is thought to be unlikely due to the high energy necessary to force Mg^{+} or Mg^{o} into four-fold coordination. Rovner (25) has presented evidence for the existence of oxygen interstitials in the intrinsic region, i.e. where properties are not controlled by impurities at oxygen pressures greater than about 10^{-1} atm. Electrical neutrality is preserved by the formation of holes which are considered localized near the interstitial defect. Rovner's ideas are based on data for diffusion of O^{18} in MgO of normal purity, MgO doped with Li, and MgO doped with Cr. At 1150°C and 10^{-1} atm oxygen pressure, the contribution of oxygen interstitials to the diffusion process was only thought to be ten to 10^{2} times that of oxygen vacancies with relative contributions dependent on temperature, oxygen pressure, and crystal purity.

Like MgO, Mn_xO also crystallizes in the NaCl structure. The manganese ion is aliovalent, i.e. the deviations from stoichiometry of Mn_xO are dependent on temperature and oxygen pressure as well as purity. A comprehensive description of the system Mn-O has been presented by Hed and Tannhauser (26). The phase diagram in the system Mn-O is shown in Figure 1. Other manganese oxides such as Mn_3O_4, Mn_2O_3, and MnO_2 are known to exist and can be converted into one another through appropriate choice of temperature and oxygen pressure.

Davies and Richardson (27) report the variation in stoichiometry of Mn_xO with oxygen partial pressure at temperatures of 1500°C, 1575°C, and 1650°C. The oxide was reported to be metal deficient with compositions ranging from $MnO_{1.000}$ to $MnO_{1.045}$ as the oxygen partial pressure was raised from about 10^{-10} to 10^{-2} atm at the three experimental temperatures. The manganese vacancy concentration was assumed to be twice the concentration of trivalent manganese determined chemically from quenched samples. The results of Davies and Richardson have been questioned by Eror (28), Smyth (29), and Birchenall (30). Eror's criticism concerned the experimental procedure of Davies and Richardson, while both Smyth and Birchenall point out that Davies and Richardson ignored the concentration of electron holes in constructing their equilibrium equations. Using the data of Davies and Richardson, Smyth points out that above an oxygen partial

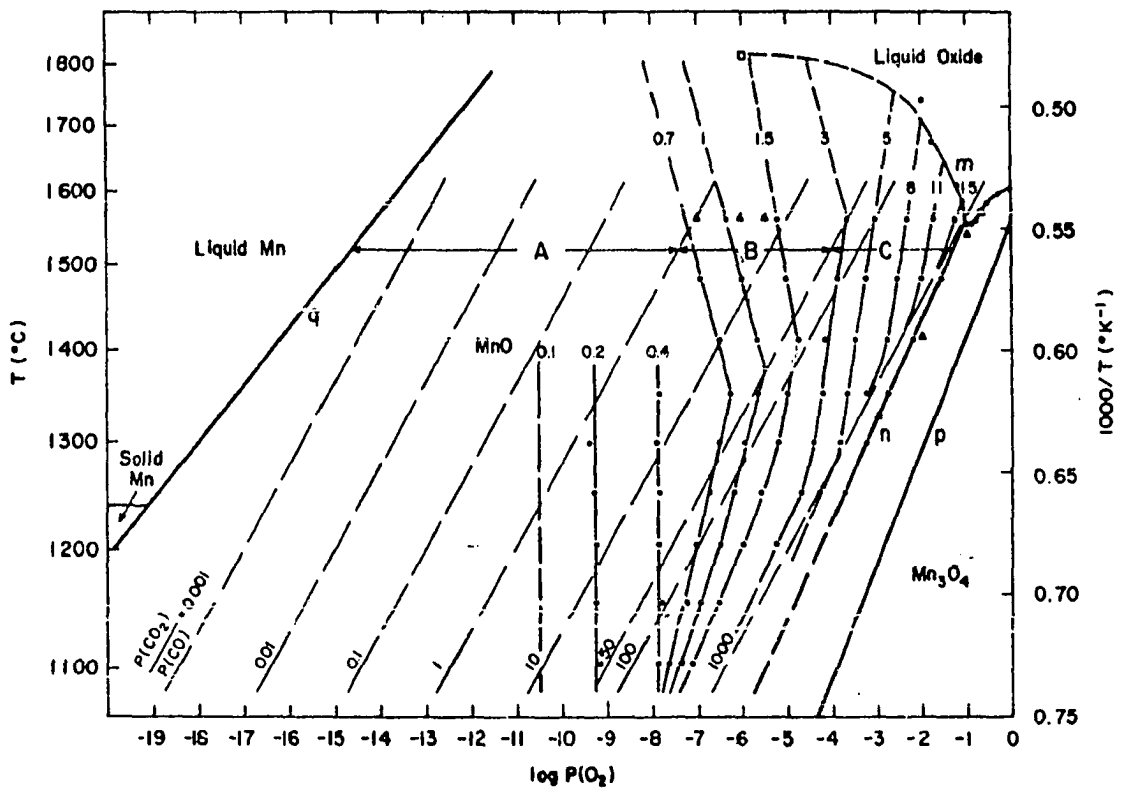

Figure 1. The system Mn-O from Hed and Tannhauser (26) showing dashed lines of constant composition with values of molar oxygen excess times 10^2

pressure of 10^{-7} atm, where the manganese vacancy concentration is proportional to $p_{O_2}^{1/6}$, the appropriate defect reaction should be

$$\tfrac{1}{2}O_2(g) = O_O + V_{Mn}'' + 2h. \tag{45}$$

The electroneutrality condition is given by

$$[V_{Mn}''] = p \tag{46}$$

and thus

$$[V_{Mn}''] = K_{45}^{1/3} p_{O_2}^{1/6}. \tag{47}$$

At or below oxygen partial pressures corresponding to $MnO_{1.000}$ or lower, the possibility of manganese interstitials exists, i.e.

$$Mn_{Mn} = Mn_i^{\cdot\cdot} + V_{Mn}'' . \tag{48}$$

The Schottky equilibrium must also be considered, i.e.

$$O = V_{Mn}'' + V_O^{\cdot\cdot}. \tag{49}$$

Since Roth (8, 9) reports extensive Frenkel disorder in Fe_xO, Birchenall (30) considers Equation 48 to be appropriate at low p_{O_2}. The oxygen pressure dependence may be deduced through consideration of the equilibrium

$$Mn_{Mn}\ O_O = \tfrac{1}{2}\ O_2(g) + Mn_i^{\cdot\cdot} + 2\ell. \tag{50}$$

If the appropriate electroneutrality condition is

$$n = 2[Mn_i^{\bullet\bullet}] \tag{51}$$

then

$$[Mn_i^{\bullet\bullet}] = K_{50}^{1/3} p_{O_2}^{-1/6} \ . \tag{52}$$

It is important to note that the vacancy concentration reported by Davies and Richardson (27) was independent of temperature for the three reported temperatures suggesting that a "quenched" disorder was measured.

Eror (28) investigated the nonstoichiometry of $Mn_{1-x}O$ using electrical conductivity and thermogravimetric techniques. The p-n boundary, i.e. where $\sigma_p = \sigma_n$, was located at a p_{CO}/p_{CO_2} ratio of 1.0 for 900°C < T < 1150°C. Eror found that $[V_{Mn}^{''}]$ exhibited a dependence of $p_{O_2}^{1/6}$ in the p-type region in accordance with Equations 50 and 52 over two orders of magnitude of p_{O_2} above the p-n boundary. At the highest pressures investigated, a dependence on $p_{O_2}^{1/5}$ was found. This dependence may be explained on the basis of formation of singly ionized cation vacancies, i.e.

$$\tfrac{1}{2}O_2(g) = O_O + V_{Mn}^{'} + p \ . \tag{53}$$

If the electroneutrality condition is

$$[V_{Mn}^{'}] = p \tag{54}$$

then it may be shown that

$$[V'_{Mn}] = K_{55}^{1/2} \, p_{O_2}^{1/4} \quad . \tag{55}$$

Since Kevane (31) has demonstrated that an oxygen pressure dependence of $p_{O_2}^{1/5.0002}$ is an allowable intermediate dependence during a transition from $p_{O_2}^{1/6}$ to $p_{O_2}^{1/4}$, Eror postulated the existence of singly ionized manganese vacancies in the high p_{O_2} region.

The electrical conductivity measurements on n-type Mn_xO, yield a pressure dependence of $\sigma \alpha p_{O_2}^{-1/6}$. Eror suggests the following defect model

$$Mn_{Mn}O_O = \frac{1}{2} O_2(g) + Mn_i^{\cdot\cdot} + 2e \quad . \tag{56}$$

Assuming the electrical neutrality condition

$$n = [Mn_i^{\cdot\cdot}] \tag{57}$$

then

$$n = K'_{56} p_{O_2}^{-1/6} \tag{58}$$

Since the electrical conductivity, σ, is given by

$$\sigma = ne\mu_e \tag{59}$$

then

$$\sigma \alpha p_{O_2}^{-1/6} \quad . \tag{60}$$

Hed and Tannhauser (32), include the possibility of oxygen vacancies in the n-type region according to

$$O_O = \frac{1}{2} O_2(g) + V_O^{\cdot\cdot} + 2e \qquad (61)$$

which may be shown to yield $\sigma \alpha p_{O_2}^{-1/6}$ if $2[V_O^{\cdot\cdot}] = e$. Hed and Tannhauser also discuss the possibility that a doubly ionized cation vacancy model may be dominant in the n-type region and yet show a pressure dependence of $\sigma \alpha p_{O_2}^{-1/6}$. Such a possibility could exist if

$$\mu_e >> \mu_p \ . \qquad (62)$$

As the oxygen partial pressure decreases the number of holes decreases and the electron contribution to the conductivity dominates because of Equation 62 even though $n_p > n_e$. Gvishi Tallan, and Tannhauser (33) have experimentally confirmed Equation 62 in n-type Mn_xO.

Price and Wagner (34) add more support to the cation vacancy model for n-type Mn_xO in a tracer diffusion study of Mn^{55} in Mn_xO. Their data show no inflection point in D^*_{Mn} as the p-n boundary is crossed into the n-type material. Such an inflection would be expected if a change existed in the majority defect species. Price and Wagner have extrapolated the data of Boquet et al. (35) in support of their argument. In n-type Mn_xO the enthalpy of motion for cations was found to be 22.2 kcal/mole. Since Eror (28) and Boquet et al. (35) found the motion enthalpy to be about 25 kcal/mole in p-type

Mn_xO at 10^{-10} atm p_{O_2}, Price and Wagner suggest that this is further support for the manganese vacancy model in the n-type material.

A gravimetric study of Mn_xO was reported by Bransky and Tallan (36). Their results are of the form $[V'_{Mn}] \alpha p_{O_2}^{1/4}$ for $x < 0.02$ in MnO_{1+x}, thus supporting a model for singly ionized manganese vacancies in the low p_{O_2} regions. At values of $x > 0.02$ a pressure dependence of weight change on $p_{O_2}^{1/3.3}$ was found. This value suggests existence of the equilibrium

$$O_2(g) = 2O_O + (V_{Mn}V_{Mn})'' + 2h. \tag{63}$$

If electrical neutrality is preserved through

$$2[(V_{Mn}V_{Mn})''] = p \tag{64}$$

then

$$[(V_{Mn}V_{Mn})''] = K'_{63}p_{O_2}^{1/3} . \tag{65}$$

However, a complex defect model could also be visualized including manganese interstitials according to

$$\frac{1}{2} O_2(g) + Mn_{Mn} = O_O + (V_{Mn}Mn_iV_{Mn})' + h \tag{66}$$

and would result in a dependence of $[V_{Mn}] \alpha p_{O_2}^{1/4}$. A higher degree of ionization would only decrease the pressure dependence. Higher order complexes would be necessary to increase the pressure dependence. Bransky and Tallan conclude

that the existence of manganese interstitials while unlikely cannot be discounted without further X-ray or neutron diffraction study.

Both Price and Wagner (34) and Eror (28) found the enthalpy of formation of manganese vacancies to be a negative quantity. Thus disorder will decrease in Mn_xO as it is heated at constant oxygen pressure. Conversely, disorder in Mn_xO will increase as it is cooled in constant p_{O_2}. It is on this basis that Eror was critical of the experimental technique of Davies and Richardson (27).

Nickelous oxide, Ni_xO, like Mn_xO, crystallizes in the NaCl structure. Unlike Mn_xO, Ni_xO is the only stable oxide of nickel. Ni_xO exhibits p-type semiconductivity but does not exhibit wide deviations from stoichiometry as found in Mn_xO or Co_xO (30). The small change in stoichiometry in Ni_xO over its stable phase field renders gravimetric measurements practically useless for investigations of defect structure. The volatility of Ni_xO at high temperature and low oxygen partial pressure also complicates gravimetric measurements.

Wagner and Baumback (37) measured the electrical conductivity of Ni_xO at temperatures of 800°C, 900°C, and 1000°C. The conductivity was found proportional to the fourth root of p_{O_2} suggesting the following defect equilibrium

$$\frac{1}{2} O_2(g) = O_O + V'_{Ni} + h \ . \qquad (67)$$

Mitoff (38) presents evidence to support a doubly-ionized cation vacancy model through

$$\frac{1}{2} O_2(g) = O_O + V''_{Ni} + 2h. \qquad (68)$$

Equation 68 leads to a dependence of $[V''_{Ni}] \alpha p_{O_2}^{1/6}$. Several investigators (39, 40) have found that Mitoff's data could be represented by a $p_{O_2}^{1/4}$ dependence. Some of Mitoff's quantitative data are presented in Figure 2.

Eror (28) found the electrical conductivity of Ni_xO to be proportional to $p_{O_2}^{1/4}$ in the range 900°C - 1200°C and one atm to 10^{-4} p_{O_2}. This pressure dependence suggests the singly ionized cation vacancy model. The data of Eror and Mitoff are in good agreement at one atmosphere oxygen pressure.

Tretyakov and Rapp (41) investigated deviations from stoichiometry of Ni_xO using high temperature electrochemical cell measurements. Their data from 836°C to 1086°C and from one atm to 10^{-4} atm p_{O_2} offer support for the doubly-ionized vacancy model. Near p_{O_2} = 1 atm the vacancy concentration is expressed as

$$[V''_{Ni}] = 0.51^{+0.21}_{-0.15} \ p_{O_2}^{1/6} \ \exp\left(\frac{-19{,}000 \pm 8{,}700}{RT}\right) \qquad (69)$$

which is in good agreement with the expression of Mitoff, i.e.

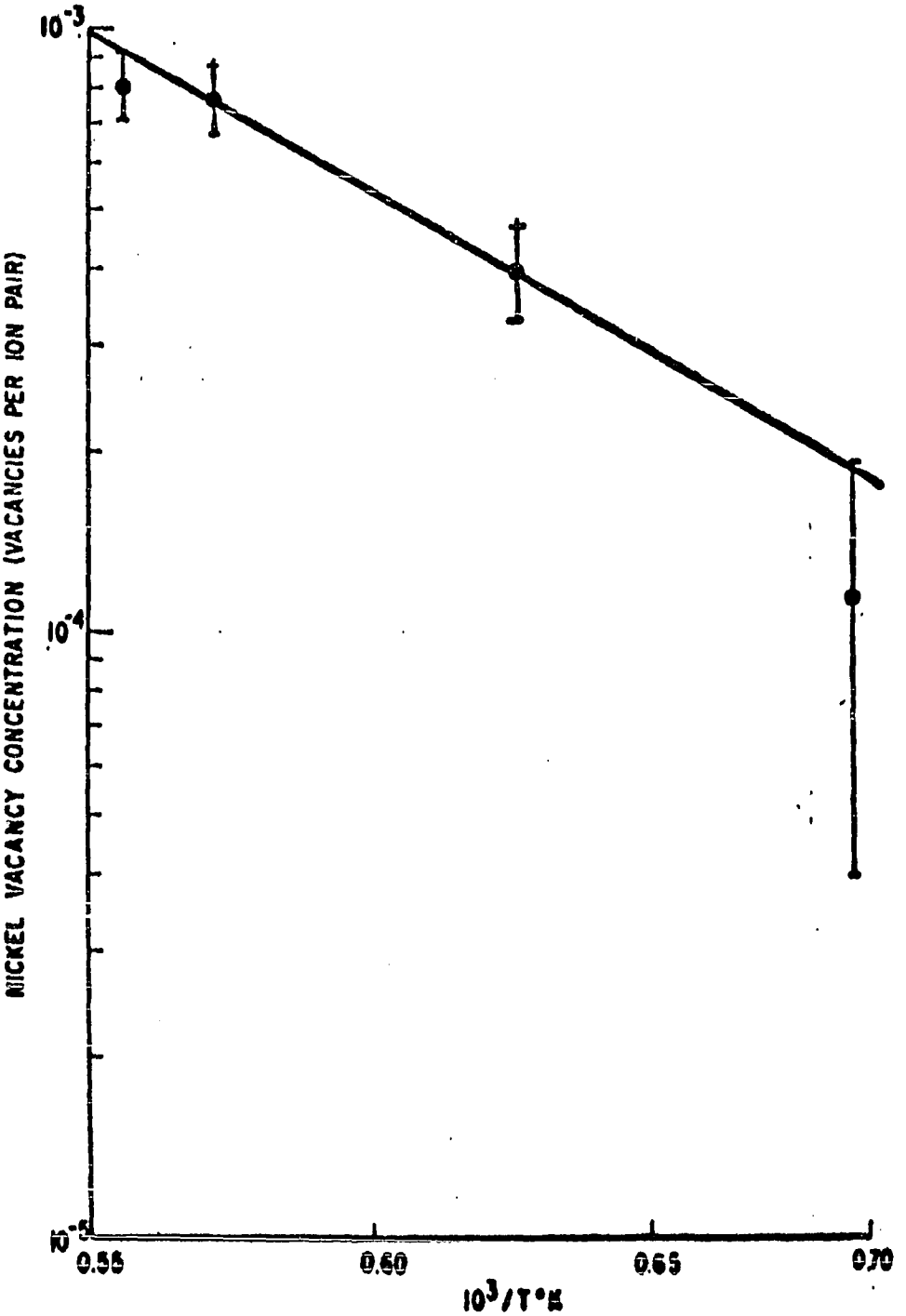

Figure 2. Nickel vacancy concentration in Ni_xO at $p_{O_2} = 1$ from Mitoff (38)

$$[V_{Ni}''] = 0.11\ p_{O_2}^{1/6}\ \exp\left(\frac{-17,800}{RT}\right). \qquad (70)$$

At 1000°C and p_{O_2} = 0.21 atm, the Tretyakov-Rapp expression yields a vacancy concentration of 2.1×10^{-4} per ion pair whereas the Mitoff expression yields 0.74×10^{-4} per ion pair. Zintl (39) has used chemical analysis to determine the amount of Ni^{3+} in Ni_xO and reports $[n_i^{3+}] = 2.5\times10^{-4}$ per ion pair. Sockel and Schmalzried (40) also report a dependence of $[V_{Ni}'']$ on $p_{O_2}^{1/6}$.

Bransky and Tallan (36) measured the electrical conductivity and Seebeck coefficient in Ni_xO. In the range 1000°C - 1600°C and p_{O_2} from one atm to 10^{-5} atm, the conductivity was proportional to $p_{O_2}^{1/4}$ suggesting singly-ionized vacancies. The enthalpy of formation of V_{Ni}' was reported to be 0.66 ± 0.03 ev.

Cobaltous oxide crystallizes in the NaCl structure and exhibits large deviations from stoichiometry. Experiments involving electrical conductivity, gravimetry, diffusion, and thermoelectric measurements confirm the existence of cation vacancies; however, as in the case of Ni_xO there is little agreement as to the ionization state of the majority vacancy species.

The first investigations of Co_xO as a function of p_{O_2} were those of Wagner and Koch (42) who found the conductivity to depend on $p_{O_2}^{1/4}$. This dependence was also found by

Duquesnoy and Marion (43) who investigated Co_xO in the range 900°C to 1200°C and p_{O_2} ranging from about two atm to 10^{-12} atm. These results suggest the following defect equilibrium:

$$\frac{1}{2} O_2(g) = O_O + V'_{Co} + h . \qquad (71)$$

Others finding the $p_{O_2}^{1/4}$ conductivity dependence include Eror (28), Carter and Richardson (44 , 45), and Shelykh et al. (46).

Eror and Wagner (47) calculated the transference number of the cobaltous ion using their conductivity data and the self diffusion data of Carter and Richardson (44, 45) to be 5×10^{-5}. This indicates Co_xO is primarily an electronic conductor. Eror's gravimetric measurements also suggest $[V'_{Co}] \alpha p_{O_2}^{1/4}$. Eror's data for the temperature dependence of $[V'_{Co}]$ is shown in Figure 3.

Fisher and Tannhauser (48) report electrical conductivity and gravimetric measurements on Co_xO from 900°C to 1450°C and from one to 10^{-12} atm p_{O_2}. Their results, shown in Figure 4, may be separated into two regions, A and B. In region A, both conductivity and gravimetric measurements reveal a relationship between isothermal weight change and the fourth root dependence of p_{O_2} suggesting that V'_{Co} is the dominant type of cobalt vacancy. This region is seen to include the experimental conditions of Eror (28) and others. In region B the conductivity varied as the sixth root of p_{O_2} suggesting

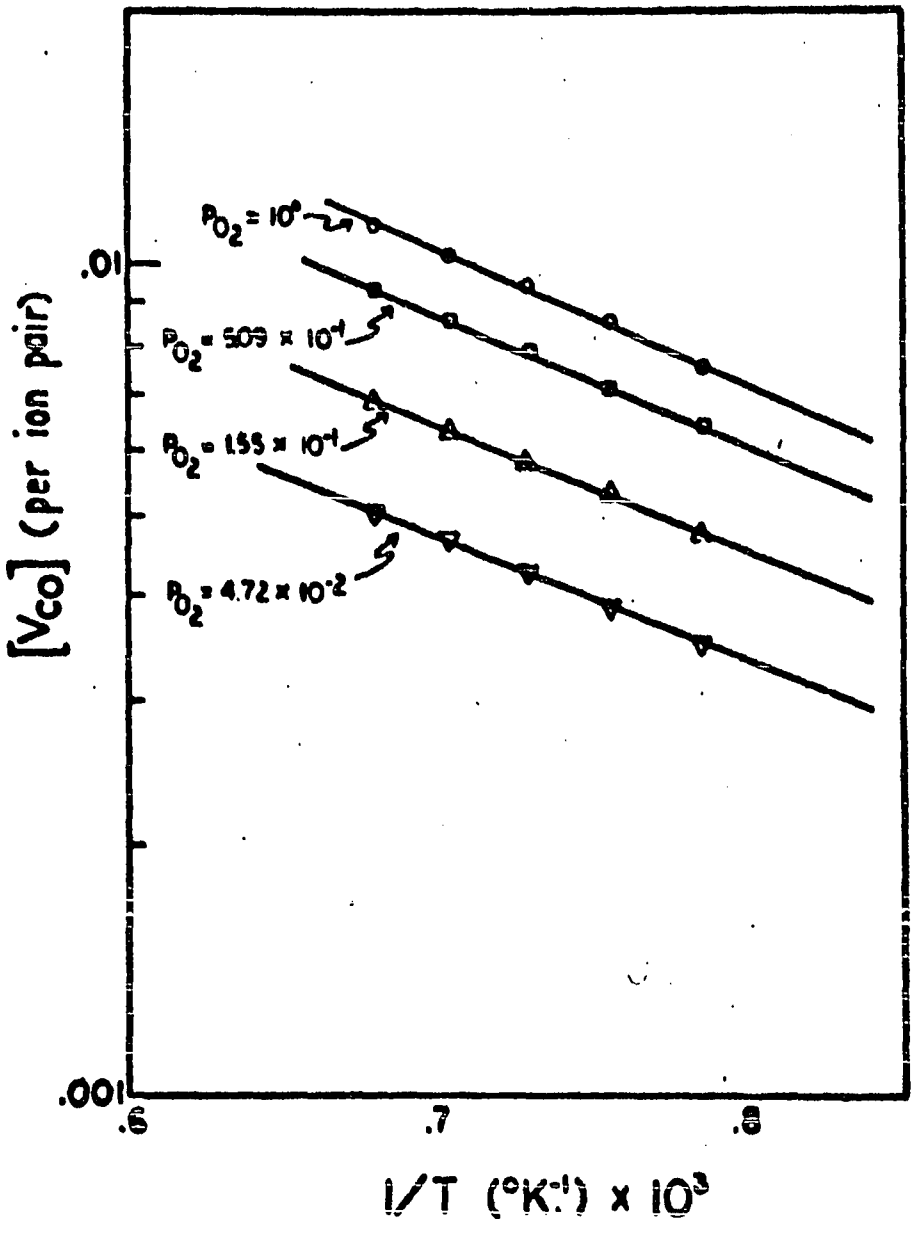

Figure 3. Cobalt vacancy concentration in Co_xO from Eror and Wagner (47)

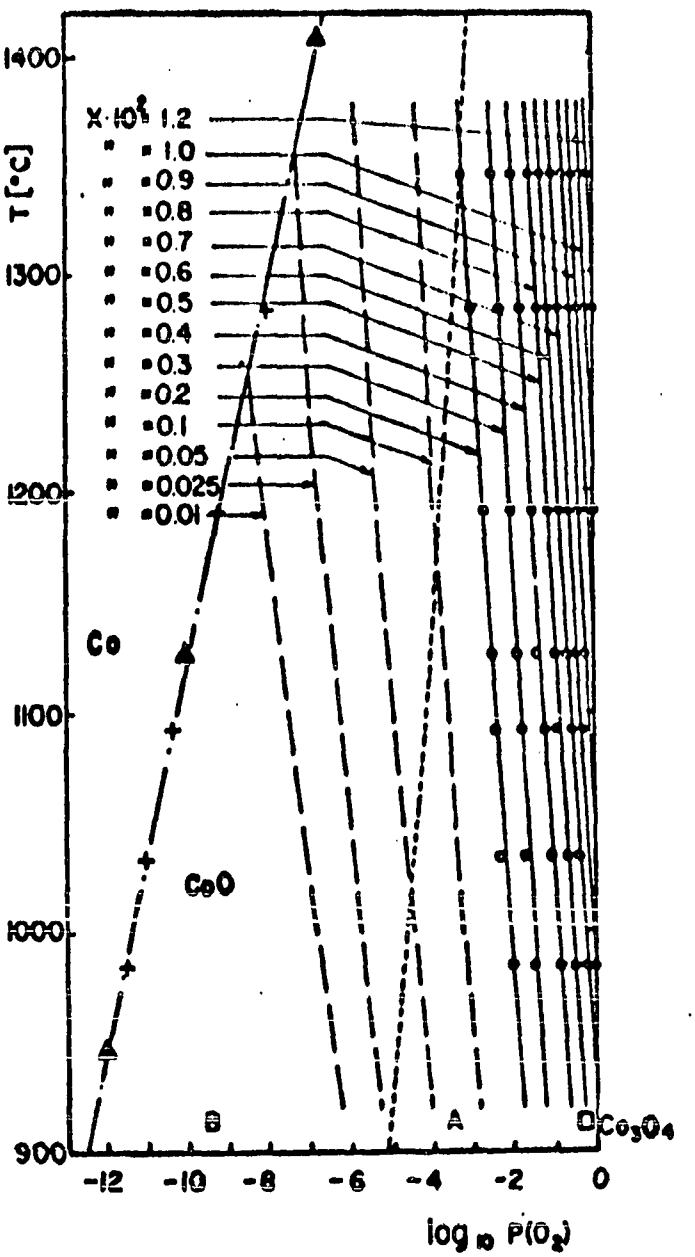

Figure 4. The system Co-O from Fisher and Tannhauser (48) showing lines of constant composition with values of molar oxygen excess, x, times 10^2

that the dominant type of cobalt vacancy is V_{Co}''. Fisher and Tannhauser do not report any of the experimental difficulty discussed by Eror (28) and Eror and Wagner (47) involving the poor reproducibility of conductivity measurements for $p_{O_2} < 10^{-4}$ in CO/CO_2 mixtures.

Crow (7) has presented a defect model for Co_xO based on his own diffusion results and the experimental work of others therefore implying that the model is valid for measurements at the given impurity level. The total electrical neutrality condition is given by Crow as

$$p + [F_M^{\cdot}] = [V_M'] + 2[V_M''] \tag{72}$$

where $F_M^{\cdot}$ represents a foreign (impurity) cation on a metal ion site. Using Brouwer's assumption (16) that one quantity predominates on both sides of the equation above, Crow divided the diagram into three regions where the principal neutrality conditions are as follows: $[F_M^{\cdot}] = 2[V_M'']$ at low p_{O_2}, $p = 2[V_M'']$ at higher p_{O_2} in accord with the results of Fisher and Tannhauser (48) and $p = [V_M']$ at highest p_{O_2} in accord with Eror (28) and Eror and Wagner (47). This behavior permits explanation of the behavior of minority species such as V_{Co}' in the region where $2[V_M''] = p$ predominates. The formation of V_{Co}' is given by

$$\frac{1}{2} O_2(g) = O_O + V_{Co}' + h. \tag{73}$$

Thus

$$[V'_{Co}] = \frac{K'_{73} p_{O_2}^{1/2}}{p} \tag{74}$$

and since $2[V''_M] = p$,

$$[V'_{Co}] = \frac{K''_{73}\, p_{O_2}^{1/2}}{[V''_{Co}]} . \tag{75}$$

The formation of V''_{Co} is given by

$$\frac{1}{2} O_2(g) = O_O + V''_{Co} + 2h \tag{76}$$

and

$$[V''_{Co}] = K'_{76}\, p_{O_2}^{1/6} . \tag{77}$$

Substituting Equation 77 into Equation 75 the resulting expression for V'_{Co} is

$$[V'_{Co}] = \frac{K''_{73}\, p_{O_2}^{1/3}}{K'_{76}} . \tag{78}$$

Similar considerations apply to other defects outside of their majority (concentration) region.

Diffusion Studies in Oxides of Interest

The first measurement of tracer diffusion of Ni^{63} in Ni_xO was made by Shim and Moore (49) who report $D^*(p_{O_2} = 0.21 \text{ atm}) = (4.4\times10^{-4}) \exp(-44.2 \text{ kcal/RT})$. Using Ni_xO crystals from the same boule as Shim and Moore, Lindner and Akerström (50) report $D^*(p_{O_2} = 0.21 \text{ atm}) = (1.72\times10^{-2}) \exp(-56 \text{ kcal/RT})$.

In both cases isotope penetration was measured by the surface decrease method suggesting possible error due to incorrect calculation involving the absorption correction. Choi and Moore (51) studied diffusion of Ni^{63} in single crystals of Ni_xO using the conventional sectioning technique and found $D^*(p_{O_2} = 0.21 \text{ atm}) = (1.83 \times 10^{-3}) \exp(-45.9 \pm 2.0 \text{ kcal/RT})$.

The diffusion of oxygen in Ni_xO has been studied by O'Keefe and Moore (52) using the technique of isotope exchange with O^{18}. The diffusion activation energy was 59.5 kcal/mole at $p_{O_2} = 0.015$ atm. At 1500°K the ratio $D^*_{Ni}(p_{O_2} = 0.015 \text{ atm})/D^*_O(p_{O_2} = 0.015 \text{ atm})$ was reported as 2×10^3.

Fueki and Wagner (53) have studied the parabolic oxidation of nickel between 900°C and 1400°C at pressures ranging from the dissociation pressure of Ni_xO to one atm p_{O_2}. The self diffusion coefficient was reported as $D_{Ni}(p_{O_2} = 0.21 \text{ atm}) = (1.1 \times 10^{-3}) \exp(-50.3 \text{ kcal/RT})$ with D_{Ni} independent of p_{O_2} for $p_{O_2} < 10^{-5}$ atm. The diffusion activation energy ranged from 43.6 kcal/mole at $p_{O_2} = 1$ atm to 36.3 kcal/mole at $p_{O_2} = 10^{-5}$ atm.

Crow (7) measured tracer diffusion of Ni^{63} in Ni_xO from 1100°C to 1400°C and from $p_{O_2} = 1$ atm to $p_{O_2} = 10^{-5}$ atm. Crow found $D^*_{Ni}(p_{O_2} = 1.0 \text{ atm}) = (8.9 \times 10^{-3}) \exp(-54.7 \text{ kcal/RT})$ and $D^*_{Ni}(p_{O_2} = 5 \times 10^{-5} \text{ atm}) = (1.2 \times 10^{-3}) \exp(-51.8 \text{ kcal/RT})$. The value of D^*_{Ni} at a given temperature was found to increase with increasing oxygen partial pressure.

Price and Wagner (54) report a chemical diffusion coefficient in Ni_xO using an electrical conductivity technique. Volpe and Reddy (55) have discussed reasons for apparent disagreement between their conductivity and tracer diffusion results in Ni_xO.

Carter and Richardson (44, 45) have observed the diffusion of Co^{60} in Co_xO in the range 1000°C to 1350°C as a function of p_{O_2}. The value of D^*_{Co} was found to be proportional to $p_{O_2}^{0.31}$. Carter and Richardson also report the parabolic oxidation of cobalt at 1148°C from p_{O_2} = 1 atm to p_{O_2} = 5.5×10^{-3} atm. The parabolic rate constant was found proportional to $p_{O_2}^{0.29}$.

Price and Wagner (54) report a chemical diffusion coefficient in Co_xO using an electrical conductivity technique. Between 800°C and 1100°C they found $\tilde{D} = (4.33\times10^{-3})$ exp(-24 kcal/RT).

Crow (7) reports diffusion of Co^{60} in Co_xO between 1100°C and 1400°C and between p_{O_2} = 1 atm and $p_{O_2} = 5\times10^{-5}$ atm. At p_{O_2} = 1 atm he reports $D^*_{Co}(p_{O_2} = 1 \text{ atm}) = (4.8\times10^{-3})$ exp (-35.9 kcal/RT). The tracer diffusion coefficient was found to depend on the sixth root of p_{O_2} at low p_{O_2} and on the fourth root of p_{O_2} at higher p_{O_2}.

Boquet et al. (35) have studied diffusion of Mn^{54} into single crystal and polycrystalline Mn_xO from 900°C to 1150°C and from $p_{O_2} = 10^{-25}$ atm to $p_{O_2} \simeq 10^{-10}$ atm. For $p_{O_2} < 10^{-17}$

atm they found D^*_{Mn} proportional to $p_{O_2}^{1/n}$ with n ranging from 6 to 8. For $p_{O_2} > 10^{-15}$, they found D^*_{Mn} proportional to $p_{O_2}^{1/6}$. The conductivity in Mn_xO was found proportional to $p_{O_2}^{-1/6}$ below $p_{O_2} \simeq 10^{-17}$ atm and proportional to $p_{O_2}^{1/6}$ above $p_{O_2} \simeq 10^{-15}$ atm.

Price and Wagner (34) studied diffusion of Mn^{54} in Mn_xO at 1032°C from $p_{O_2} = 10^{-8}$ atm to $p_{O_2} = 10^{-18}$ atm. The diffusion coefficient was found to increase with the sixth root of p_{O_2} over the entire range of p_{O_2} studied. No inflection point in the value of D^*_{Mn} was found in the region $p_{O_2} = 10^{-14}$ atm as was reported previously by Boquet et al. (35). The fact that an inflection point was absent suggested that the same majority defect species was present over the range of p_{O_2} studied.

Wuensch and Vasilos (56) have reported the interdiffusion of several transition metal monoxides with MgO. Results in the temperature range 1000°C to 1850°C for single crystal MgO are given below.

$$\tilde{D}_{Fe_xO/MgO} = (8.83\times10^{-5}) \exp(-1.81 \text{ ev/RT}) \qquad (79)$$

$$\tilde{D}_{Co_xO/MgO} = (5.78\times10^{-5}) \exp(-2.06 \text{ ev/RT}) \qquad (80)$$

$$\tilde{D}_{Ni_xO/MgO} = (1.80\times10^{-5}) \exp(-2.10 \text{ ev/RT}) \qquad (81)$$

Wuensch and Vasilos conclude that the diffusion process is controlled in these cases by the extrinsic impurity level.

The change in diffusion activation energy in Equations 79 through 81 may be correlated to the ratio of ionic radius to ionic polarizability for the ions involved.

Rigby and Cutler (57) report the effect of cation vacancy concentration on the value of the interdiffusion coefficient in the system Fe_xO-MgO. The concentration of cation vacancies was determined by chemically analyzing for ferric ions as a function of concentration, temperature, and p_{O_2} and by assuming that $2[V''_{Mg}] = [\dot{Fe}_{Mg}]$. The interdiffusion coefficient was found to vary linearly with cation vacancy concentration between 1105°C and 1315°C up to about four percent of total cation sites vacant. The diffusion activation energy was reported as 47.5 kcal/mole and was independent of cation vacancy concentration.

Interdiffusion studies in the system Fe_xO-MgO have been reported by Blank and Pask (58). Their results disagree with Rigby and Cutler (57) and others (56, 59) in that Blank and Pask found both the interdiffusion coefficient and the diffusion activation energy to depend on concentration. Their results are given below:

$$\tilde{D}_{Fe_xO/MgO}(\text{vacuum, } 1150°C) = (8.10\times10^{-12}) \exp(0.345[Fe]) \quad (82)$$

$$\tilde{D}_{Fe_xO/MgO}(\text{vacuum, } 1250°C) = (1.60\times10^{-11}) \exp(0.398[Fe]) \quad (83)$$

$$\tilde{D}_{Fe_xO/MgO}(\text{vacuum, } 1350°C) = (2.40\times10^{-11}) \exp(0.437\ [Fe]). \quad (84)$$

The change in diffusion activation energy with concentration found by Blank and Pask is given in Table 2.

Table 2. Diffusion factors in Fe_xO-MgO in vacuum (1150°C-1350°C) after Blank and Pask (58)

Composition (atomic % Fe)	D_o cm^2/sec	ΔH kcal/mole
5	6.34×10^{-7}	29.6
10	4.49×10^{-6}	32.9
15	5.04×10^{-5}	37.7
20	8.40×10^{-4}	43.5

The increase in the interdiffusion coefficient is explained on the basis of an increase in cation vacancy concentration due to $Fe_{Mg}^{\bullet}$. Brynestad and Flood (60) found the ratio Fe^{3+}/Fe^{2+} to decrease as $[Mg^{2+}]$ increased in the solid solution. The increase in diffusion activation energy with increasing iron concentration is attributed to tetrahedrally coordinated ferric ions which involve greater strain at the saddle point configuration than for octahedrally coordinated ferrous ions. Evidence of tetrahedrally coordinated ferric ions has been reported by Koch and Cohen (61), Blank and Pask (58) and Roth (8, 9).

Appel and Pask (62) report on the interdiffusion of

Ni_xO and MgO. In air at 1346°C they found the relation

$$\tilde{D}_{Ni_xO/MgO}(\text{air, } 1346°C) = (7.19\times10^{-12}) \exp\{(4.31 \pm 0.01)[Ni]\} \quad (85)$$

where [Ni] is in terms of atomic fraction of nickel. Blank and Pask (58) have also reported interdiffusion in the system Ni_xO-MgO. The interdiffusion coefficient was found to be exponentially dependent on nickel concentration as shown below:

$$\tilde{D}_{Ni_xO/MgO}(\text{air, } 1200°C) = (7.75\times10^{-12}) \exp(5.37[Ni]) \quad (86)$$

$$\tilde{D}_{Ni_xO/MgO}(\text{air, } 1300°C) = (4.1\times10^{-12}) \exp(5.37[Ni]) \quad (87)$$

$$\tilde{D}_{Ni_xO/MgO}(\text{air, } 1370°C) = (7.6\times10^{-12}) \exp(5.37[Ni]) \quad (88)$$

$$\tilde{D}_{Ni_xO/MgO}(\text{air, } 1400°C) = (1.05\times10^{-11}) \exp(5.37[Ni]) \quad (89)$$

where [Ni] is in terms of atomic fraction. No change is observed in the activation energy for diffusion with increasing nickel concentration. This result coupled with knowledge of the high octahedral site preference energy of Ni^{+3} led Blank and Pask to conclude that there was no signifi-

cant amount of tetrahedrally coordinated nickel in the system Ni_xO-MgO.

Zintl (39) has reported the hole concentration in solid solutions of Co_xO-MgO and Co_xO-Ni_xO. At 1000°C in air the data may be represented by an equation of the form

$$p = H \exp\{-\beta(1 - [CoO]\} \tag{90}$$

where all concentrations are given in terms of mole fractions and H is a constant. For the system Co_xO-MgO the constant β was 5.76 and for the system Ni_xO-Co_xO β was 3.5. Schmalzried and Holt (63) have used Zintl's result to interpret the work of Blank and Pask (58) in the system Ni_xO-MgO. Since the system Ni_xO-MgO has been shown to behave as an ideal solution (64), Darken's equation is given as

$$\tilde{D} = (1-N_{MgO})\ D_{Mg}{}^{2+} + N_{MgO}\ D_{Ni}{}^{2+} \tag{91}$$

with

$$D_{Ni}{}^{2+} = D^{o}_{Ni}{}^{2+} \exp(-\beta\ N_{MgO}) \tag{92}$$

and

$$D_{Mg}{}^{2+} = D^{o}_{Mg}{}^{2+} \exp(-\beta\ N_{MgO}), \tag{93}$$

therefore

$$\tilde{D} = [D^{o}_{Mg}{}^{2+} + N_{MgO}(D^{o}_{Ni}{}^{2+} - D^{o}_{Mg}{}^{2+})]\ \exp(-\beta\ N_{MgO}). \tag{94}$$

If $D^{o}_{Ni^{2+}} \simeq D^{o}_{Mg^{2+}}$ Equation 94 simplifies to the following

$$\tilde{D} = D^{o}_{Mg^{2+}} \exp(-\beta N_{MgO}). \quad (95)$$

With Equation 95, Schmalzried and Holt were able to reproduce Blank and Pask's data with $\beta = 2.7$. The assumption that $D^{o}_{Ni^{2+}} \simeq D^{o}_{Mg^{2+}}$ is justified upon extrapolation of Equation 95 to $N_{MgO} = 0$ which yields $D^{o}_{Ni^{2+}}(air) = 2.7 \times 10^{-11}$ cm^2/s at 1370°C in approximate agreement with the data of Shim and Moore (49) of D^{*}_{Ni} (air) $= 13 \times 10^{-11}$ cm^2/sec at 1200°C.

Jones and Cutler (65) have recently found an equation of the type discussed by Schmalzried and Holt (63) to describe their interdiffusion data in the system Mn_xO-MgO at $p_{O_2} = 10^{-9}$ atm and 1500°C. The variation of the interdiffusion coefficient with manganese concentration was found to obey an equation similar to Equation 94, i.e. Jones and Cutler give

$$\tilde{D} = [D^{o}_{Mg^{2+}} + N_{MgO}(D^{o}_{Mn^{2+}} - D^{o}_{Mg^{2+}})]\, C \exp(-\beta N_{MgO}) \quad (96)$$

where C is a constant intended to correct for any nonideality of the solution. If $D^{o}_{Mg^{2+}} = D^{o}_{Mn^{2+}}$, Equation 96 is reduced to

$$\tilde{D} = C\, D^{o}_{Mg^{2+}} \exp(-\beta N_{MgO}). \quad (97)$$

Jones and Cutler also report interdiffusion in Mn_xO-MgO in air atmosphere at 1380°C, 1480°C, and 1565°C. The interdiffusion coefficient was found to vary linearly with cation

vacancy concentration (revealed chemically) up to approximately 1.5 percent of total cation sites vacant. The diffusion activation energy in air was not found to vary with manganese concentration.

Stiglich (10) has investigated $Ni_xO + Co_xO$ solid solutions using X-ray techniques and has found significant evidence of occupation of tetrahedral sites. These results are supported by Hed (66) who investigated electrical conductivity of Co_xO from 800°C to 1200°C and $p_{O_2} = 10^{-0.88}$ atm to $p_{O_2} = 10^{-2.88}$ atm. Hed found a negative enthalpy of formation of defects. Furthermore, a plot of log conductance versus $10^4/T$ yielded nonparallel and curved isobars. On the basis of such evidence Hed rejected a simple association model as proposed by Bransky and Tallan (36) in the case of Mn_xO. Hed proposes a defect complex involving cobalt interstitials defined by the equilibrium

$$\tfrac{1}{2}O_2(g) + Co_{Co} = (V_{Co}Co_iV_{Co})^{\cdot} + O_O + h. \qquad (98)$$

Stiglich (10) has investigated interdiffusion between Ni_xO and Co_xO from 950°C to 1600°C in air and from 1000°C to 1480°C at $p_{O_2} = 5\times10^{-3}$ atm. An increase in $\tilde{D}$ with increasing Co_xO concentration in the solid solution was explained on the basis of increasing tetrahedral coordination with increasing Co_xO concentration. On the basis of the existence of a knee in the Arrhenius plot for his diffusion data,

Stiglich proposed that at least two mechanisms are operable in Ni_xO-Co_xO under the experimental conditions investigated. At low temperatures, for a given composition, Stiglich proposed that an interstitialcy mechanism is operating. At higher temperatures Stiglich proposed that either voidal diffusion proceeds through octahedral-tetrahedral-octahedral jumps or through direct octahedral to octahedral jumps. At high Co_xO content, for a given temperature, the direct octahedral to octahedral jump may become more important due to higher concentrations of octahedral vacancies. At reduced p_{O_2} Stiglich found the knee in the activation plot to be shifted to a lower temperature for a given concentration adding more support to his proposed mechanism.

EXPERIMENTAL PROCEDURE

Experimental Materials

Single crystals of magnesium oxide were obtained from a commercial source (Norton Research Corporation Ltd., Chippawa, Canada). The crystals were cleaved to the approximate dimensions 1/8 in. x 1/4 in. A representative chemical analysis is shown in Table 3.

Table 3. Chemical analysis of magnesium oxide single crystals

Impurity	Concentration (ppm)
SiO_2	20 - 30
Fe_2O_3	110 - 140
TiO_2	8 - 12
Al_2O_3	44 - 64
CaO	30
ZrO_2	14 - 20
MnO_2	3 - 25
NiO	5

Polycrystalline specimens of Mn_3O_4 were prepared from reagent grade manganous carbonate (Mallinckrodt Chemical Works). The chemical analysis of the $MnCO_3$ is shown in Table 4. The $MnCO_3$ was heated to 1000°C in an air atmosphere forming Mn_3O_4. Specimens of Mn_3O_4 were pressed at 8000 psi using a 1/4 in. diameter hardened steel die. These specimens were sintered

Table 4. Chemical analysis of manganous carbonate

Impurity	Maximum limit of impurity
Alkali carbonate (as Na_2CO_3)	0.02%
Alkalies and earths	0.15%
Chloride	0.01%
Heavy metals (as Pb) insoluble in nitric acid or hydrogen peroxide	0.01%
Iron	0.001%
Nickel	0.001%
Sulfate (SO_4)	0.01%
Water	6.0%
Zinc	0.05%
Assay (Mn)	43.0% - 48.0%

at 1550°C for two hours in an argon atmosphere. The resulting material was sectioned using a diamond saw into specimens of the approximate dimensions 7/32 in. diameter by 3/16 in. The stoichiometry of these specimens was not determined; however, their black appearance suggested the presence of the spinel phase Mn_3O_4. The microstructure of these specimens is shown in Figure 5b.

Water immersion determination of the bulk density of the sintered material showed it to have a density of 4.92 g/cm^3. Attempts to achieve greater density by sintering at higher

Figure 5. Macrostructure and microstructure of materials

(a) Co_xO boule (low purity) showing polycrystalline cap at the point of arc initiation with large single crystal growing from a seeded area on the cap. Approximately 0.9X.

(b) Mn_3O_4 polycrystal, 120X.

(c) Co_xO boule (low purity). (Approximately 0.5X)

(d) Cross section, Co_xO boule (low purity). (Approximately 1.5X)

Photographs reduced to 81.5% of original size for publication.

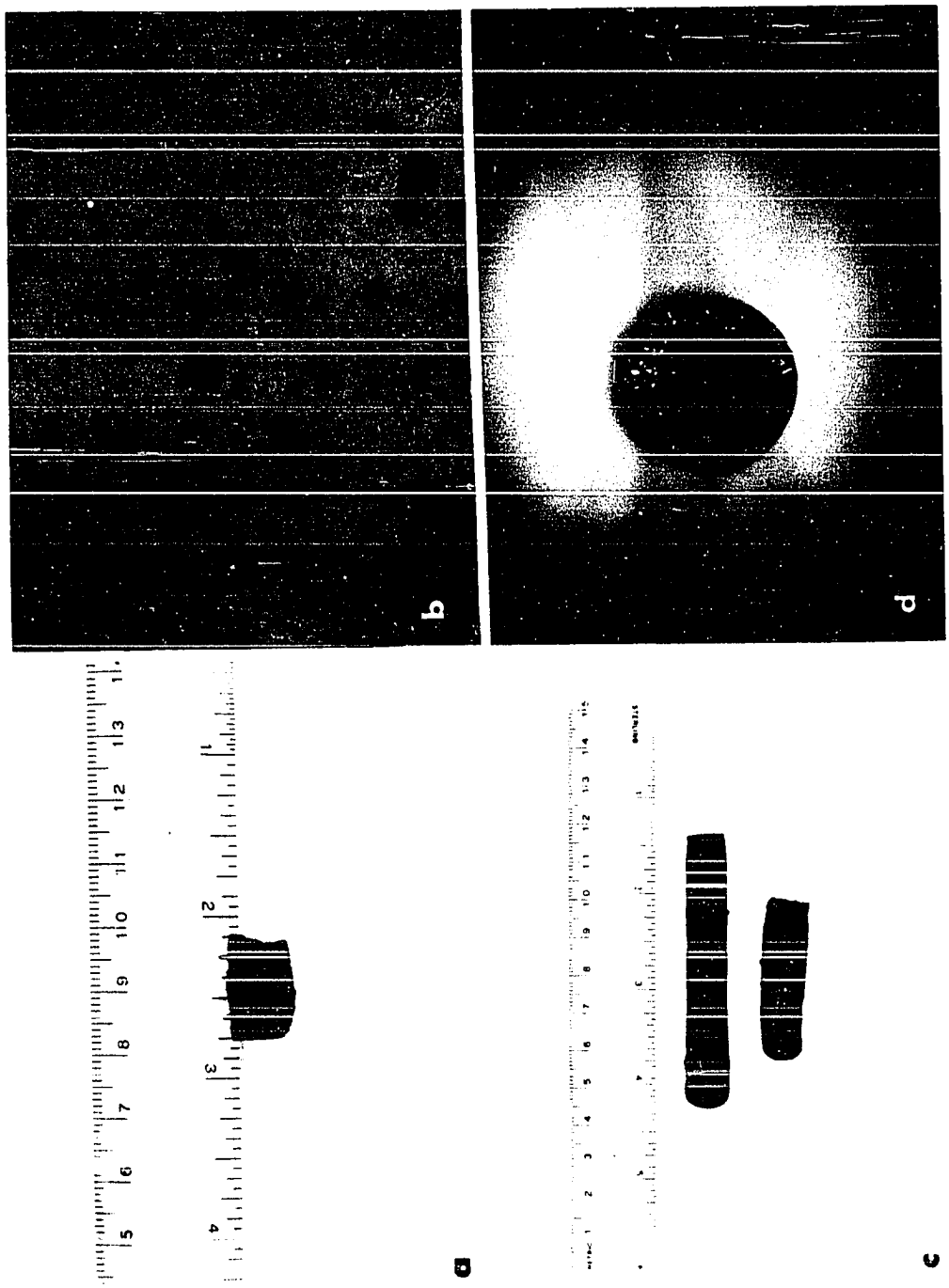
b
d
a
c

temperature were unsuccessful. At sintering temperatures of 1650°C or higher the samples volatilized.

Single crystals of nickelous oxide and cobaltous oxide were grown for this study by the arc-transfer technique. This technique which has been described in the literature (67, 68, 69) consists of the transfer of material from a cathode through a d.c. arc to an anode which is the growing single crystal of the desired material. The arc serves the two-fold purpose of transfer of material to the growing crystal and generation of the heat necessary to liquefy the metal oxides.

Preliminary crystal growth experiments were performed with the following materials: cobalt rod, reactor grade (99.5% Co), five mm diameter (Kulit Tungsten Co., Ridgefield, N.J.); and nickel rod, high purity (99.4% Ni), five mm diameter (Central Steel and Wire Co., Des Moines, Iowa). These materials were used in the characterization and refinement of the crystal growth techniques.

In early experiments the metal anode was mounted directly over the metal cathode. The arc was initiated and a current of six A was maintained for a period of one hour. The current was then brought to seven A and maintained throughout the growth process. All experiments were carried out in an air atmosphere. Crystals produced were typically 1.4 cm in diameter while growth rates were on the order of 0.15 cm/hr

for an arc gap maintained at 2.0 mm. In other experiments the cathode was mounted directly below the anode with resultant mass transfer in the upward direction. Crystal boules produced by this technique were typically 0.7 cm in diameter. These smaller diameter boules as compared to those produced by the cathode-over-anode configuration may be explained by the gravitational effect on the pool of molten oxide maintained at the anode tip with resultant "necking down". Growth rates with the anode-over-cathode configuration were typically 0.35 cm/hr. The largest single crystals with either configuration were obtained from seeded melts. The seeding procedure was to place a small chip of single crystal on the cathode with a (100) face perpendicular to the electrode axis prior to initiating the arc.

In an effort to obtain the largest possible single crystals, several experimental approaches to the arc-transfer method were considered. Drabble and Palmer (67) report that the largest single crystals were obtained through the use of oxide electrodes. Due to the low electrical conductivity of the oxide electrodes it was found necessary to reduce the surface of the oxide electrode through a hydrogen anneal.

A technique was found experimentally which incorporated the advantages of the oxide electrode while using metal electrodes. Upon the use of greater currents, the arc heat led to the oxidation of the cathode tip during the growth

process. In the case of NiO growth, the arc was initiated and maintained at six A for one hour to allow the electrodes to heat. The current was then raised to the range 11 A to 18 A causing the lower end of the cathode to oxidize. The molten cap on the cathode would then be transferred to the anode. The process of mass transfer was thus an intermittent one. Attempts to create a continuous process by raising the current to even greater values were unsuccessful and had the undesirable effect of producing smaller single crystals. In the case of CoO growth, a continuous mass transfer was achieved. The arc was initiated and rapidly brought to 12 A. The current was slowly raised to 15 A over a period of about two hours. The feed rod was continuously oxidized with an apparent oxide tip maintained on the lower 1/2 in. of the cathode. An added advantage of the use of the highest current for growth of both Co_xO and Ni_xO was the stabilization of the arc. A nonstable or wandering arc invariably resulted in growth of smaller single crystals than those grown with a stable arc.

Under the growth conditions described, the Ni_xO boules produced were typically 1.2 cm in diameter with a growth rate of approximately 1 cm/hr. The fact that the growth process was intermittent in the case of NiO did not apparently detract from crystal quality. The CoO boules produced were typically 1.5 cm in diameter with growth rates on the order of 0.9 cm/hr.

Boules of CoO were produced as long as 8.5 cm. In the case of both Ni_xO and Co_xO the <100> crystal direction was apparently aligned with the axis of the boule. Photographs showing the largest CoO boule produced are presented in Figure 5.

Higher purity metal electrodes (than those used in the preliminary studies) were used for preparation of single crystals for experimental use. Five millimeter diameter rods of nickel (99.999% purity) and cobalt (99.999% purity) were obtained from United Mineral & Chemical Co. The quantitative analyses of these materials are shown in Table 5. A qualitative analysis obtained of both types of as-grown crystals indicated similar impurity levels as those of the metal feed rods. A quantitative analysis of the as-grown crystals was unavailable due to the small quantity of material available for analysis, and the assumption is made that the quantitative analysis of the as-grown crystals is essentially that of the metal feed material.

Table 5. Quantitative spectrographic analysis of nickel (99.999%) and cobalt (99.999%) metal rods (ppm)

Impurity element	Co	Ni
Al	< 1	< 1
Ca	< 1	
Cu	< 1	
Fe	3	9
Mg	1	< 1
Mn	2	
Si	3	< 1
Ag	< 1	4

Characterization of Single Crystals

The back-reflection Laue Method of X-ray analysis was used to determine: (1) that cleaved specimens were single crystals, (2) the orientation of cleavage faces, (3) the degree of strain, and (4) the presence of polygonized structures. The apparatus used included a Siemens Kristalloflex 4 X-ray Generator (Siemens America, Inc.) equipped with a chromium X-ray tube, and a special Polaroid XR-7 X-ray camera (Polaroid Land Corp.). Representative samples of the resulting Laue photographs are shown in Figure 6.

In all cases (100) cleavage was observed as shown by the familiar pattern for cubic crystals seen in Figure 6. The diffraction pattern for MgO, Figure 6c, shows well defined spots indicating negligible strain or substructure. In the cases of Ni_xO and Co_xO the diffraction spots appear as doublets indicating the presence of a polygonized structure. This result is in agreement with that of chemical etching for dislocations presented later in this chapter. The doublets are seen to be pronounced in Figure 6 in the case of low purity CoO. This is most likely due to strain in the single crystal resulting from the formation of Co_3O_4 as the crystal cooled in the growth assembly. There was no observable difference in the diffraction pattern of high and low purity Ni_xO or high and high and low purity Co_xO (cooled in argon atmosphere).

Figure 6. Laue photographs of single crystals

(a) Laue photograph, Co_xO as-grown (high purity), back reflection, Cr radiation, 25 keV, 18 mA, d =5 cm, 33 minute exposure.

(b) Laue photograph, Ni_xO as-grown (high purity), back reflection, Cr radiation, 25 keV, 18 mA, d=5 cm, 1 hour expsoure.

(c) Laue photograph, MgO (Norton Co.), back reflection, Cr radiation, 20 keV, 22 mA, d=5 cm, 20 minute exposure.

(d) Laue photograph, Co_xO as-grown (low purity), back reflection, Cr radiation, 20 keV, 22 mA, d=5 cm, 1 hour exposure.

Photographs reduced to 81.5% of original size for publication.

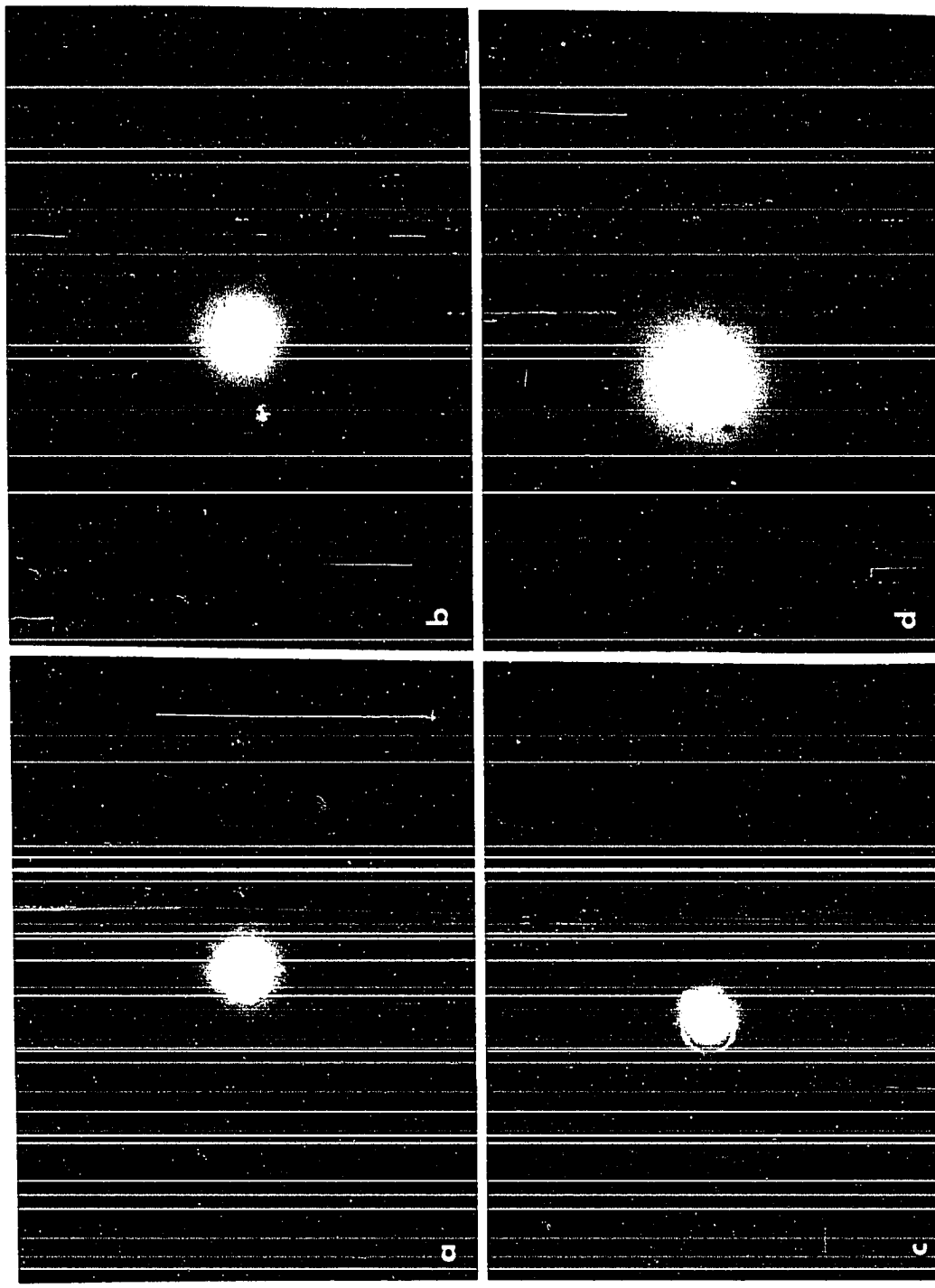
b
d
a
c

The dislocation density of single crystals was observed using a chemical etching procedure. Ghosh and Clarke (70) chemically etched MgO using a saturated aqueous solution of NH_4Cl and concentrated H_2SO_4 in equal parts. In this study the same etchant was used with etchant maintained at 70°C. Freshly cleaved specimens were immersed in this etchant for a period of one minute and were subsequently washed with water and acetone. The resulting dislocation pattern for MgO is shown in Figure 7c. Average values of dislocation densities are 3.2×10^7 per cm^2 near a cleavage edge and 1.4×10^5 per cm^2 near the center of a cleaved surface. The value found for the center of a cleaved surface is in excellent agreement with values in the literature reported for this commercial brand of MgO single crystals (71).

No literature was found pertaining to the chemical etching of Co_xO; however, knowledge of the slight solubility of CoO in nitric acid suggested its use as an etchant for dislocations. Successful etching of CoO was accomplished by submerging fresh cleaved surfaces in boiling 70% HNO_3. Etching times were typically 40 minutes. The result of this effort is shown in Figure 7. In the case of the as-grown Co_xO, a dark phase is shown preferentially clustered about dislocation sub-boundaries. Since X-ray diffraction measurements indicate the presence of both CoO and Co_3O_4, it is probable that the dark phase is the spinel which precipitated

Figure 7. Dislocation etch pits on Co_xO and MgO

(a) Co_xO as-grown, chemically etched, 120X.

(b) Co_xO annealed and cooled in argon atmosphere, 960X, chemically etched.

(c) MgO (Norton Company), chemically etched, 960X.

(d) Co_xO annealed and cooled in argon atmosphere, 480X, chemically etched.

Photograph reduced to 81.5% of original size for duplication.

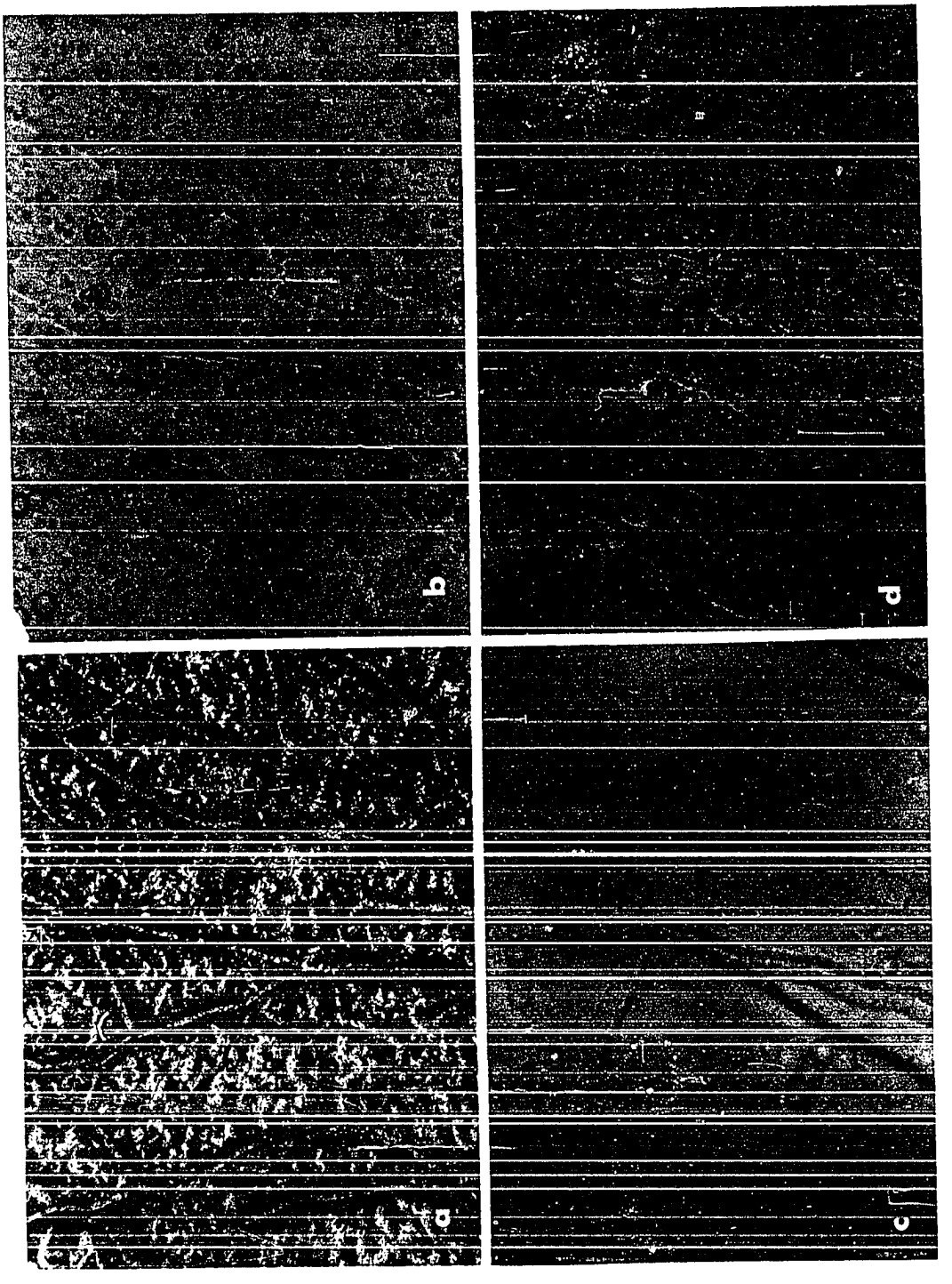
b
d
a
c

preferentially in the high disorder areas as the boule cooled. Since the presence of the spinel made viewing of the dislocation structure impossible, it was desirable to eliminate it. In an effort to eliminate the Co_3O_4 phase single crystals of Co_xO were heated to 800°C in a flowing argon atmosphere and held for four hours. The furnace with the samples undisturbed was cooled at approximately 75°C per hour with the continuous flowing argon atmosphere. These crystals were etched as previously described. The dislocation structure is shown in Figure 7 at two magnifications. The average dislocation density near the center of the cleaved surface is 8.1×10^5 per cm^2. This value is representative of both the high and low purity grades of CoO grown.

Dislocation etch pits in Ni_xO have been chemically revealed through procedures reported by Takeda and Kondoh (72) involving the use of hot nitric acid etchant. In this study freshly cleaved specimens were immersed in boiling 70% HNO_3. Etching times were typically ten minutes. Etched Ni_xO surfaces are shown in Figure 8. The average dislocation density near the center of the cleavage surface is 2.2×10^6 per cm^2. This value is representative of both the high and low purity grades of Ni_xO grown.

An experiment was conducted to verify that the etched relief did represent dislocation etch pits instead of other phenomena such as selective dissolution near impurity centers.

Figure 8. Dislocation etch pits on Ni_xO

(a) Ni_xO as-grown, chemically etched, 960X.

(b) Matched cleavage surface of Ni_xO, as-grown, 720X, chemically etched, "right half," (See Figure 4d for "left half.")

(c) Ni_xO as-grown, chemically etched, 480X.

(d) Matched cleavage surface of Ni_xO, as-grown, 720X, chemically etched, "left half," (See Figure 4b for "right half.").

Photograph reduced to 81.5% of original size for publication.

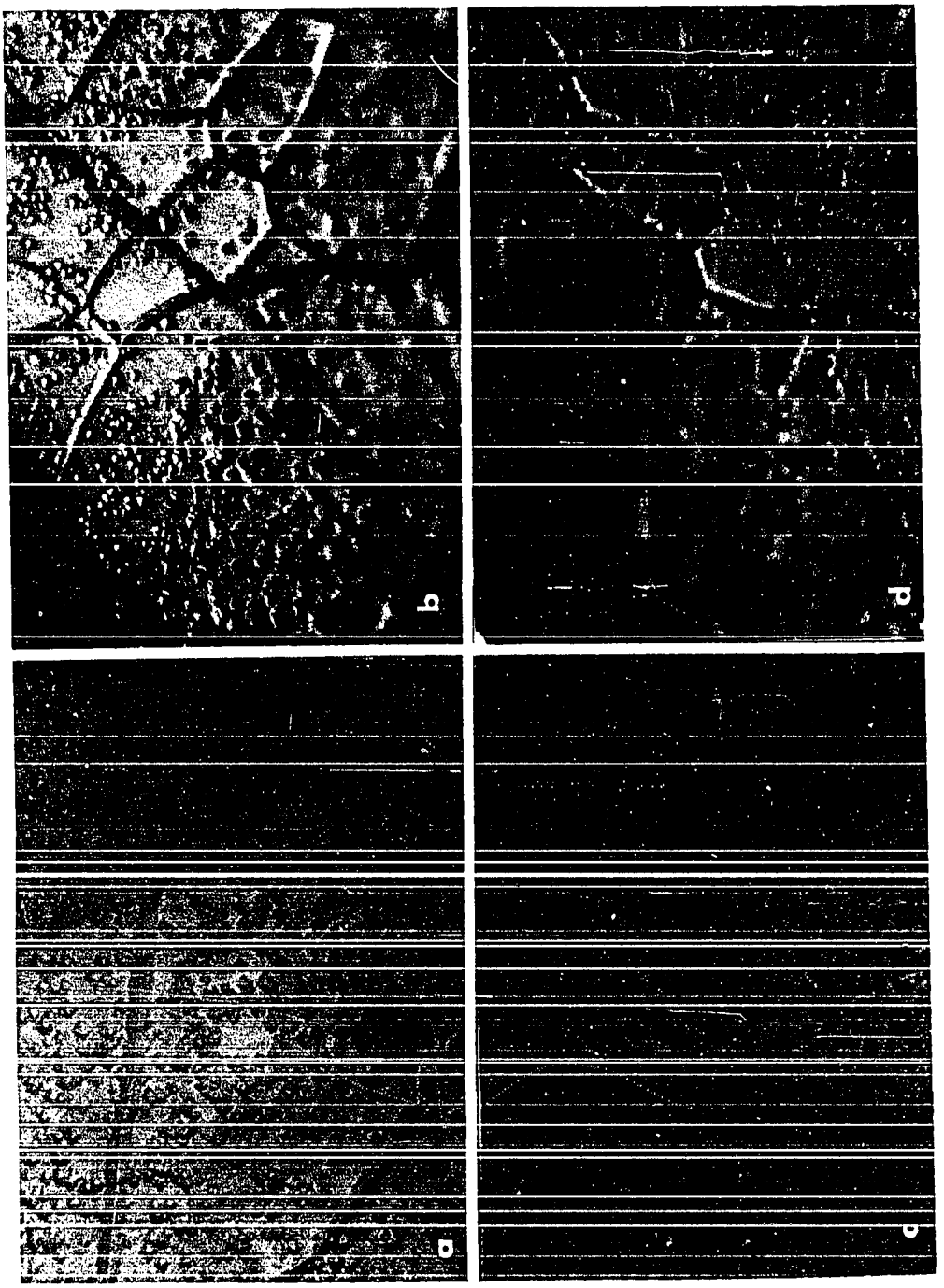
a
b
c
d

Matching faces of two halves of a cleaved boule were etched using the treatment described above. The resulting surface relief is shown in Figure 8. Since there is approximate correspondence between both halves of the cleaved piece and because the shape of the etch pits corresponds to the familiar inverted pyramid shape, there is no question that the etch pits correspond to dislocation sites.

Preparation of Specimen Surfaces

In order to determine the effect on the diffusion process of the physical condition of the original interface between halves of the diffusion couples, an effort was made to characterize the fit at the interface.

In order to obtain highly polished surfaces while maintaining flatness, a combination of manual and automatic polishing procedures were employed. Special specimen holders were fabricated for this purpose. These holders were hollow rings of 316 stainless steel of the dimensions 2 in. OD, 1 in. ID, by 1/2 in. height. Specimens were mounted centrally in these rings with sealing wax (Rigidax Type WI Green, M. Argülso & Co., Inc.). The mounting procedure consisted of heating a glass plate and aluminum foil spacer on a hot plate. The ring was placed on the spacer, and specimens were placed in the central opening face down on the glass plate. The wax was melted into the ring, and after subsequent cooling, the ring with specimens in place was removed from the spacer

and the glass plate.

Grinding was accomplished on a rotating disk with 600 grit SiC abrasive paper (water lubricant). Preliminary polishing was accomplished using a 6μm diamond abrasive paste on a nylon faced lap (oil lubricant). Polishing required approximately five minutes for moderate pressure and the disk rotating at 120 rpm. The ring assembly was cleaned with acetone and placed on a 12-in. vibratory wax lap charged with 0.3 μm Al_2O_3 suspended in water. The vibratory lap was adjusted such that ring assemblies moved about the circumference at about 5 rpm about the radius of the lap. A small quantity of detergent was added to the lap charge to prevent wax buildup on the sample surface. Typical polishing treatments with the wax lap were six to ten hours. Final polishing was accomplished with an auxiliary head to the vibratory lap employing a napless cloth surface (AB Metcloth, Buehler Ltd.) and a charge of 0.05 μm Al_2O_3 suspended in water. Typical treatments were a 20 minute polish at ten rpm about the circumference of the twelve in. diameter lap.

Two procedures were employed to determine the characteristics of the polished surfaces. The first procedure involved the measurement of surface flatness and consisted of observing the optical interference between the polished surfaces and optical flats using monochromatic light. Optical flats certified to one-tenth wavelength (Edmund Scientific

Co.) were employed with sodium light, λ = 5500Å, and laser illumination, λ = 6328Å. In this method, horizontal spacing between interference bands represents a vertical displacement of one-half wavelength of the illuminating light. Perfectly parallel bands indicate a flat test surface with the number of bands determined by the magnitude of the optical wedge (air wedge). A spherical surface in contact with a flat surface results in an interference pattern of a number of concentric rings (Newton's rings). Surface waviness results in waviness of interference bands.

Interference patterns from mechanically polished specimens are shown in Figures 9, 10 and 11. These specimens are typical of the results produced. It was found that MgO characteristically exhibited a high point at one end of the specimen while flatter surfaces were generally produced for Ni_xO and Co_xO as compared to MgO.

The second method of surface characterization involved the use of a commercial stylus device (Bendix Profilimeter, Bendix Automotive and Automation Co.) to measure surface roughness. The mechanically driven stylus was oscillated across the polished sample in a linear trace with electronic readout in root-mean-square microinches. The average roughness value for MgO was 1.5 microinch (0.037 μm) rms. Microroughness values were not available for Ni_xO, Co_xO, or Mn_xO (polycrystal).

Figure 9. Flatness measurement of polished MgO single crystals

(a) Interference pattern of MgO sample, mechanical polish only, 60X, sodium light.

(b) Interference pattern of MgO sample, sodium light, chemical polish, 85% H_3PO_4 at 160°C for 5 minutes, 120X.

(c) Interference pattern of MgO sample, sodium light, mechanical polish only, 120X.

(d) Interference pattern of MgO sample, sodium light, mechanical polish followed by chemical polish, 85% H_3PO_4 at 160°C for 5 minutes, 120X.

Photograph reduced to 81.5% of original size for duplication.

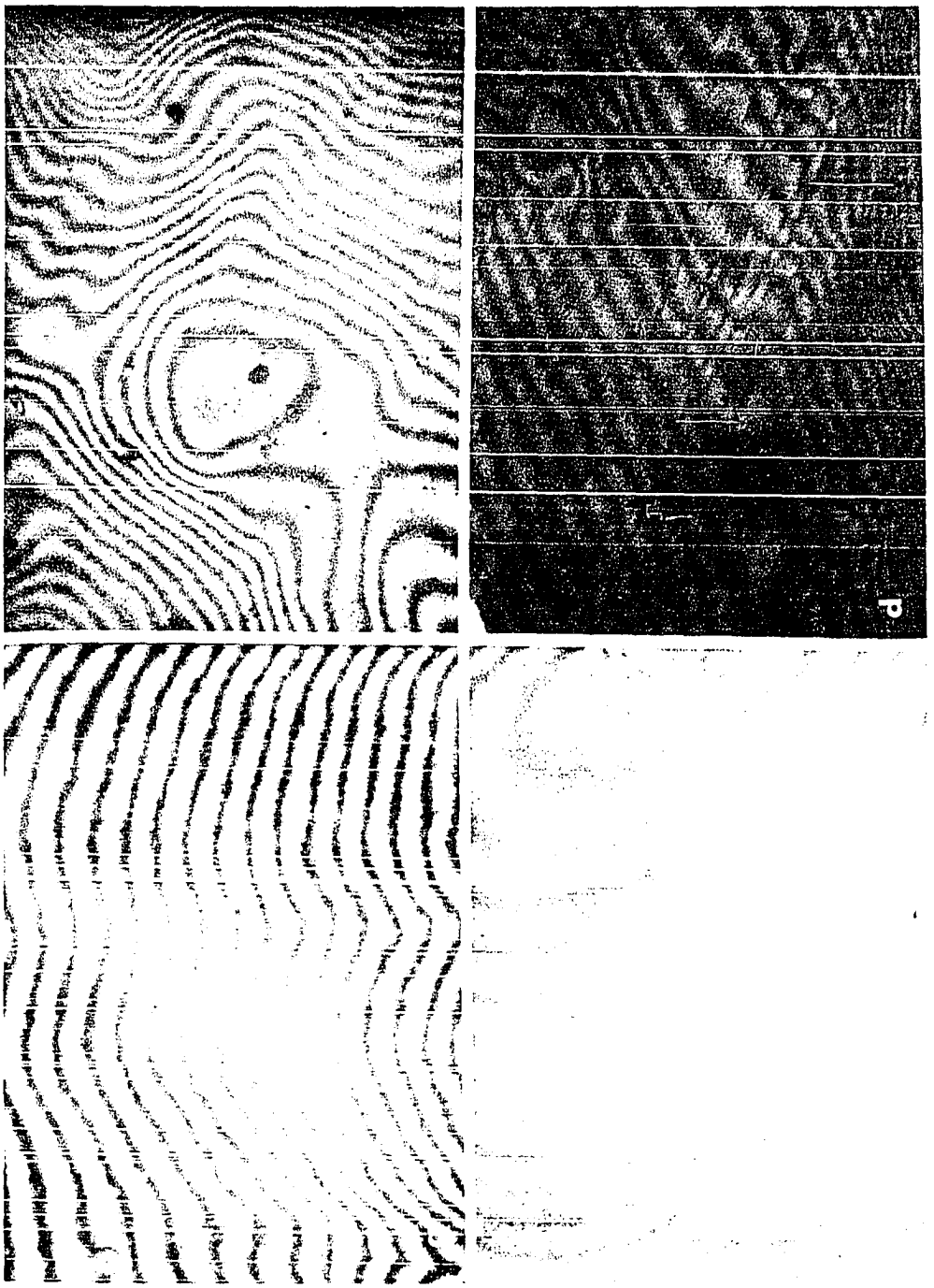
a

Figure 10. Measurement of polishing damage in MgO single crystals

(a) Dislocation etch pattern of polished MgO surface, 480X.

(b) Dislocation etch pattern of polished MgO surface after chemical removal of 50 μm layer adjacent to surface, 480X.

(c) Interference pattern of surface shown in (a) before dislocation etch, 60X, sodium light.

(d) Interference pattern of surface shown in (b) after chemical removal of material and prior to dislocation etch, 60X, sodium light.

Photographs reduced to 81.5% of original size for publication.

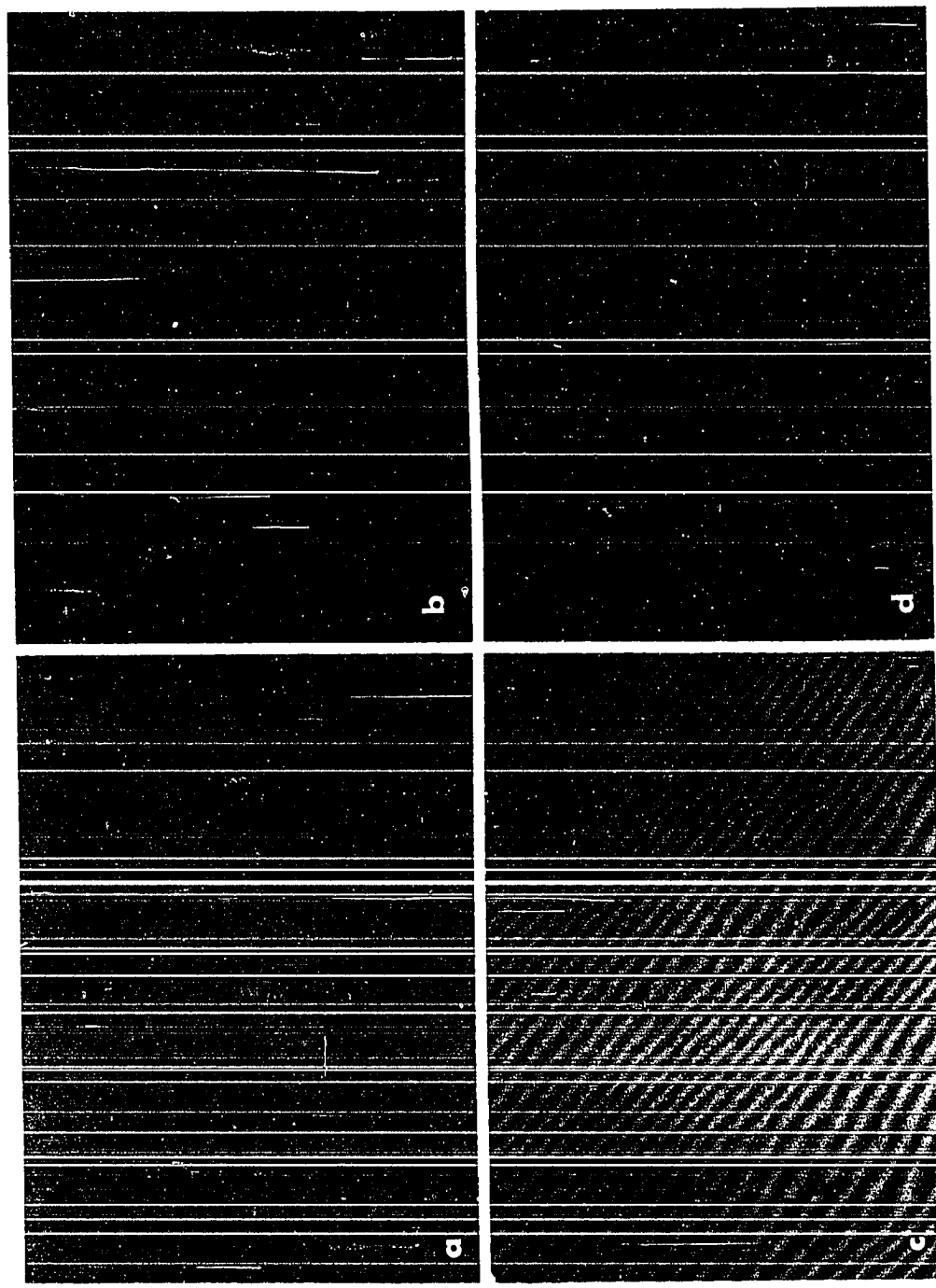
b
d
a
c

Figure 11. Flatness measurement of Co_xO and Ni_xO single crystals; microstructure of specimens after diffusion anneal

(a) Interference pattern of mechanically polished Co_xO crystal, sodium light, 60X.

(b) Ni_xO-Co_xO diffusion couple showing pore line, Specimen 9, 120X.

(c) Interference pattern of mechanically polished Ni_xO crystal, sodium light, 60X.

(d) Mn_xO-MgO diffusion couple, Specimen 3, 150X.

Photographs reduced to 81.5% of original size for publication.

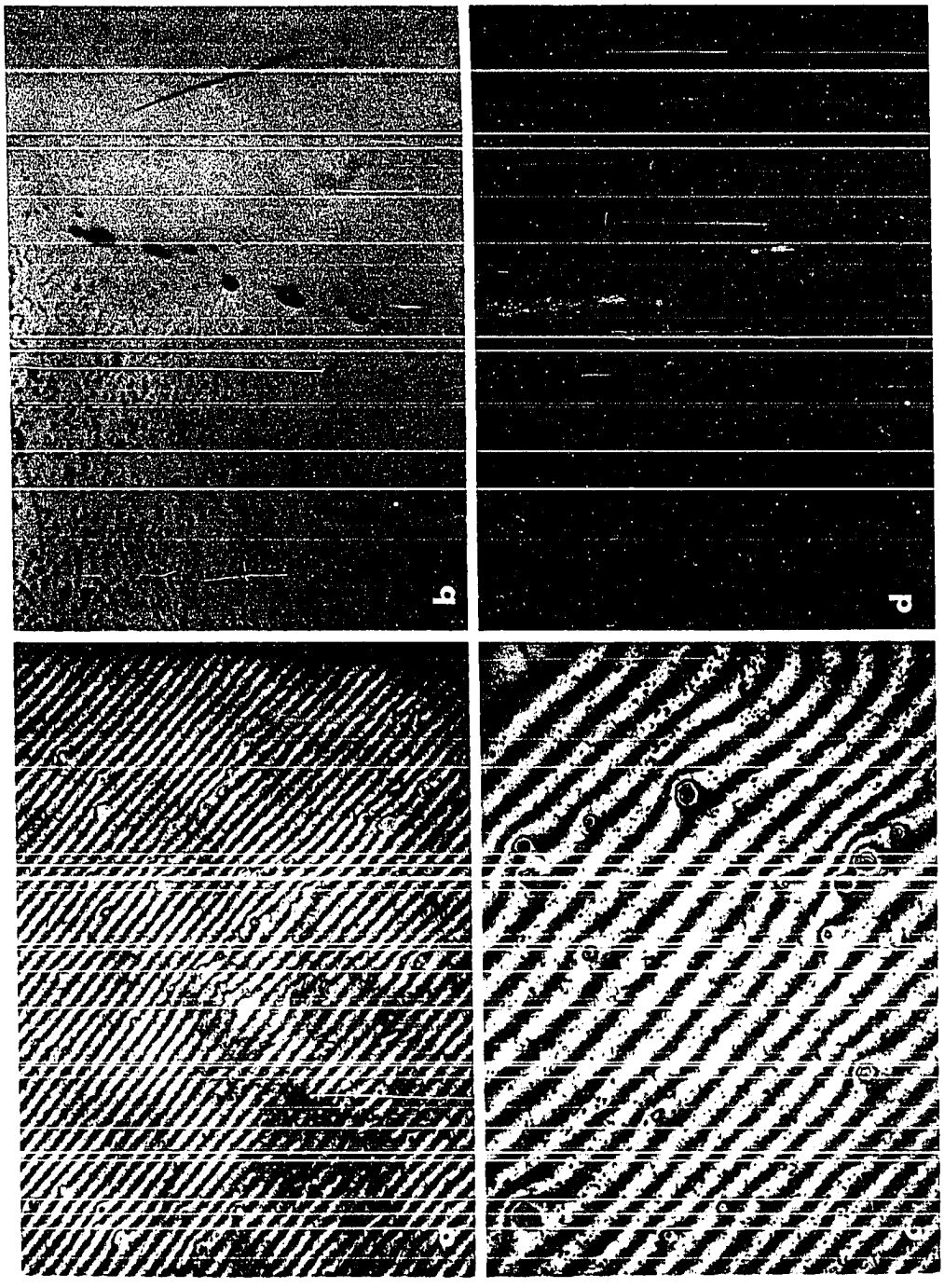
b
d

Measurement of Polishing Damage

The dislocation damage induced in MgO single crystals by the polishing procedure was observed through a procedure of chemical etching for dislocation concentration with subsequent chemical removal of bulk surface layers. The dissolution rate was first measured by immersing MgO single crystals in 85% H_3PO_4 for one to ten minutes at 160°C with constant agitation. The crystals were withdrawn and quenched in a large water bath at 30°C. After washing in acetone, the dimensions of the crystals were measured with an optical microscope using a graduated ocular and movable stage. The average dissolution rate was found to be 24 μm/min (6.09×10^{-3} in./min). This value agrees well with an extrapolation of the value of Ghosh and Clarke (70) of 2×10^{-3} in/min. at 160°C. The results of this study are shown in Figure 9. The dislocation density is seen to approach native concentration at 50 μm below the polished surface. A mechanically polished specimen which was subsequently chemically polished appeared to be only a compromise between the flat surface produced by the mechanical polish and the wavy surface produced by a chemical polish. Since it was anticipated that diffusion measurements would involve concentration changes over several hundred microns, the effect of a damaged layer was thought to be negligible, and the chemical polishing procedure was abandoned. Interference patterns of mechanically polished Ni_xO and Co_xO crystals are shown in Figure 11.

Preparation of Diffusion Couples and Anneal Procedure

Diffusion couples were prepared from Ni_xO and Co_xO crystals and from sintered specimens of Mn_xO and MgO single crystal. In all cases only the mechanical polishing procedure was used. Prior to diffusion experiments the samples were annealed separately at the temperature and oxygen partial pressure of the subsequent diffusion anneal in an attempt to stabilize the structure and stoichiometry of the crystals. All anneals were of a six hour duration. The results indicated that a constant state of disorder prevailed in specimens air quenched after the short pre-anneal. Furthermore, d-c conductivity of the quenched specimens was independent of anneal temperatures. These results indicate that the disorder of quenched specimens was not typical of the high temperature defect condition, and therefore approach to equilibrium could not be established by this method.

Polished and annealed single crystals were examined by the Laue method to determine any misalignment in crystal orientation produced by the polishing procedure. The crystals were then ultrasonically cleaned in an acetone bath. The appropriate crystals were brought together, and the assembly was wrapped with platinum wire prior to insertion into the furnace. A given diffusion couple was constructed of specimens (crystals) of the same approximate size to insure one dimensional diffusion.

Diffusion Anneal Furnace and Atmosphere Control Apparatus

A furnace was constructed for diffusion anneals with the following features: adequate control and capability of reaching temperatures of 1600°C or greater, atmospheric control in conjunction with the use of a purified flowing gas mixture, and capability of rapid insertion of the sample into the furnace and rapid withdrawal of the sample from the furnace. The furnace configuration is shown in Figure 12. The heating elements were Kanthal Super (Kanthal Corporation). The hot face insulation consisisted of 60% bubbled Al_2O_3 mixed with 40% Al_2O_3 castable (97.5% Al_2O_3). Additional insulation consisted of 2800°F insulating firebrick (I.F.B.). A closed end impervious tube (99.7% Al_2O_3) was fixed in the center of the furnace with the open end extending down below the furnace. A smaller impervious tube (99.7% Al_2O_3) was used as a pedestal to hold experimental samples and was inserted vertically into the larger tube. A Pt - Pt 10% Rh thermocouple extended upward through the center of the pedestal tube to allow continuous monitoring of the sample temperature. When flowing gas mixtures were employed, the gas was directed upward through the pedestal tube. This tube was packed with 99.7% Al_2O_3 chips in order to create turbulent mixing as the gases passed up the tube. The gases flowed around the sample position near the top of the pedestal tube and were exited downward in the annular opening between

Figure 12. Diffusion anneal furnace

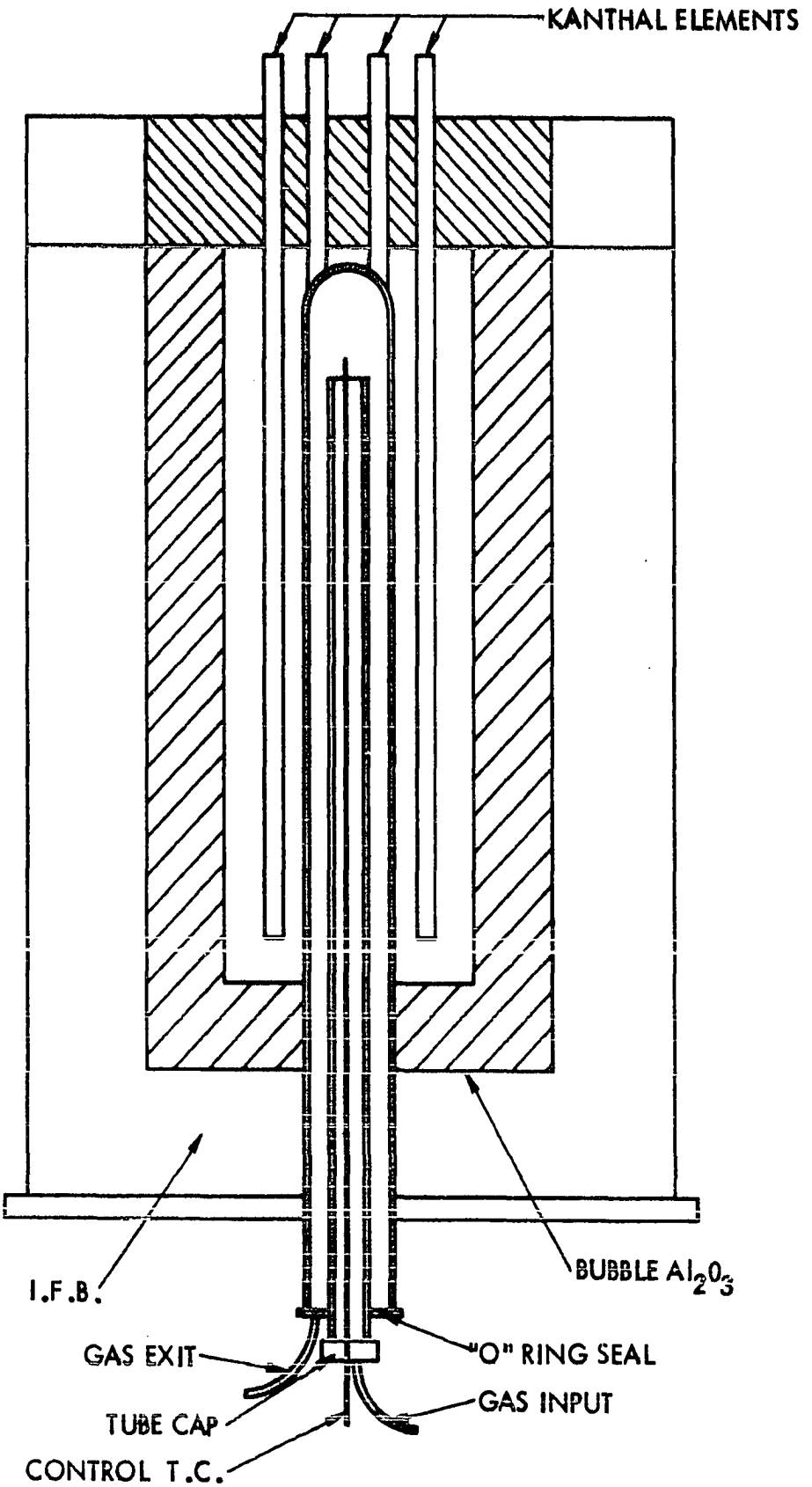
KANTHAL ELEMENTS
I.F.B.
BUBBLE Al_2O_3
GAS EXIT
"O" RING SEAL
TUBE CAP
GAS INPUT
CONTROL T.C.

the tubes.

The system for mixing and metering of various gas atmospheres is shown in Figure 13. Gas mixtures used were CO and CO_2, Ar and O_2, and a commercially premixed tank of 91 ppm O_2 in Ar. These gases are described in Table 6. All gases were dried by passage through plexiglass columns filled with anhydrous calcium sulfate (Drierite).

Table 6. Description of gases used in experimental work

Gas	Grade	Purity	Remarks
O_2	Extra dry	99.6%	
Ar	Prepurified	99.998%	
CO_2	Bone dry	99.8	
CO	Technical	99.0%	
Mixture	-	-	91 ppm (Vol.) O_2 in Ar supplied with certified analysis.

Argon and CO_2 were passed through a furnace for oxygen removal which consisted of a column packed with copper turnings maintained at 550°C. Carbon monoxide was passed through a plexiglass column containing "Ascarite" (A. H. Thomas Co.) to remove CO_2. Gas flow rates were metered on precalibrated orifice flowmeters employing differential manometers filled with di-butyl phthalate indicator.

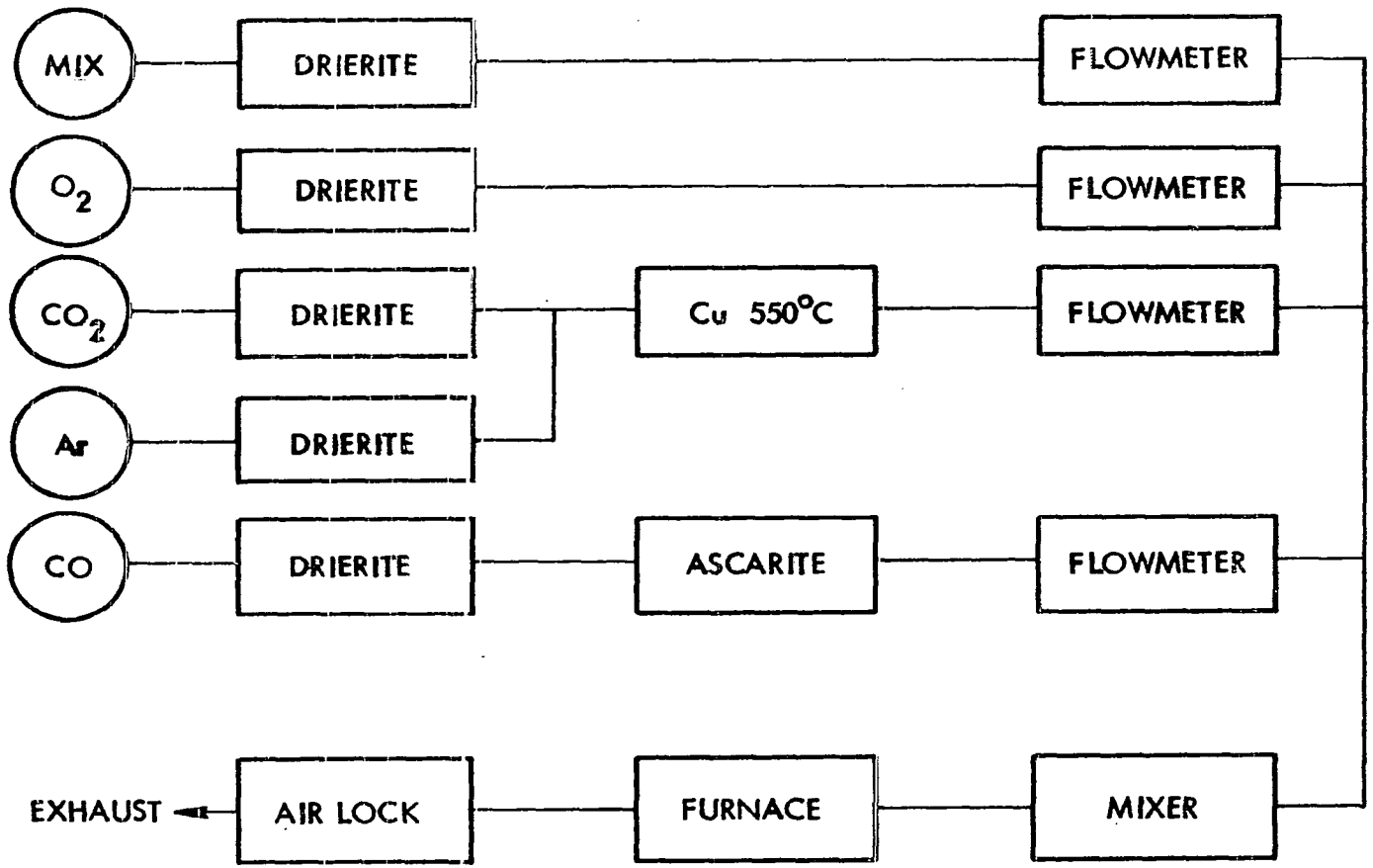

Figure 13. Gas control system

Flowmeters were calibrated by observing the rate of rise of a soap bubble in a vertically fixed pyrex column following a procedure described by Levy (73). Immediately after the metering step, gases were mixed in a plexiglass column packed with glass beads. The furnace flow rate was fixed at 2.3 cm^3/s in accordance with the suggestion of Darken and Gurry (74) as a rate sufficient to prevent cooling of experimental samples and thermal gas demixing. For argon-oxygen mixtures the furnace flow rate was kept at approximately one cm^3/s.

Control of oxygen partial pressure was accomplished in two ways. In one method a flowing mixture of oxygen in argon was passed through the furnace at a total pressure of one atmosphere. The oxygen partial pressure is dependent on the concentration of oxygen in the mixture and not on temperature if the gases behave ideally. In the second method the oxygen partial pressure was fixed by controlling the chemical equilibrium represented by

$$CO_2(g) = CO(g) + \frac{1}{2}O_2(g). \qquad (99)$$

The equilibrium represented by Equation 99 has been studied and thermodynamic data are available in the literature (75). This equilibrium may be described by

$$\log p_{O_2} = 2 \log\left(\frac{p_{CO_2}}{p_{CO}}\right) - \frac{2\Delta F^\circ}{2.303\ RT} \qquad (100)$$

where

$$\Delta F^\circ = \Delta F^\circ_{CO} - \Delta F^\circ_{CO_2} \qquad (101)$$

and ΔF° is the standard free energy of formation. Since the assumption has been made that the gases are ideal, the terms p_{CO_2} and p_{CO} in Equation 100 may be replaced by R_{CO} and R_{CO_2}, the volumetric flow rates of CO and CO_2.

Experimental specimens were placed in crucibles on the pedestal tube, and the assembly was raised into the furnace. Crucibles were constructed of platinum foil for experiments in Ar-O_2 mixtures and of molybdenum foil for experiments in CO-CO_2 mixtures.

Eighteen diffusion couples were processed under the experimental conditions given in Table 7. Specimens 3 and 4 were annealed during the same experiment for differing lengths of time to test the accuracy of the mathematical analysis of the diffusion profile. Specimens 6 and 7 were annealed simultaneously in a test of the effect of diffusion couple configuration on the experimental results. Specimens 10 and 11 were composed of the low purity Ni_xO and Co_xO crystals and were annealed simultaneously to test the effect of surface roughness at the diffusion couple interface on the experimental results.

Table 7. Details of diffusion experiments

Specimen	Couple constituents	Temperature (°C)	Time (10^4 s)	p_{O_2} (atm)
1	Mn_xO-MgO	1171 ± 3	4.038	10^{-9}
2	"	1348 ± 4	6.144	10^{-9}
3	"	1150 ± 2	8.670	10^{-9}
4	"	1150 ± 2	12.960	10^{-9}
5	"	1449 ± 4	6.780	10^{-9}
6	"	1529 ± 4	4.170	10^{-9}
7	"	1529 ± 4	4.170	10^{-9}
8	Ni_xO-Co_xO	1170 ± 2	2.178	0.21
9	"	1170 ± 2	1.435	0.21
10	"	1170 ± 2	1.435	0.21
11	"	1145 ± 1	15.570	0.21
12	"	1043 ± 2	4.680	0.21
13	"	1283 ± 3	9.600	0.21
14	"	1367 ± 4	8.508	0.21
15	"	1359 ± 3	5.694	$9x10^{-5}$
16	"	1268 ± 2	5.934	$9x10^{-5}$
17	"	1188 ± 1	0.712	$9x10^{-5}$
18	"	1410 ± 3	0.863	$9x10^{-5}$

Electron Microprobe Analysis of Annealed Samples

The electron microprobe permits quantitative chemical analysis of areas on polished samples the order of one micron in diameter. The apparatus consists of an electron gun supplying a current which is focused electromagnetically and strikes the sample surface. The collision of electrons with atoms on the specimen surface results in the generation of X-rays of wavelength characteristic of the element under irradiation. These X-rays are analyzed for wavelength and counted. The quantitative chemical composition of the specimen is deduced on the basis of comparison with standards and on the application of certain correction factors including the atomic number correction, X-ray absorption correction, and the X-ray fluorescence correction. Many reviews are available in the literature (76, 77, 78) on the subject of electron microprobe analysis.

To prepare diffusion specimens for microprobe analysis it was necessary to section the diffusion couple, mount the sectioned specimen in a metallographic mounting media, polish to sufficient smoothness, check orientation of the polished surface, and coat the specimen with an electrically conducting coating. Sectioning was accomplished by mounting the samples in a cold setting acrylic and cutting with a petrographic saw with diamond impregnated blade of one mm thickness. The halves of the diffusion couple were then remounted in acrylic

and polished according to the following procedure: (1) 600 grit SiC paper on rotating lap with water lubricant, (2) 6 μm diamond paste (AB-metadi, Buehler Ltd.) with oil lubricant on nylon cloth-covered rotating lap, (3) 1 μm diamond paste (AB-metadi, Buehler Ltd.) with oil lubricant on nylon cloth-covered rotating lap, (4) 0.25 μm diamond paste (AB metadi, Buehler, Ltd.) with oil lubricant on nylon-covered rotating lap, and (5) 0.05 μm Al_2O_3 with water lubricant on Syntron lap with cloth base for 20 minutes. After polishing the orientation of single crystals was checked using the Laue technique to insure that diffusion measurement was made parallel to the <100> direction. The polished specimens were cleaned ultrasonically in a detergent solution and washed in distilled water. A conductive coating of carbon was evaporated onto the polished specimen surface in a vacuum chamber with the coating thickness controlled by noting the deposition on a white porcelain chip. Specimens were then stored over desiccant until later analysis.

The electron microprobe was a Hitachi-Perkin Elmer XMA-5 equipped with three spectrometers capable of X-ray analysis, back scattered electron analysis, and absorbed electron analysis. Readout of X-ray count data was available in the following modes: (1) spot analysis with digital readout in counts per unit time, (2) line analysis with specimen driven automatically under the beam with recorder readout, (3) line

analysis with electron beam electromagnetically deflected in a linear trace and oscilloscope readout, and (4) area analysis with electromagnetic beam deflection and oscilloscope readout.

X-ray count data were converted to concentration values through use of a computer program entitled Magic III. A complete description of the data treatment utilized in this program is given in Appendix A. A discussion of contemporary computer treatment of microprobe data has been given by Beaman and Isasi (79). Standards for comparative purposes were single crystal oxides, polycrystalline metals, and polycrystalline coprecipitated oxides. Single crystals included MgO (Norton Company), high purity NiO, and CoO (annealed at 1000°C in argon and cooled in argon). A polycrystalline manganese metal standard was employed because of the difficulty of obtaining a manganese oxide standard of known stoichiometry. As a means of checking the accuracy of the analysis using end member standards, coprecipitated and sintered samples were produced with the following compositions: (1) five weight percent Mn_xO in MgO, and (2) 50 weight percent Mn_xO in MgO. The coprecipitation scheme is shown in Figure 14. The coprecipitated hydroxide was dried over gas flame and ignited at 1000°C to form the oxide. The oxide product was pressed to form small discs and sintered at 1500°C for two hours in argon atmosphere. The sintered

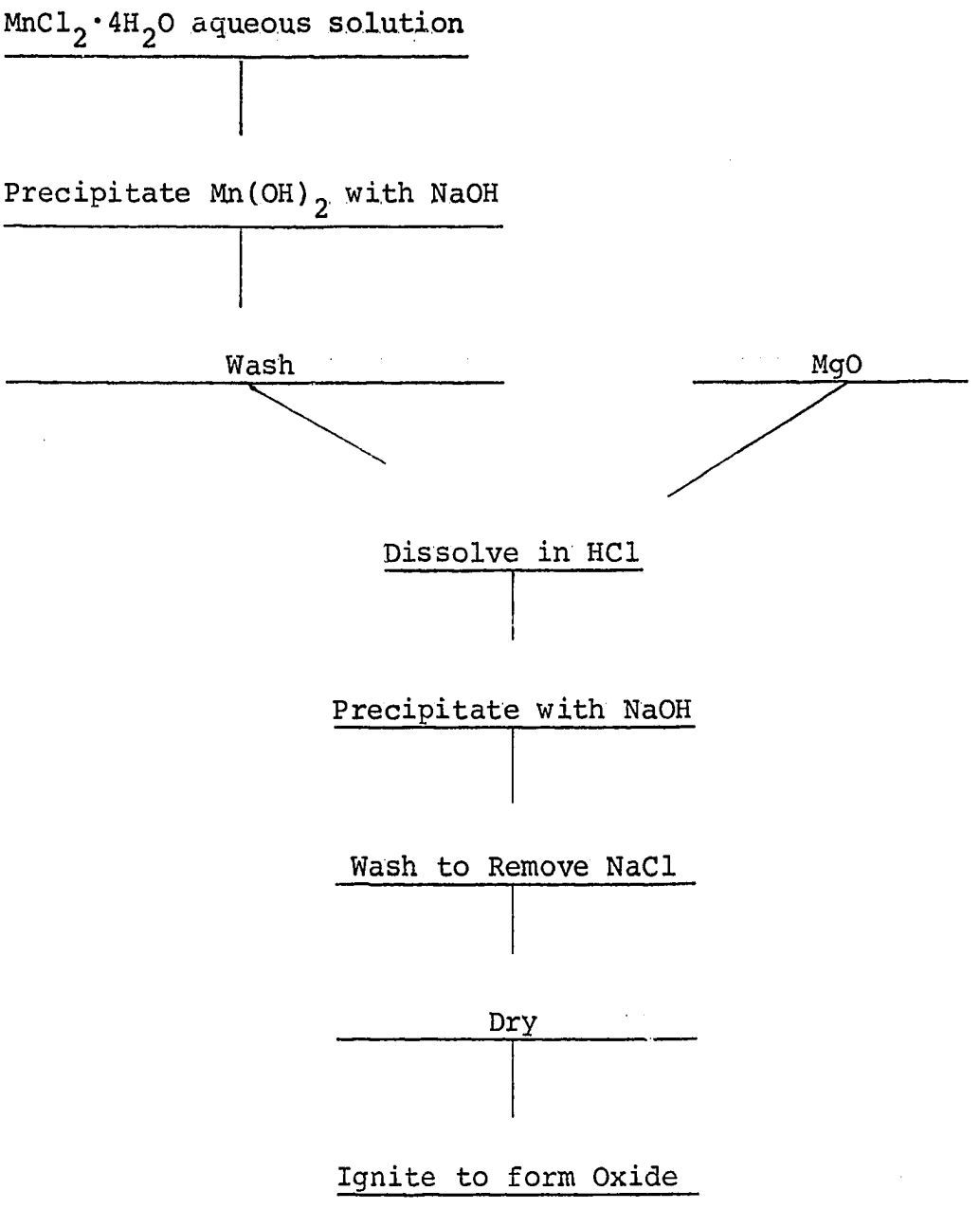

Figure 14. Coprecipitation scheme to form mixed Mn_xO-MgO oxides

polycrystals were then subjected to microprobe analysis and their computed composition was compared to their known composition. In the case of the five weight percent Mn_xO in MgO the computed and known values were within four percent of each other, the case of the 50 weight percent MnO in MgO the computed and known values were within two percent of each other. The same experiment was unnecessary with Ni_xO and Co_xO mixed oxide standards because of the very small absorption correction and subsequent higher confidence in calculations involving end member standards.

The microprobe analysis of Mn_xO-MgO experimental specimens was performed at 15 keV excitation potential at an absorbed electron current ranging from 1.5 μA to 2.0 μA. These figures were chosen in an attempt to keep the absorption correction for magnesium low while maintaining desirable counting rates and small beam size. Manganese Kα, X-rays (2.101 Å) were monitored using a lithium fluoride (LiF) analyzer crystal while magnesium Kα X-rays (9.890 Å) were simultaneously monitored using a potassium acid phthallate (KAP) analyzer crystal. Oxygen concentration was approximated by difference. The microprobe analysis of Ni_xO-Co_xO diffusion couples was performed at 20.0 keV at an absorbed electron current ranging from 1.25 μA to 2.00 μA. Nickel Kα, X-rays (1.658 Å) were monitored using one LiF analyzer while cobalt Kα, X-rays (1.789 Å) were simultaneously monitored

using another LiF analyzer. Oxygen was approximated by difference.

Typical procedure included adjustment of absorbed electron current to allow counting rates of at least five digits per twenty second period on pure oxide standards. During the course of analysis, reference was made to standards to insure against instrumental drift. Drift was nonexistent if the apparatus had been in operation for at least 30 minutes. Effort was also made to maintain focus of the electron beam during the course of the analysis since the focus directly affects the beam size and thus the counting efficiency. The beam could be directly observed on luminescent materials such as CdS and MgO. The microprobe was designed such that electron beam focus was achieved when optical focus was obtained. This feature was confirmed on luminescent materials. Experience with luminescent material showed that a beam size of no greater than five μm diameter and usually one μm diameter was maintained.

The spot analysis technique was employed in the analysis of all diffusion profiles, i.e. the specimen was stationed under the beam at optimum focus, an X-ray count was made, the specimen was moved relative to the beam using a calibrated manual adjustment, and the focus and counting continued. Typical displacement steps across the diffusion area ranged from 10 μm to 100 μm depending on the curvature of the

diffusion concentration profile. Calibration of the scale on the X and Y coordinate (horizontal) manipulators was accomplished optically by using a graduated microscope slide.

An attempt was made to measure the Lα/Lβ X-ray intensity ratios because of recent references pertaining to the analysis of stoichiometry of transition metal oxides using the technique (80, 81, 82). The manganese Lα (19.45 Å) and Lβ (19.11 Å) were completely invisible using the KAP analyzer crystal. This was probably due to the thickness of the counter window. The nickel Lα(14.56 Å) and Lβ (14.27 Å) and the cobalt Lα (15.97 Å) and Lβ (15.67 Å) were attainable using the mica and KAP analyzer crystals. The counting rates however were unacceptable because the peak-to-background ratio was approximately 1.1 to 1.2. The study was discontinued.

RESULTS AND DISCUSSION

A polished section of diffusion specimen 3 is shown in Figure 11d. The polycrystalline Mn_xO phase is recognized due to the etching of the grain boundaries produced by the mechanical polish. The single crystal MgO contains a light colored interdiffusion zone. The polishing procedure typically produced a groove at the single crystal-polycrystal interface. There was no noticeable boundary migration in the Mn_xO-MgO system. All diffusion couples were air quenched and there was no evidence of precipitation of a spinel phase within the interdiffused zone. The polished samples showed extensive spinel precipitation in the polycrystalline region indicating the presence of Mn_3O_4.

A polished section of the diffusion specimen 9 is shown in Figure 11b. There was no groove produced at the boundary between Co_xO and Ni_xO crystals by the mechanical polish. A line of pores is shown in this figure and is located perpendicular to the direction of diffusion. This sample was air quenched and shows evidence of precipitation of Co_3O_4 outside of the diffusion zone in the region of the original Co_xO crystal.

The line of porosity shown in Figure 11b was present in all Ni_xO-Co_xO interdiffusion couples. In all specimens this line was located in what was the original Co_xO crystal based on the location of the line relative to the end of the

diffusion couple. On the average the shape of the pores was elongated in a direction perpendicular to the diffusion direction. The spacing of pores along the pore line was random. Appel and Pask (62) have noted pore migration during the interdiffusion of single crystals of Ni_xO and MgO. The pore line was perpendicular to the diffusion direction and migrated into the MgO indicating a net flux of material into the Ni_xO. The pores observed by Appel and Pask were round. Thin pores elongated in a direction perpendicular to the diffusion direction were observed to be stationary and located at the original interface between interdiffusing members of the diffusion couple. Stiglich (10) observed the migration of pores during interdiffusion of single crystals of Ni_xO and Co_xO. Pores were observed to move with the elongated axis both parallel and perpendicular to the diffusion direction. Pore movement was into the volume originally occupied by the Co_xO crystal indicating a net flux of material out of the Co_xO.

The shape of mobile pores appears to be related to the fit obtained in construction of the diffusion couple. No explanation is offered to describe how some pores are apparently trapped at the diffusion couple interface. The origin of pore movement is the existence of a net flux of material in one direction along the diffusion axis. Pores act as inert markers indicating the magnitude of the net

material movement. The result that pores move into the Co_xO crystal in the system Ni_xO-Co_xO are consistent with the higher interdiffusion coefficients at high Co_xO concentration. When marker movement is observed, both cationic and anionic contributions may exist to the relaxation flux (14). Only when no marker movement is observed as in the system Mn_xO-MgO the oxygen sublattice may be considered rigid.

Area and line X-ray scans of polished samples after diffusion anneals are shown in Figures 15 and 16. These figures are photographs of the oscilloscope readout from the electron microprobe utilizing the automatic beam scanning system. The tendency for the X-ray count rate to decrease at the extreme sweep position is due to the inefficient counting geometry maintained at this position. The image of a grain boundary in Mn_xO may be seen in Figures 15a and 15c. Quantitative analysis of concentration profiles was accomplished by step counting across the interdiffused zone. The Wagner analysis (Appendix B) was used to determine the value of the interdiffusion coefficient $\tilde{D}$ from the concentration profiles obtained by microprobe analysis. The graphical technique utilized in the Wagner analysis is illustrated in Figure 17 for diffusion specimen 6.

Concentration profiles of diffusion specimens are shown in Figures 18-35. Diffusion concentration profiles in the Mn_xO-MgO system, Figures 18-24, exhibit a greater curvature

Figure 15. X-ray scans of polished samples after diffusion anneal

(a) Specimen 3, manganese X-ray area scan showing position of subsequent line analysis (Figure 15c), area 384 μm x 384 μm.

(b) Specimen 3, magnesium X-ray area scan showing position of subsequent line analysis (Figure 15d), area 384 μm x 384 μm.

(c) Specimen 3, manganese X-ray line analysis, full scale = 2000 cps, scan width = 384 μm.

(d) Specimen 3, magnesium X-ray line analysis, full scale = 2000 cps, scan width = 384 μm.

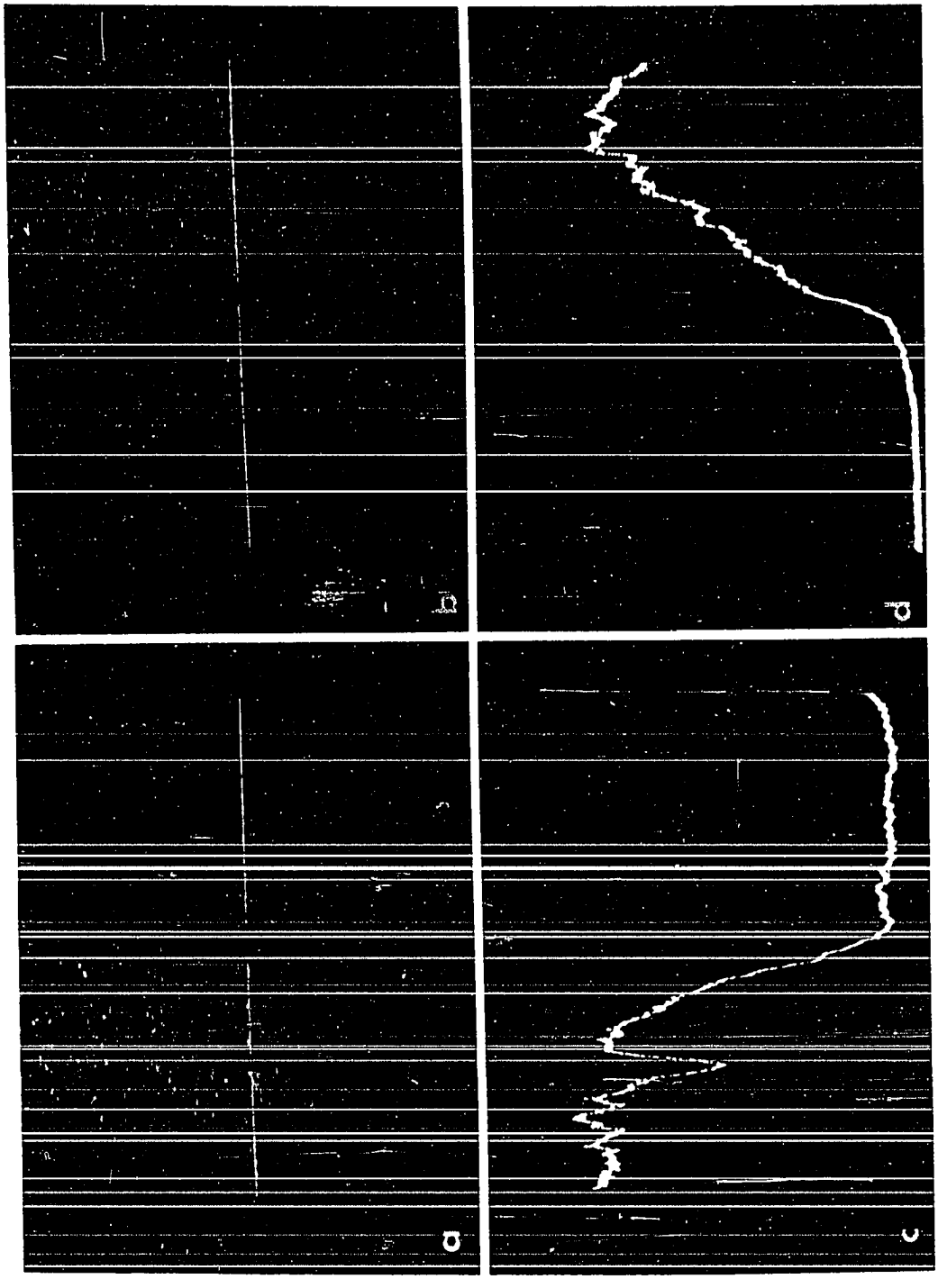
b
d
a
c

Figure 16. X-ray scans of polished samples after diffusion anneal

(a) Specimen 9, cobalt X-ray area scan showing position of subsequent line analysis (Figure 16c), area 384 μm x 384 μm.

(b) Specimen 9, nickel X-ray area scan corresponding to area shown in Figure 16a, area 384 μm x 384 μm.

(c) Specimen 9, cobalt X-ray line analysis, full scale = 5000 cps, scan width = 384 μm.

(d) Specimen 9, nickel X-ray line analysis, full scale = 5000 cps, scan width = 384 μm.

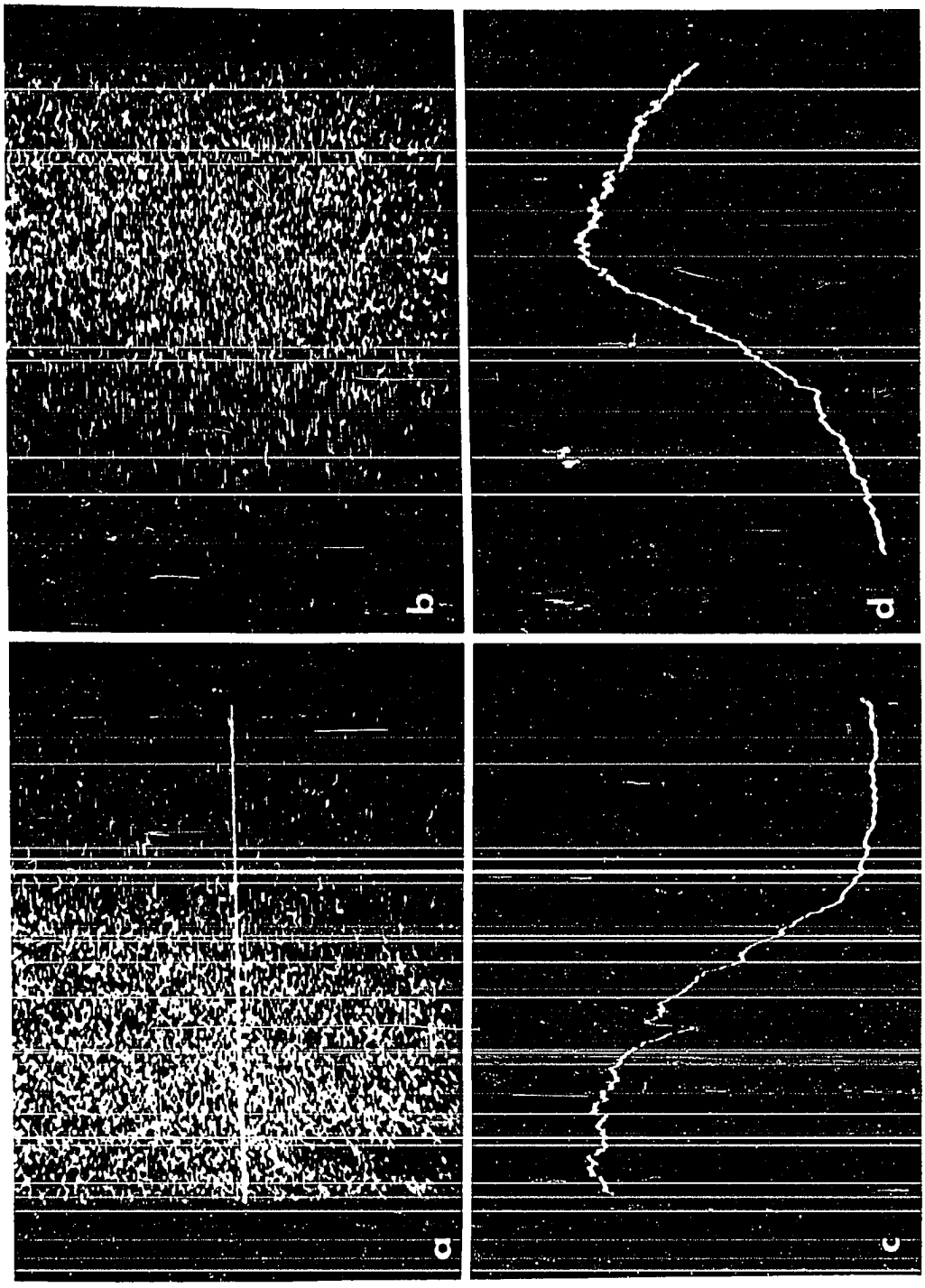
b
d
a
c

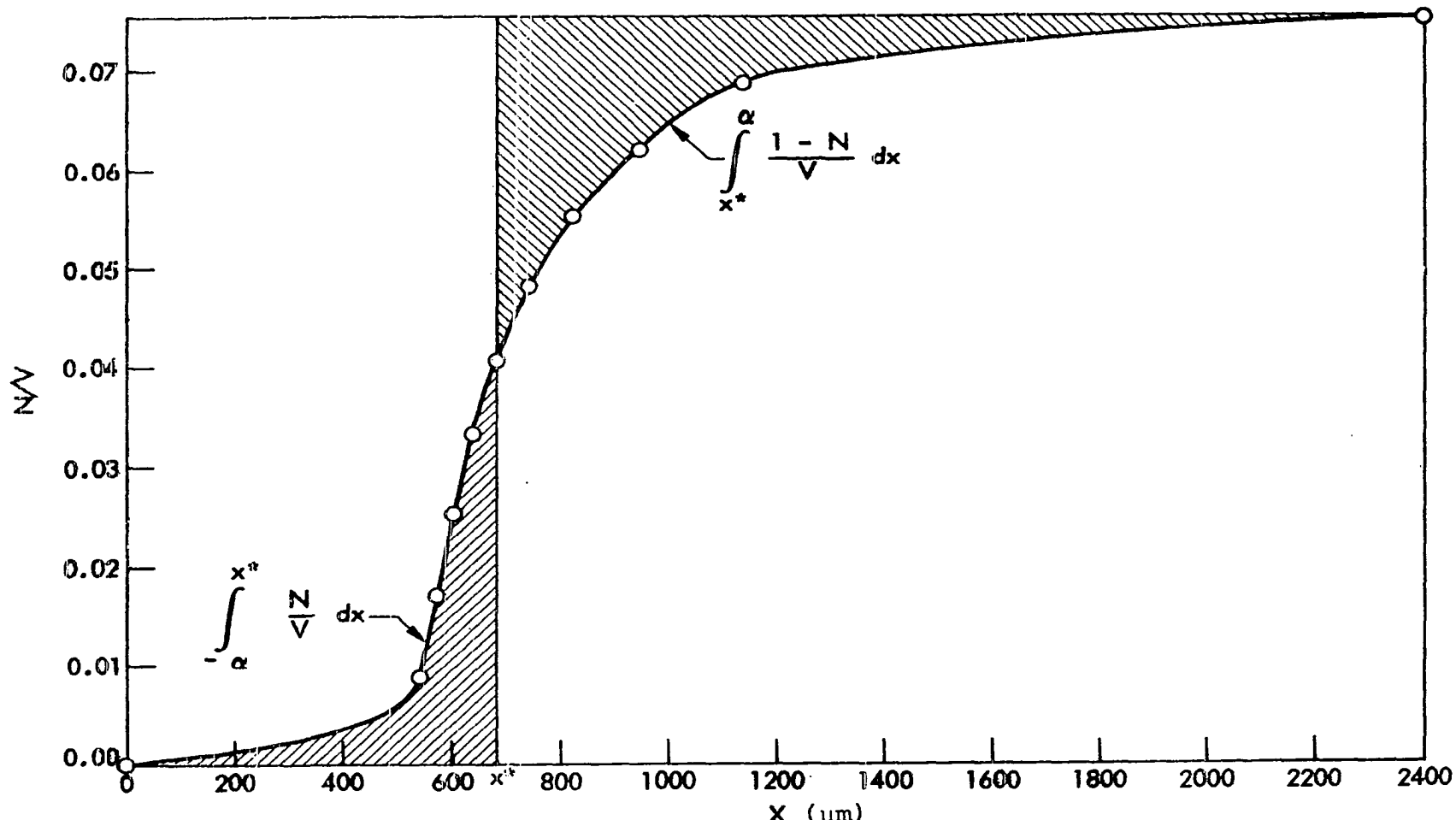

Figure 17. Illustration of the graphical technique utilized in the Wagner analysis for specimen 9

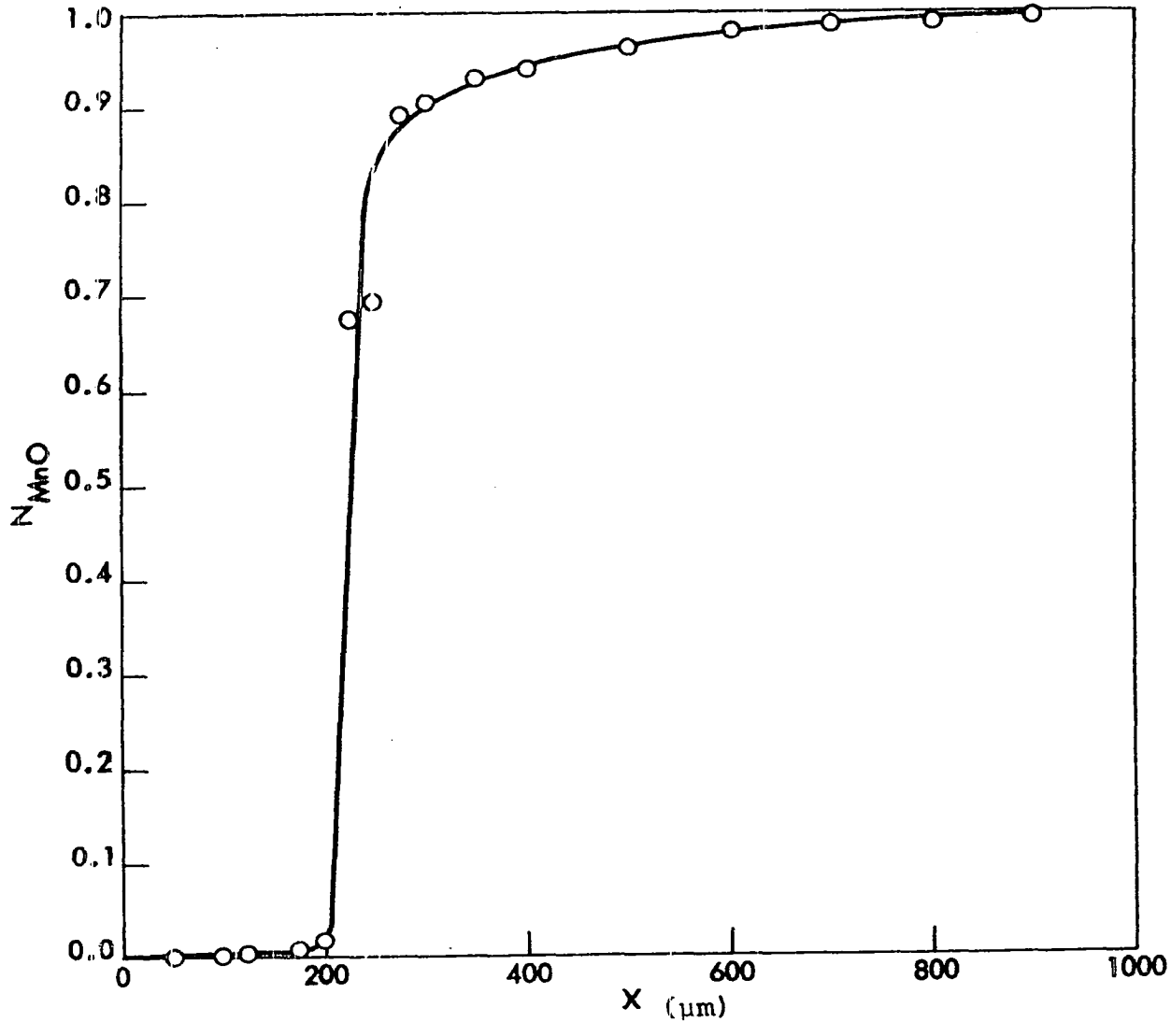

Figure 18. Concentration profile for specimen 1

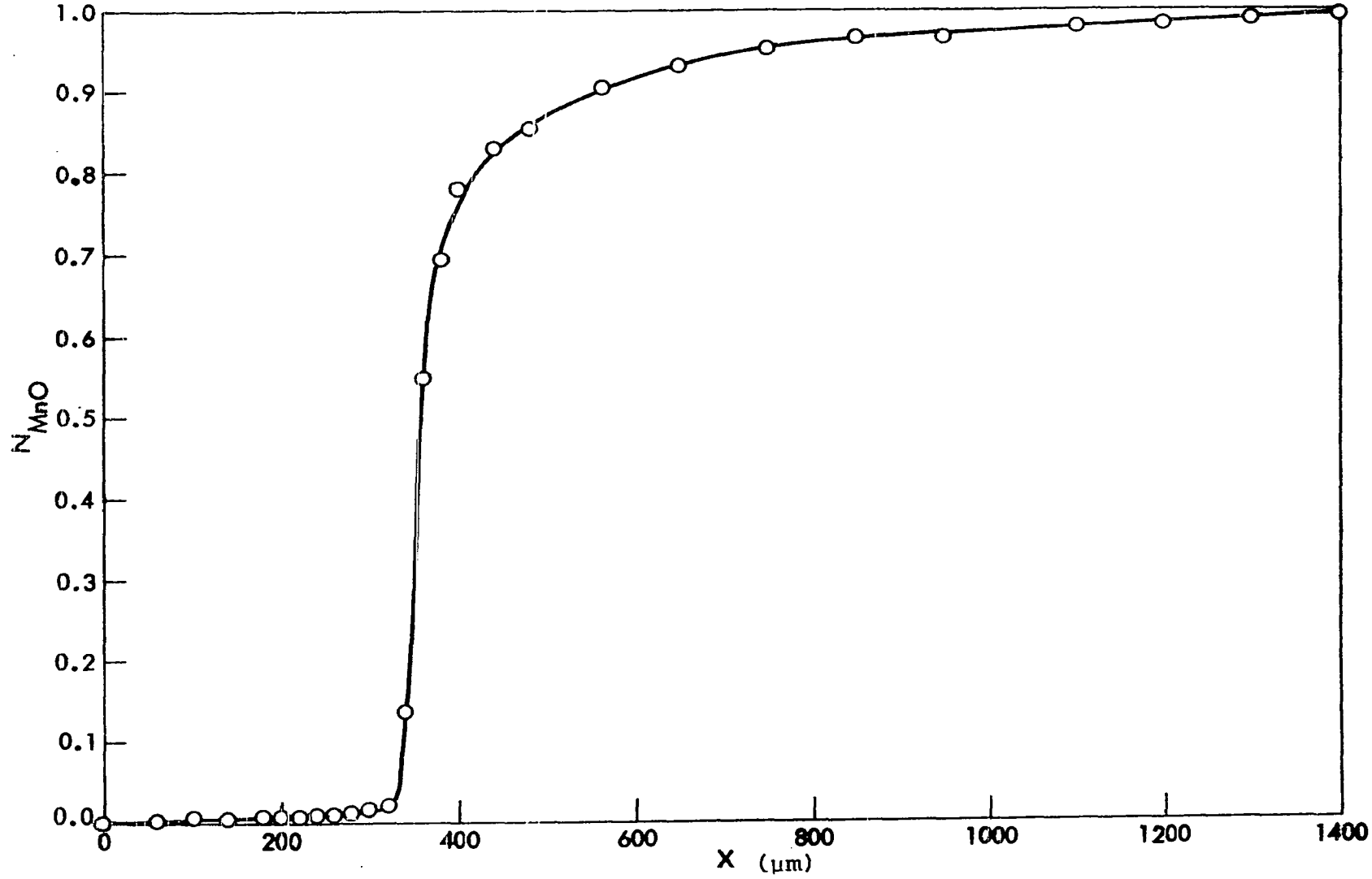

Figure 19. Concentration profile for specimen 2

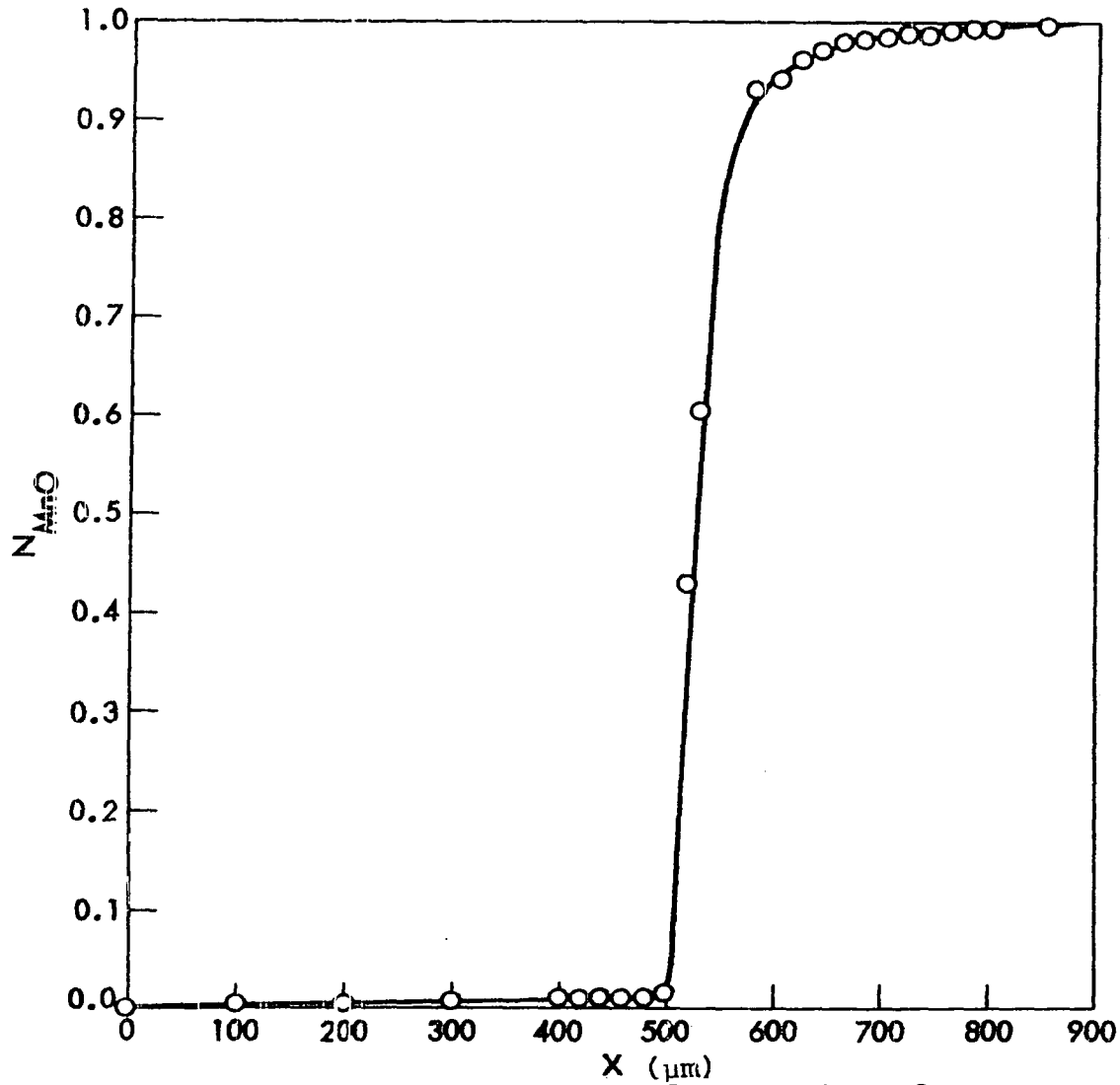

Figure 20. Concentration profile for specimen 3

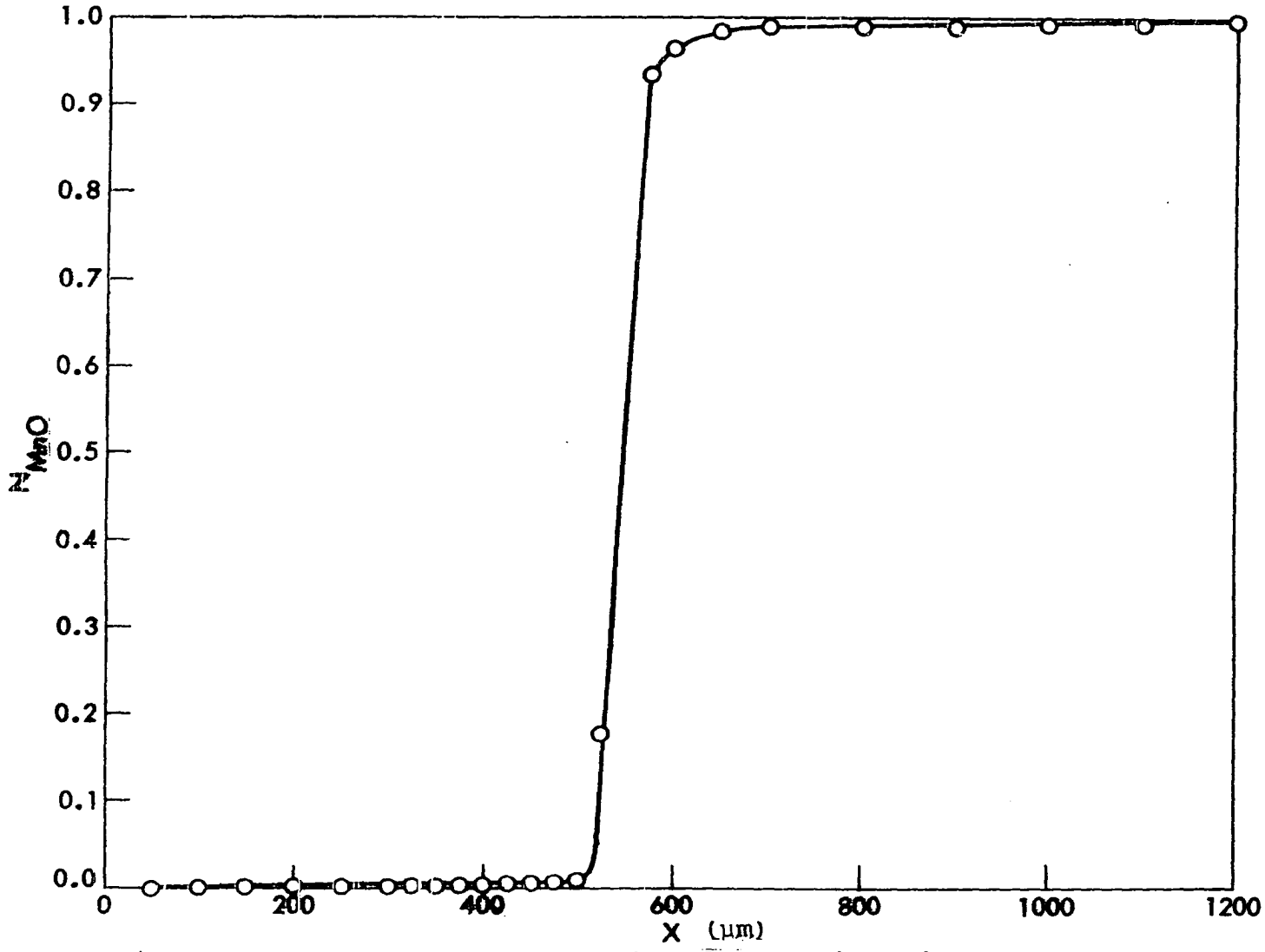

Figure 21. Concentration profile for specimen 4

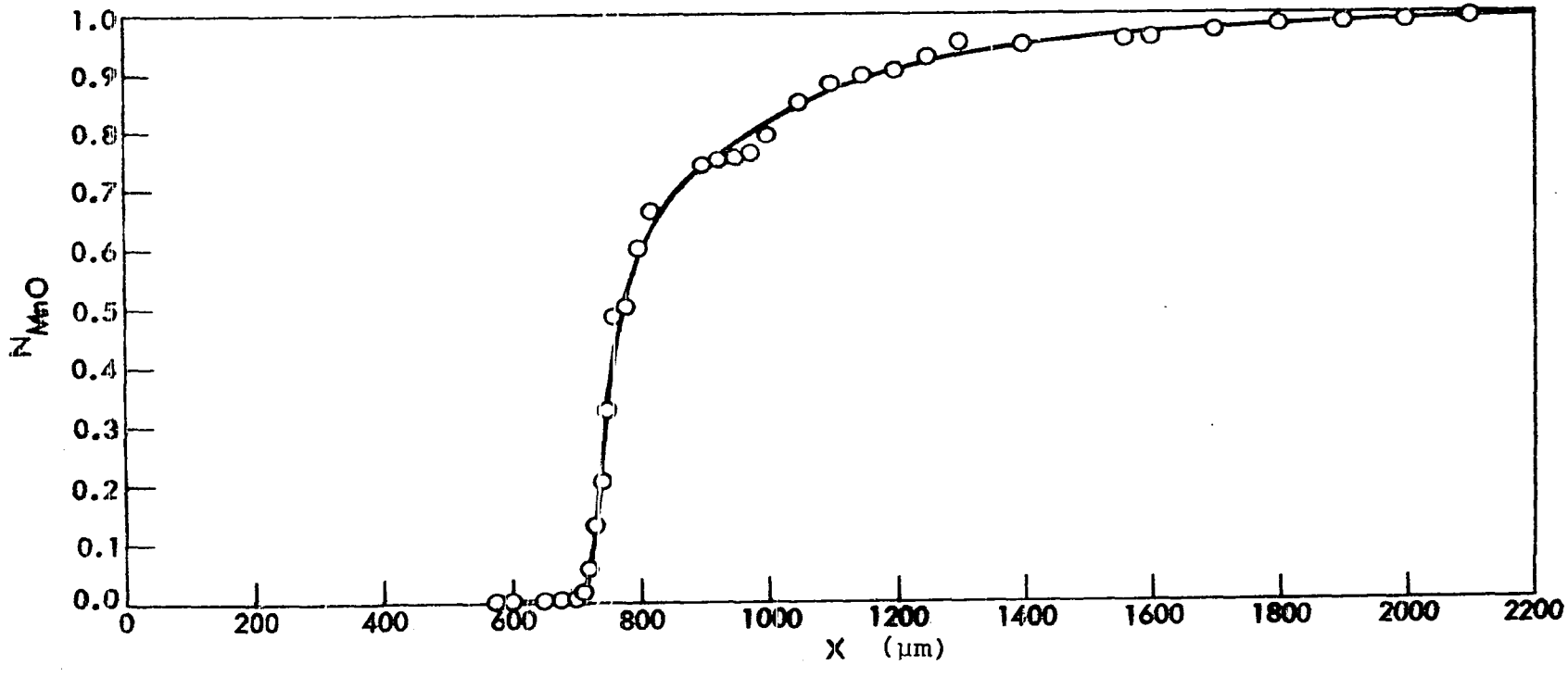

Figure 22. Concentration profile for specimen 5

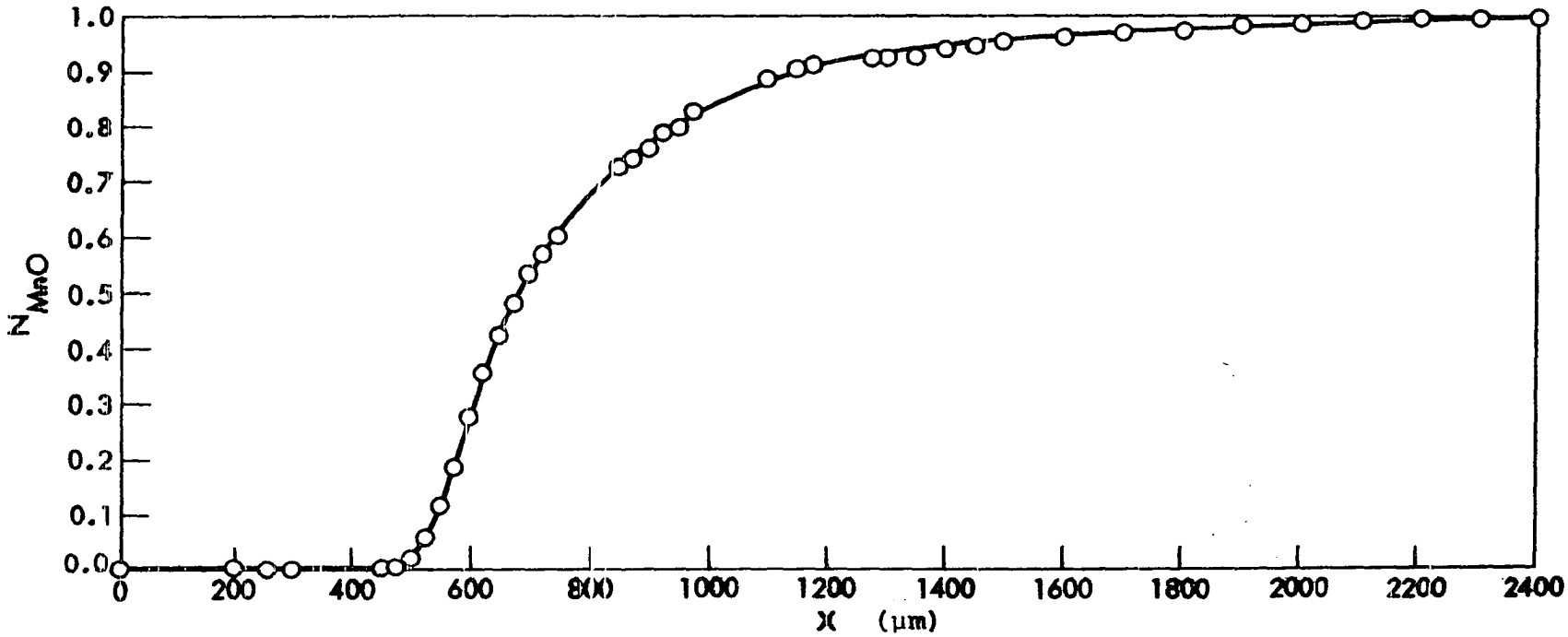

Figure 23. Concentration profile for specimen 6

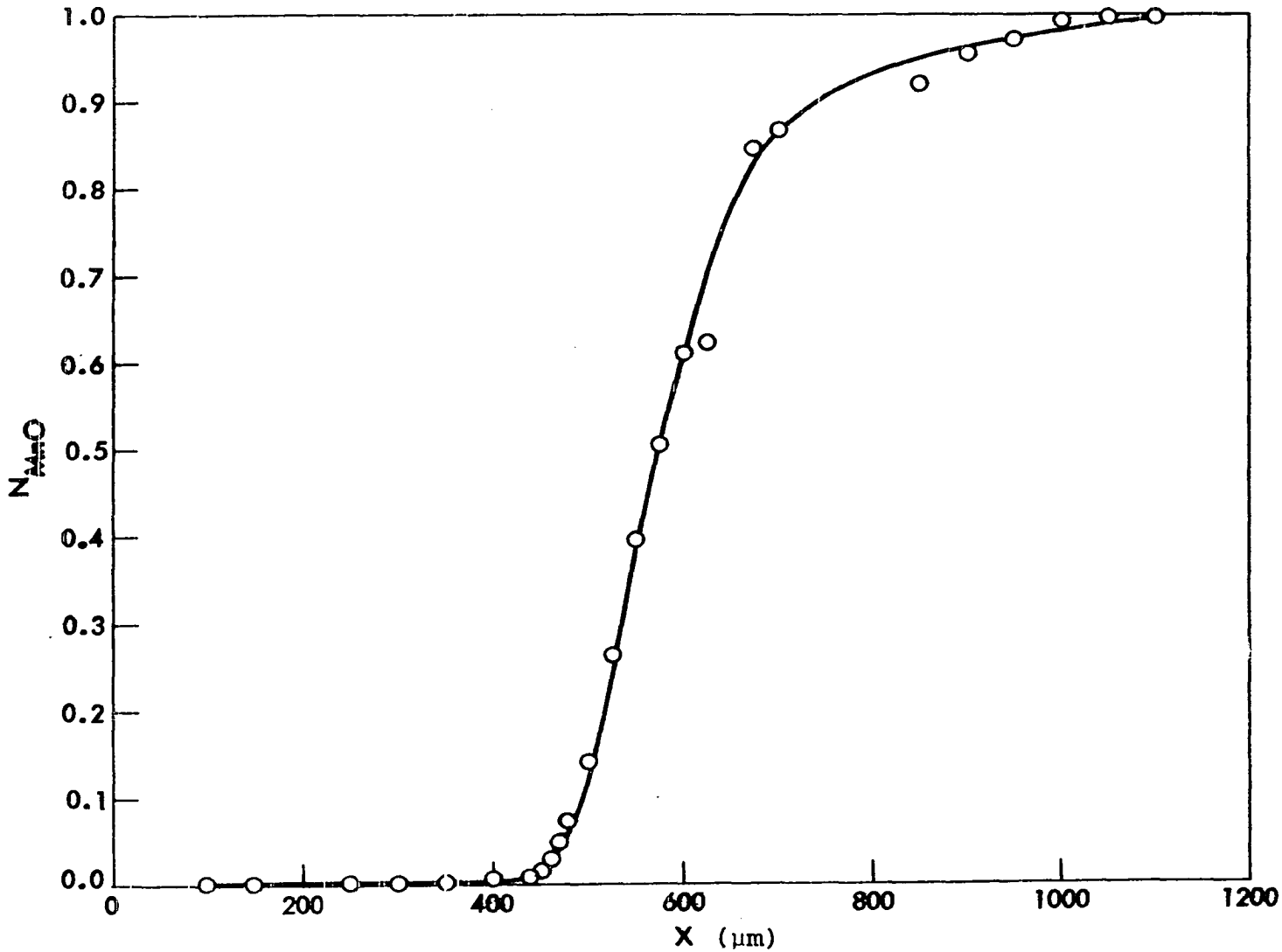

Figure 24. Concentration profile for specimen 7

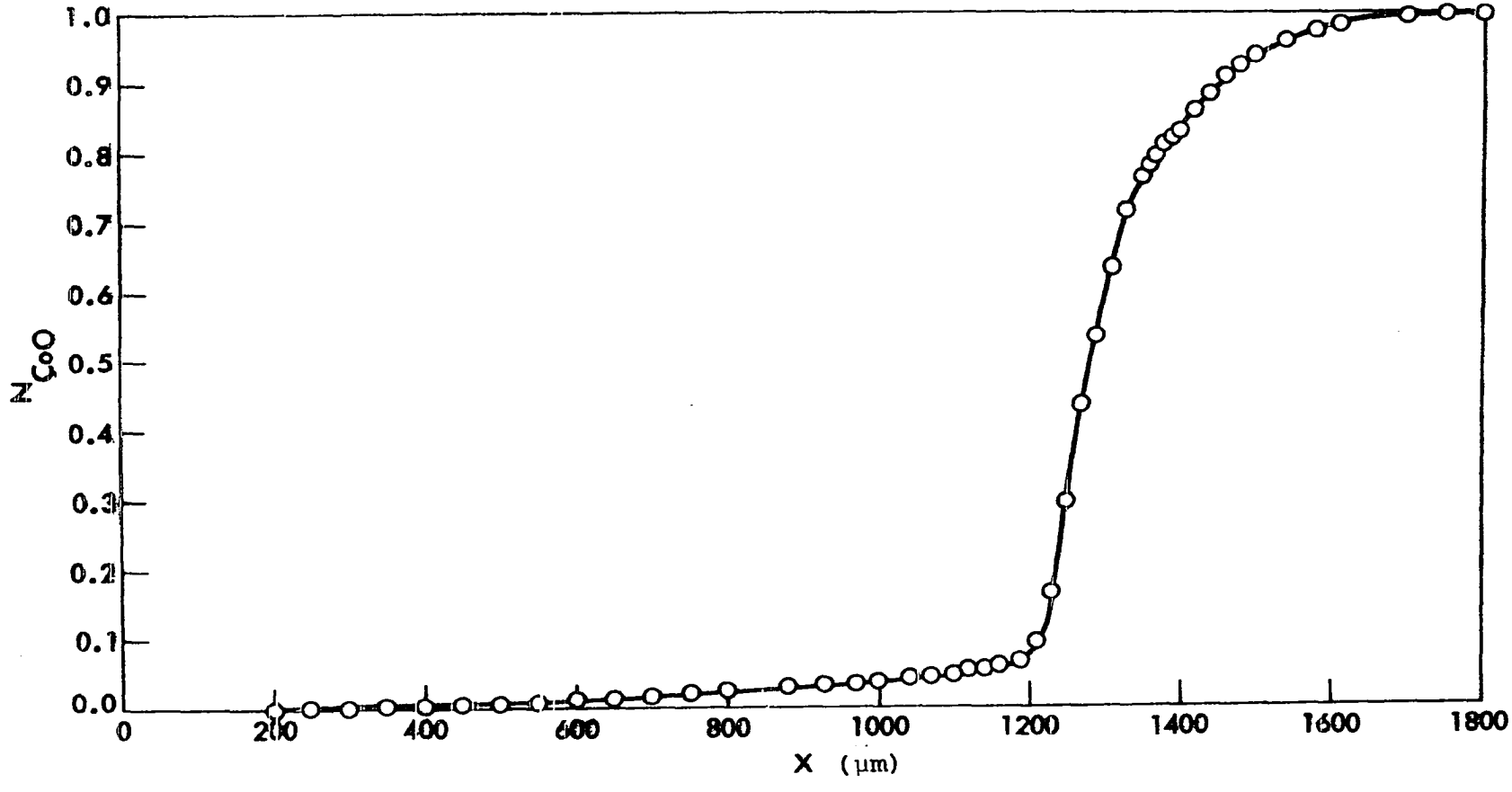

Figure 25. Concentration profile for specimen 8

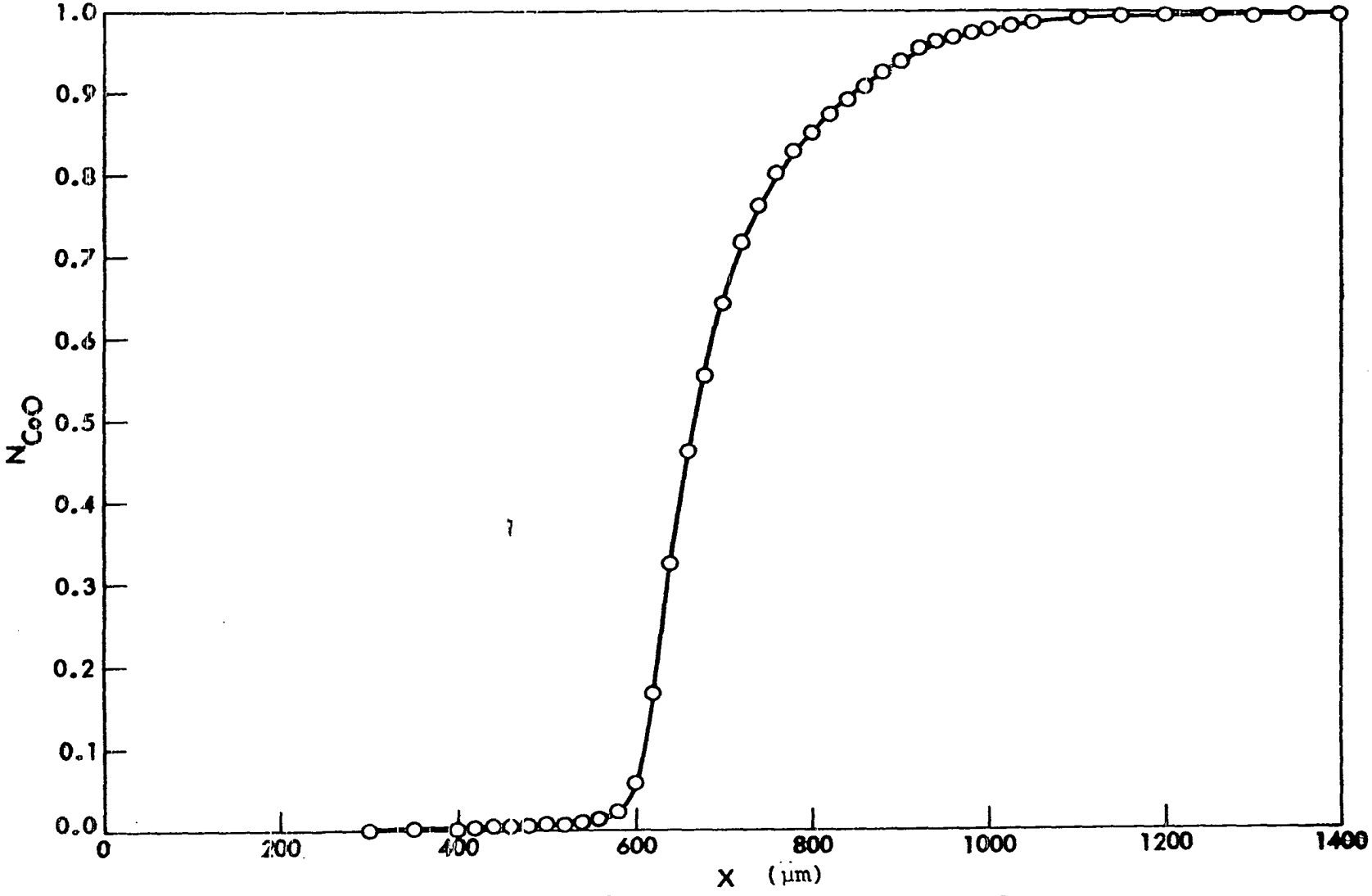

Figure 26. Concentration profile for specimen 9

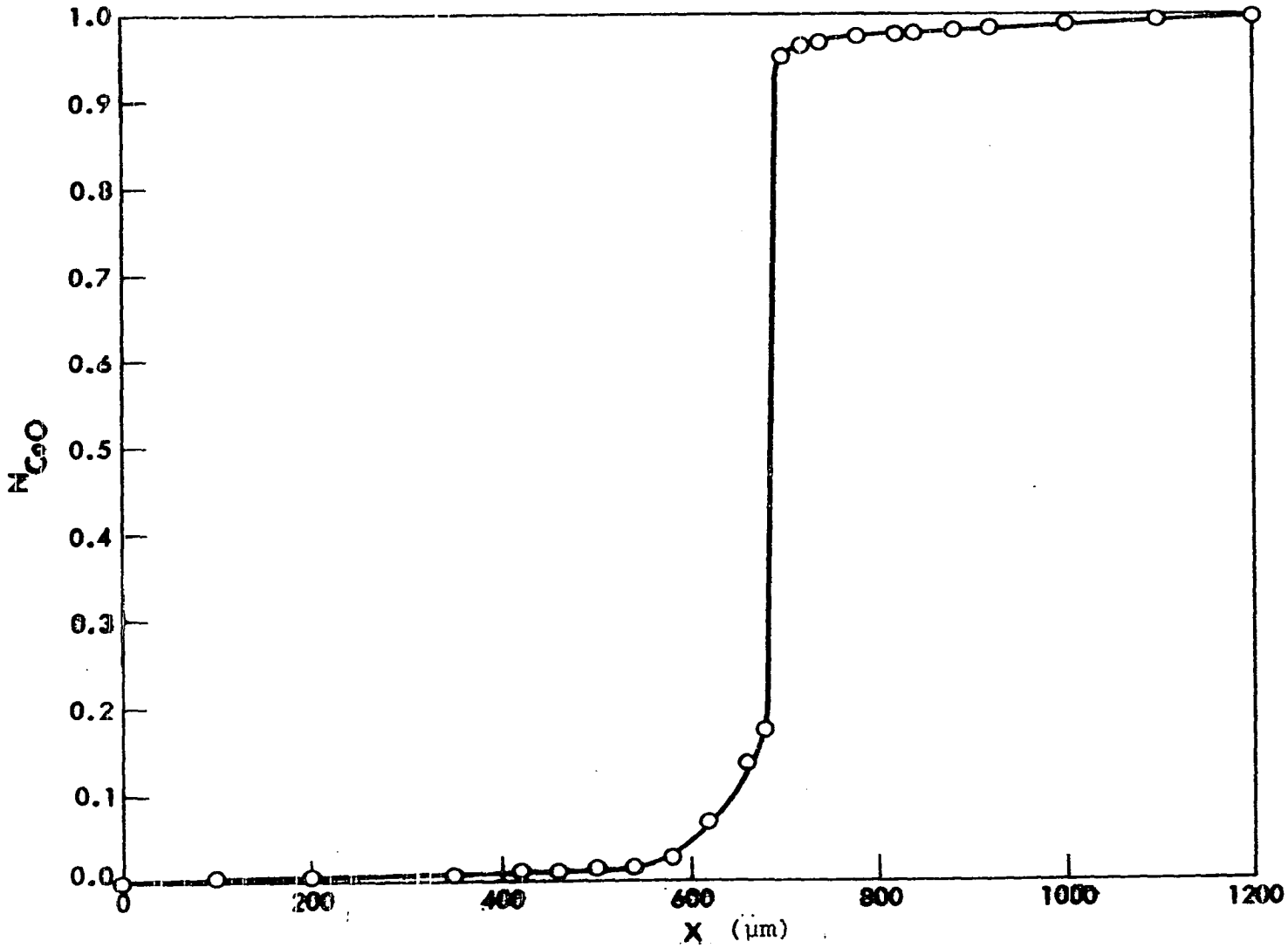

Figure 27. Concentration profile for specimen 10

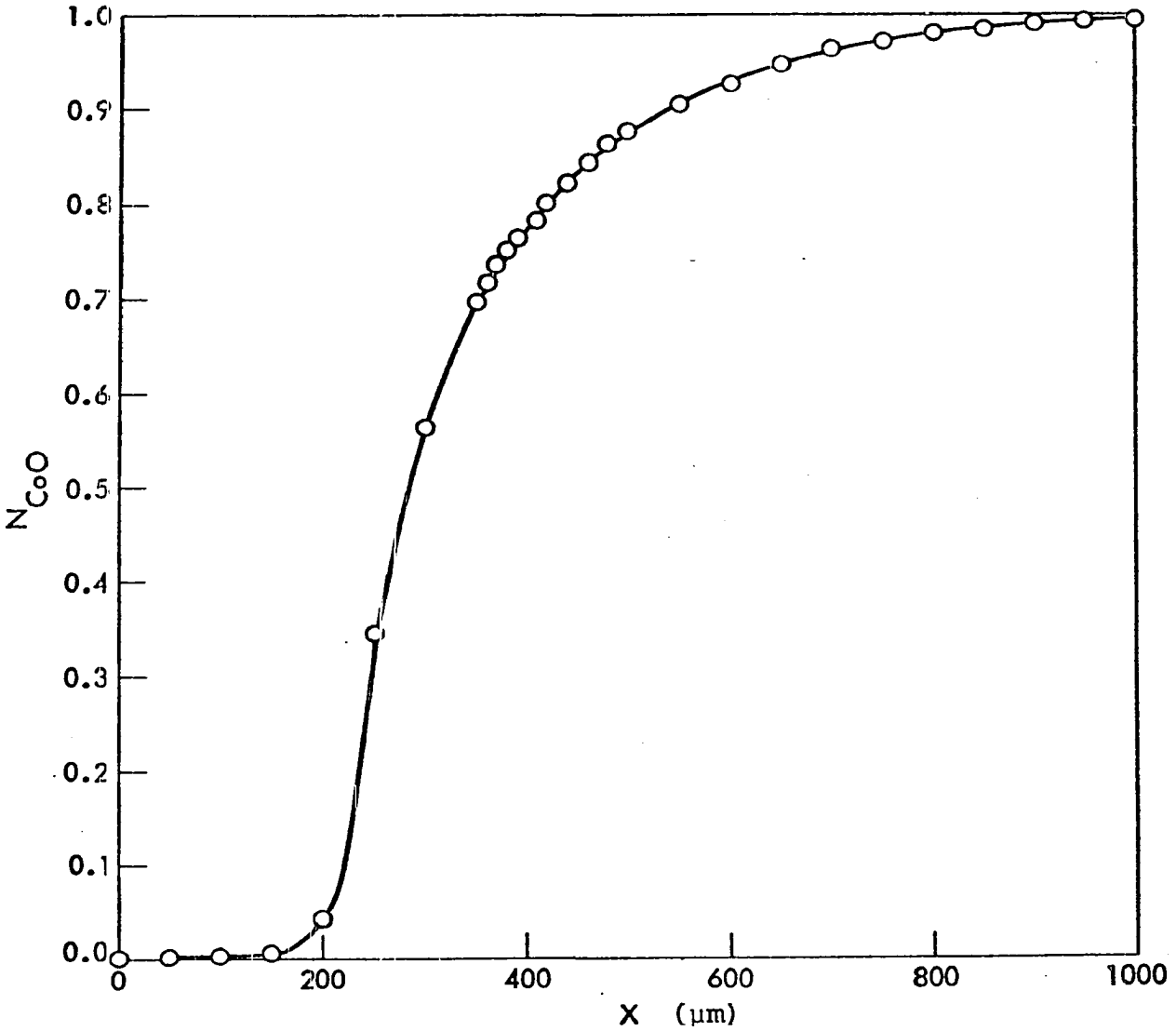

Figure 28. Concentration profile for specimen 11

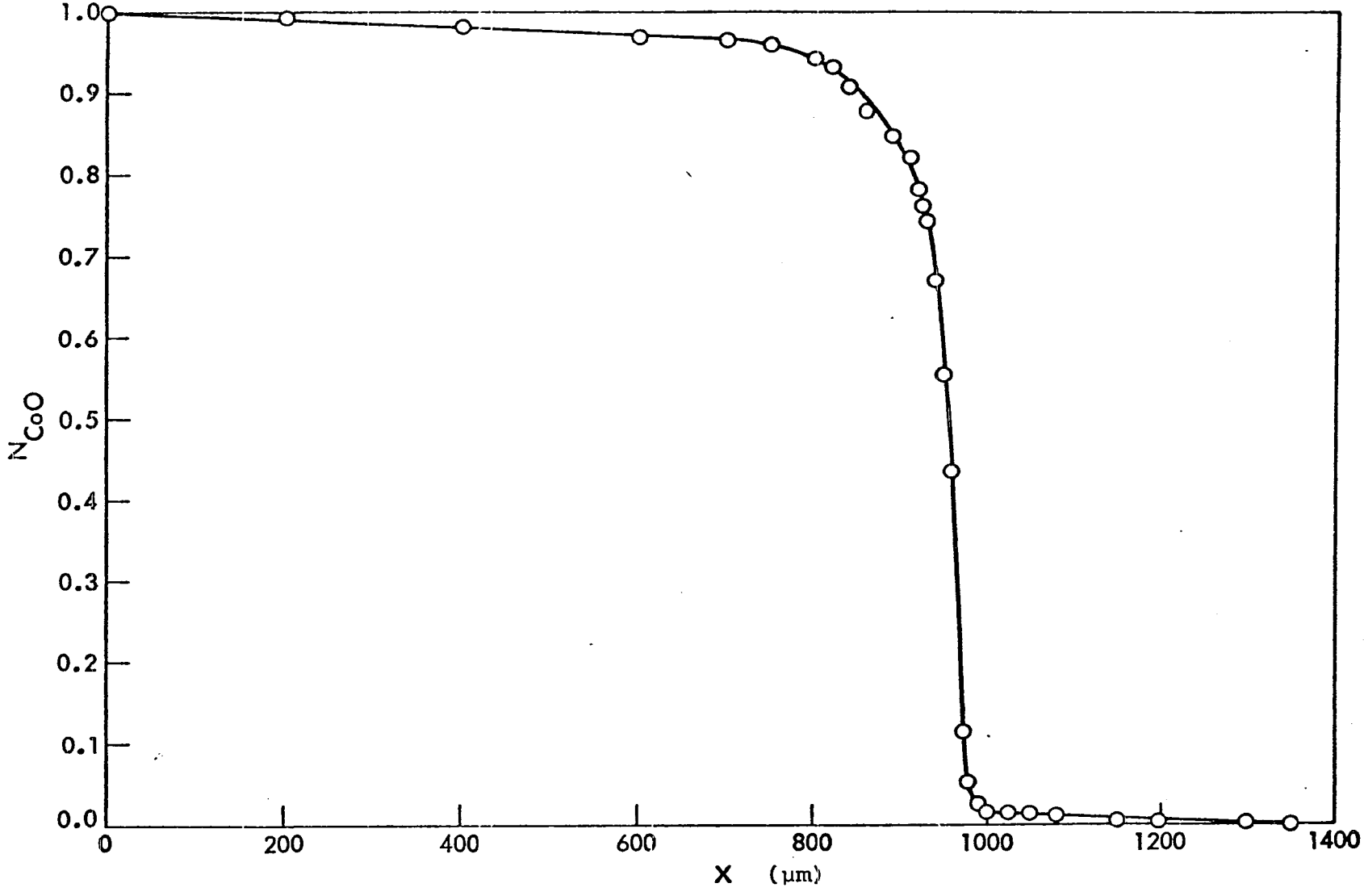

Figure 29. Concentration profile for specimen 12

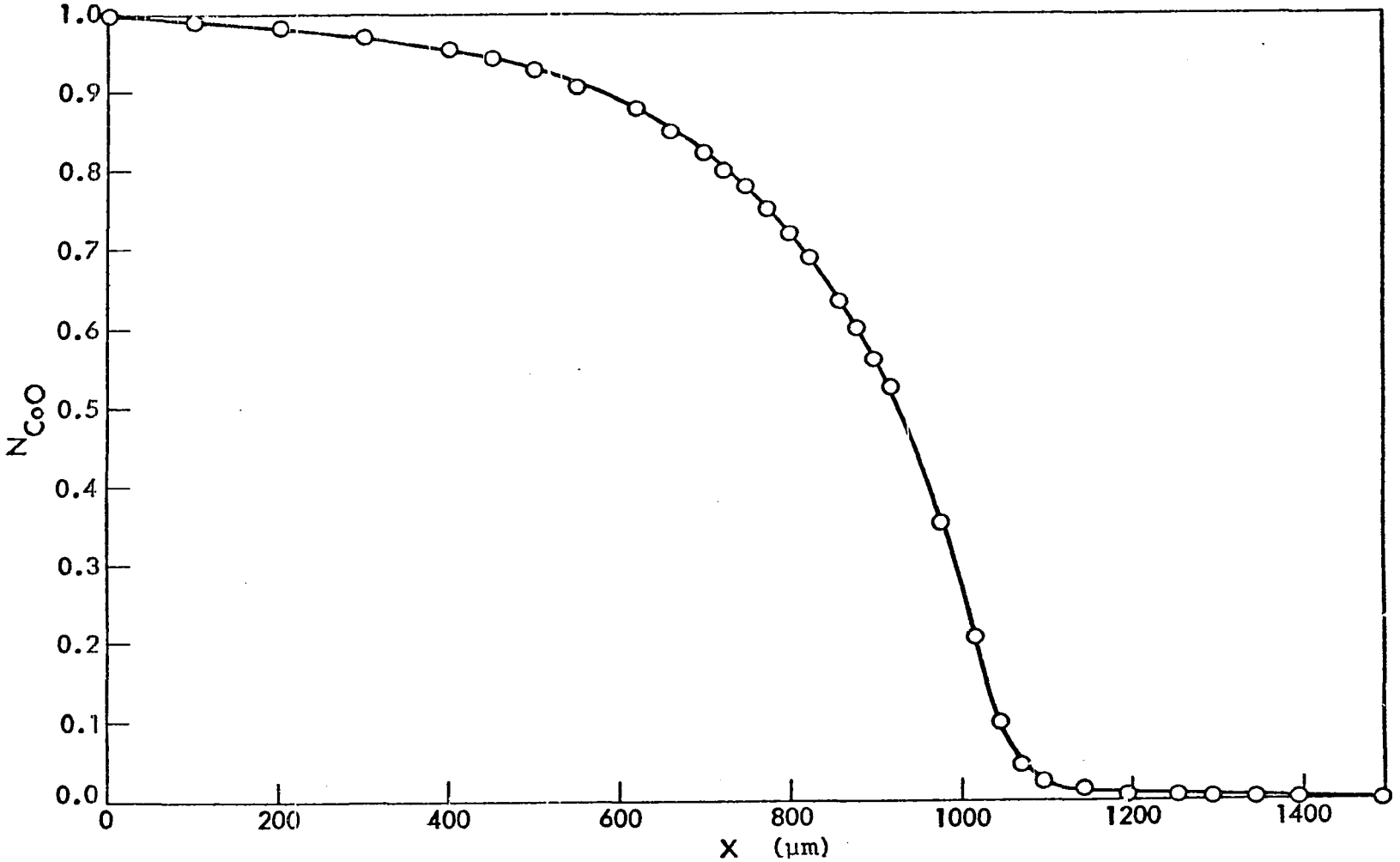

Figure 30. Concentration profile for specimen 13

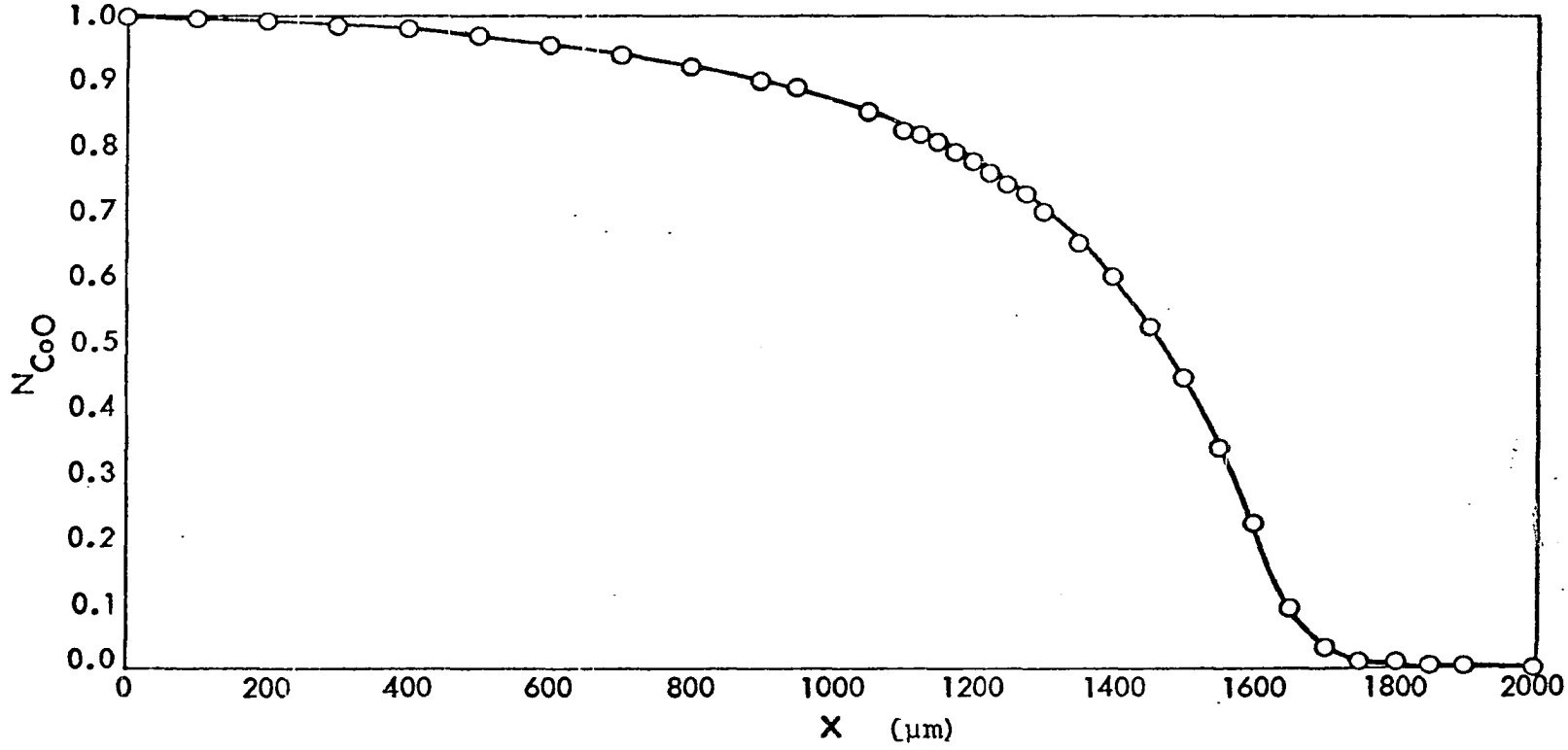

Figure 31. Concentration profile for specimen 14

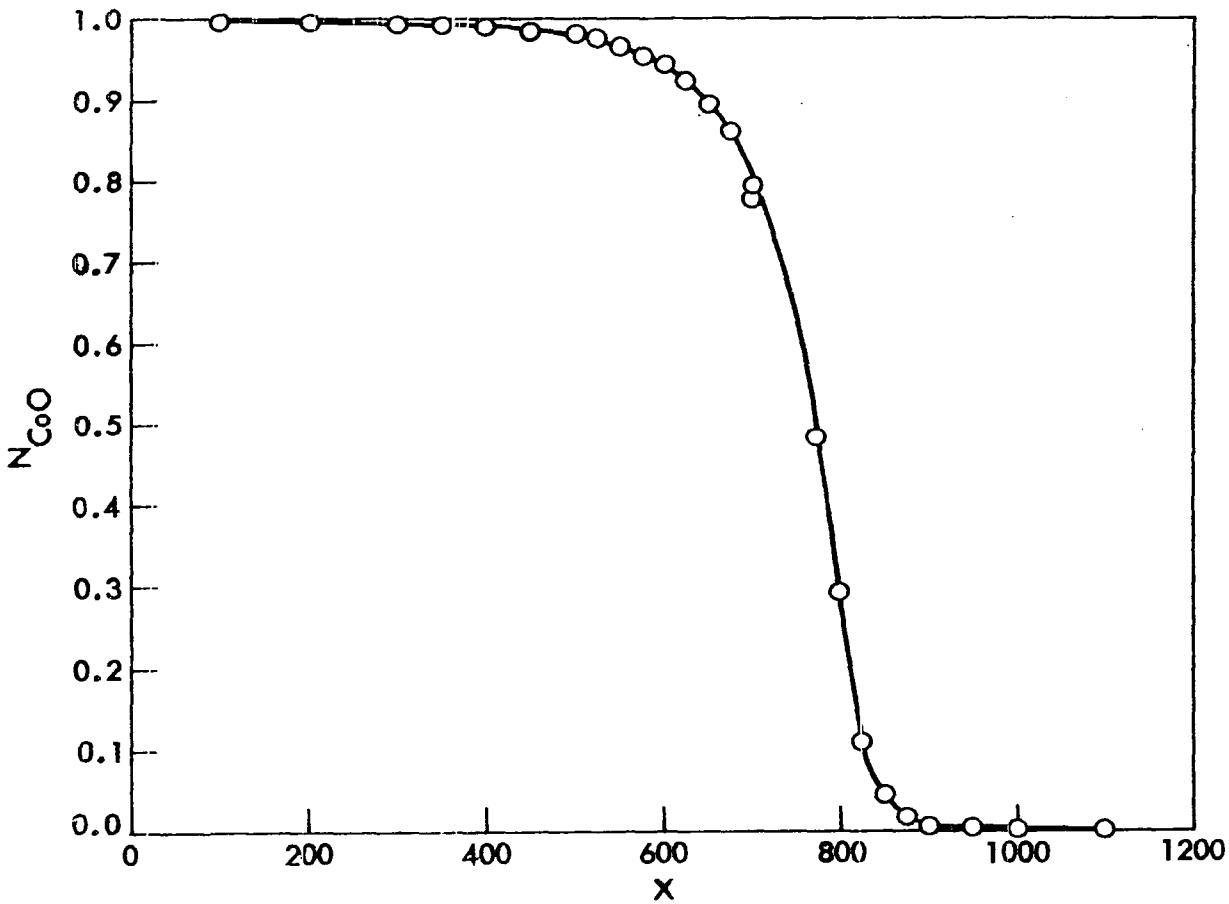

Figure 32. Concentration profile for specimen 15

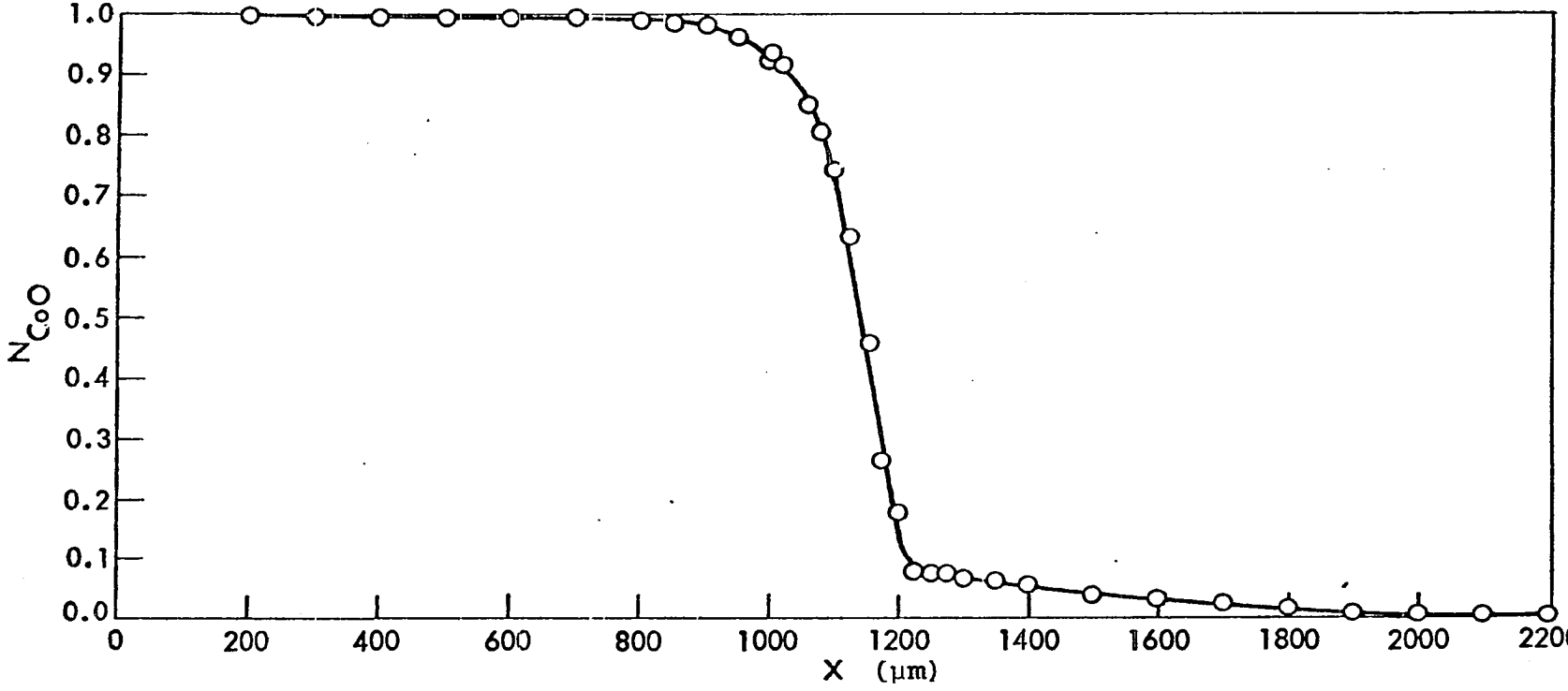

Figure 33. Concentration profile for specimen 16

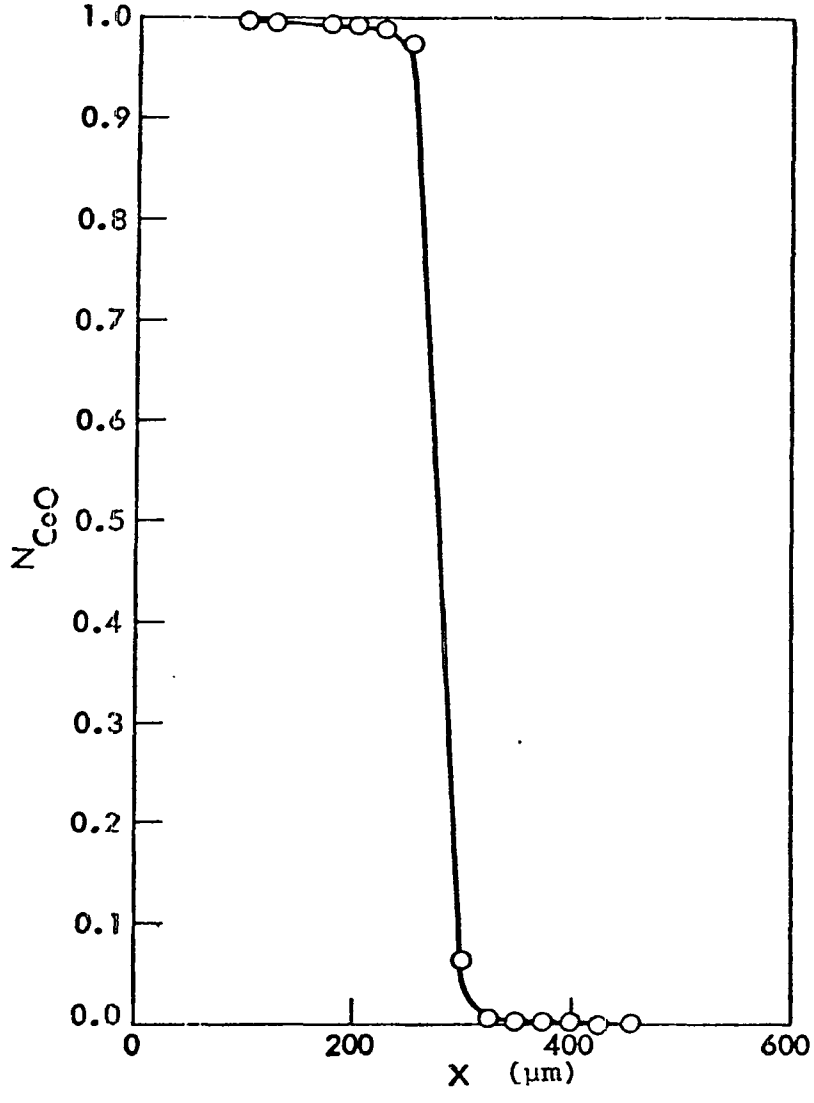

Figure 34. Concentration profile for specimen 17

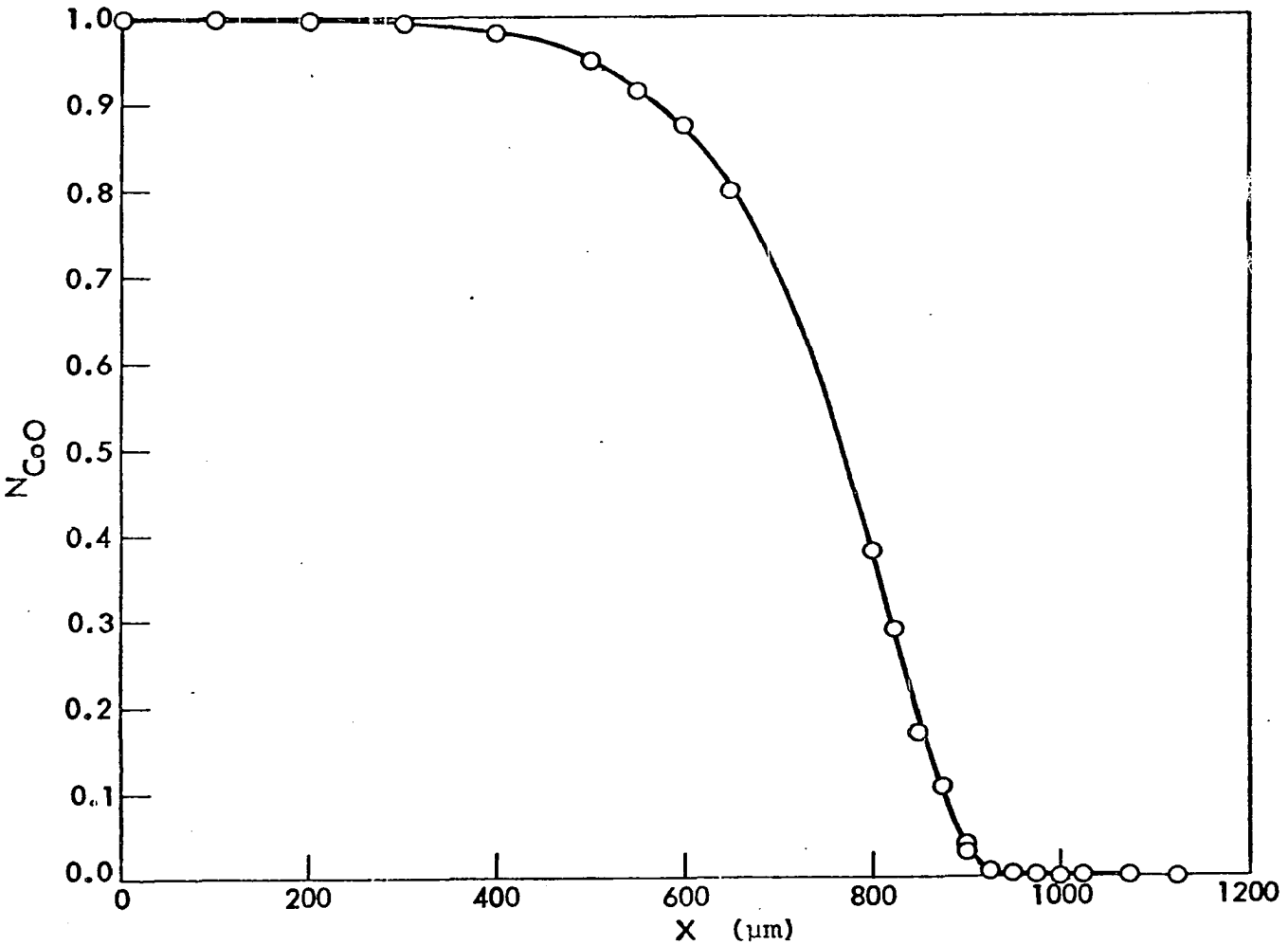

Figure 35. Concentration profile for specimen 18

on the Mn_xO rich side of the diffusion couple than on the MgO rich side allowing the qualitative conclusion that the interdiffusion coefficient is higher at higher Mn_xO concentrations. Concentration profiles in the system Ni_xO-Co_xO, Figures 25-35, exhibit greater curvature in the higher Co_xO concentration region allowing the qualitative conclusion that the interdiffusion coefficient increases as Co_xO concentration increases.

An experiment was performed to illustrate the effect of contact between constituents of the diffusion couple on the value of the interdiffusion coefficient. Diffusion specimen 6 consisted of an MgO single crystal held in contact with a polished Mn_xO polycrystal whereas diffusion specimen 7 consisted of an MgO single crystal lightly packed in finely ground Mn_xO powder. Specimens 6 and 7 were annealed simultaneously. The resulting concentration profiles are shown in Figures 23 and 24. The concentration profile for specimen 6 assumed a similar curvature to that of other samples in the Mn_xO-MgO system. The concentration profile for sample 7 exhibits a very steep slope at high Mn_xO concentrations and an exaggerated concentration tail extending into the MgO single crystal. This profile suggests that the diffusion process was limited by transfer across a boundary between the single crystal and the surrounding powder. The differences in the value of $\tilde{D}$ for specimens 6 and 7 are shown in Figure 36.

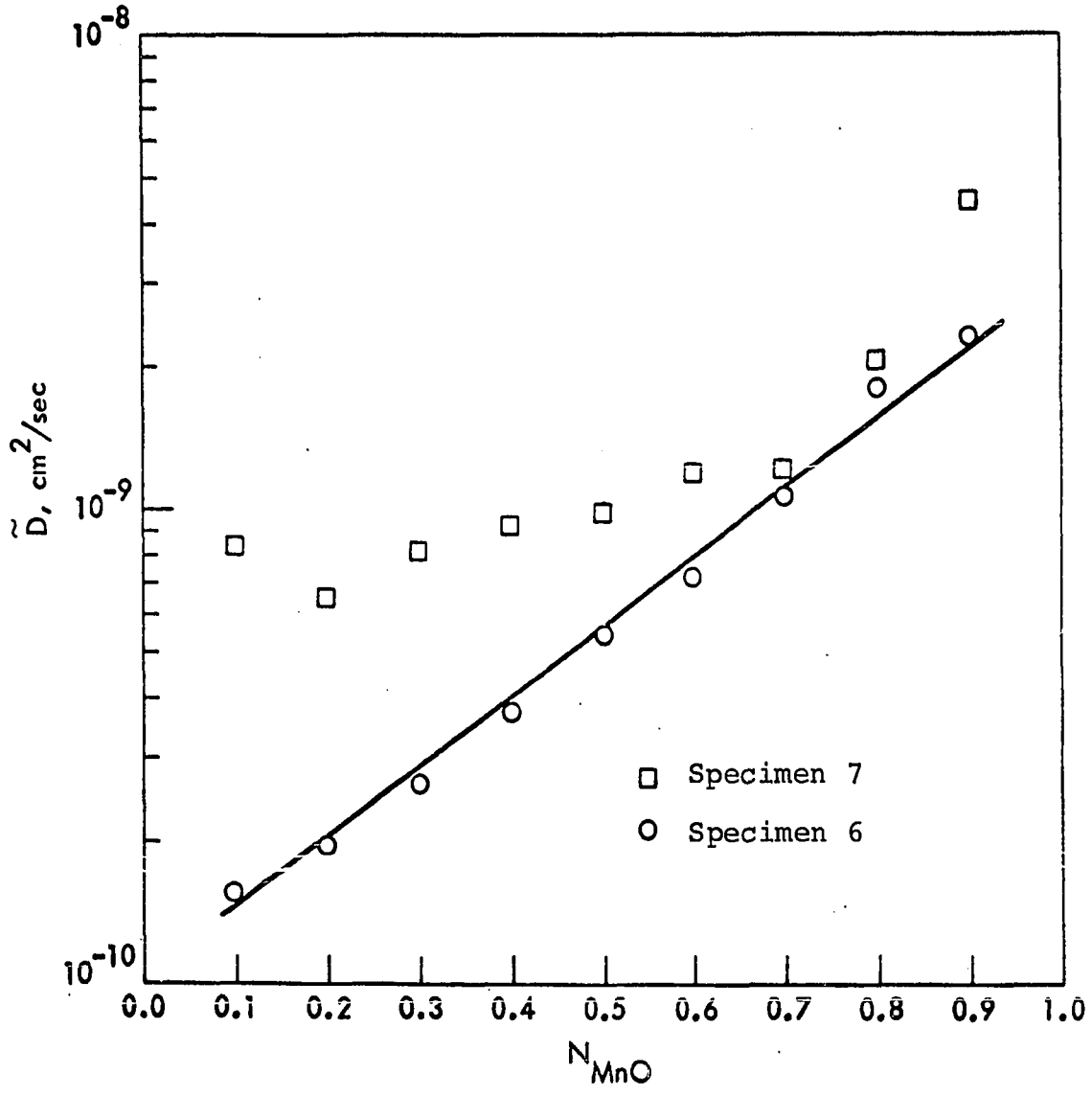

Figure 36. Effect of physical contact at diffusion interface in the system Mn_xO-MgO at 1529±4°C and p_{O_2} = 10^{-9} atm

The concentration dependence for $\tilde{D}$ for specimen 6 follows the expected linear relationship. The values of $\tilde{D}$ obtained from specimen 7 probably exhibit considerable error both from the difficult graphical analysis of a profile containing such a steep slope and from the uncertainty in locating the point $N_{Mn_xO} = 1$ in the very porous packing material.

A similar experiment was performed in the system Ni_xO-Co_xO by varying the roughness of single crystals utilized in the diffusion couple. Diffusion specimen 10 was composed of cleaved single crystals with no polishing treatment whereas specimen 9 was polished in the normal manner. The concentration profiles for these specimens which were simultaneously annealed are shown in Figures 26 and 27. Comparison of $\tilde{D}$ obtained from these concentration profiles is shown in Table 8. The values of $\tilde{D}$ for specimen 10 are lower than those for specimen 9 indicating the effect of roughness at the diffusion joint was to lower the rate of material transport. The nonlinear relationship between $\tilde{D}$ and N_{CoO} for specimen 10 is attributed to error in slope measurement.

Two experiments were performed to determine if surface diffusion or dislocation diffusion modes influenced the results of the experiments. These experiments consisted of simultaneously annealing two similar diffusion couples, quenching one couple, and annealing the remaining couple for an additional period. The resulting values of $\tilde{D}$

Table 8. Comparison of $\tilde{D}$ for specimens 9 and 10

N_{CoO}	$\tilde{D}$ (Specimen 9)	$\tilde{D}$ (Specimen 10)
0.2	1.02×10^{-9}	7.61×10^{-10}
0.3	1.16×10^{-9}	8.14×10^{-10}
0.4	1.33×10^{-9}	8.38×10^{-10}
0.5	1.76×10^{-9}	9.18×10^{-10}
0.6	2.12×10^{-9}	8.68×10^{-10}
0.7	3.7×10^{-9}	7.82×10^{-10}
0.8	5.45×10^{-9}	6.40×10^{-10}
0.9	8.19×10^{-9}	5.26×10^{-10}

computed from the appropriate concentration profiles are compared in Figure 37 for specimens 3 and 4 (Mn_xO-MgO couple) and in Table 9 for samples 8 and 9 (Ni_xO-Co_xO couple). Excellent agreement was found in both experiments. The effect of the operation of a low activation energy process such as dislocation or surface diffusion might have appeared as a concentration enhancement particularly at low concentrations. Such an effect apparently did not influence results under these stated experimental conditions.

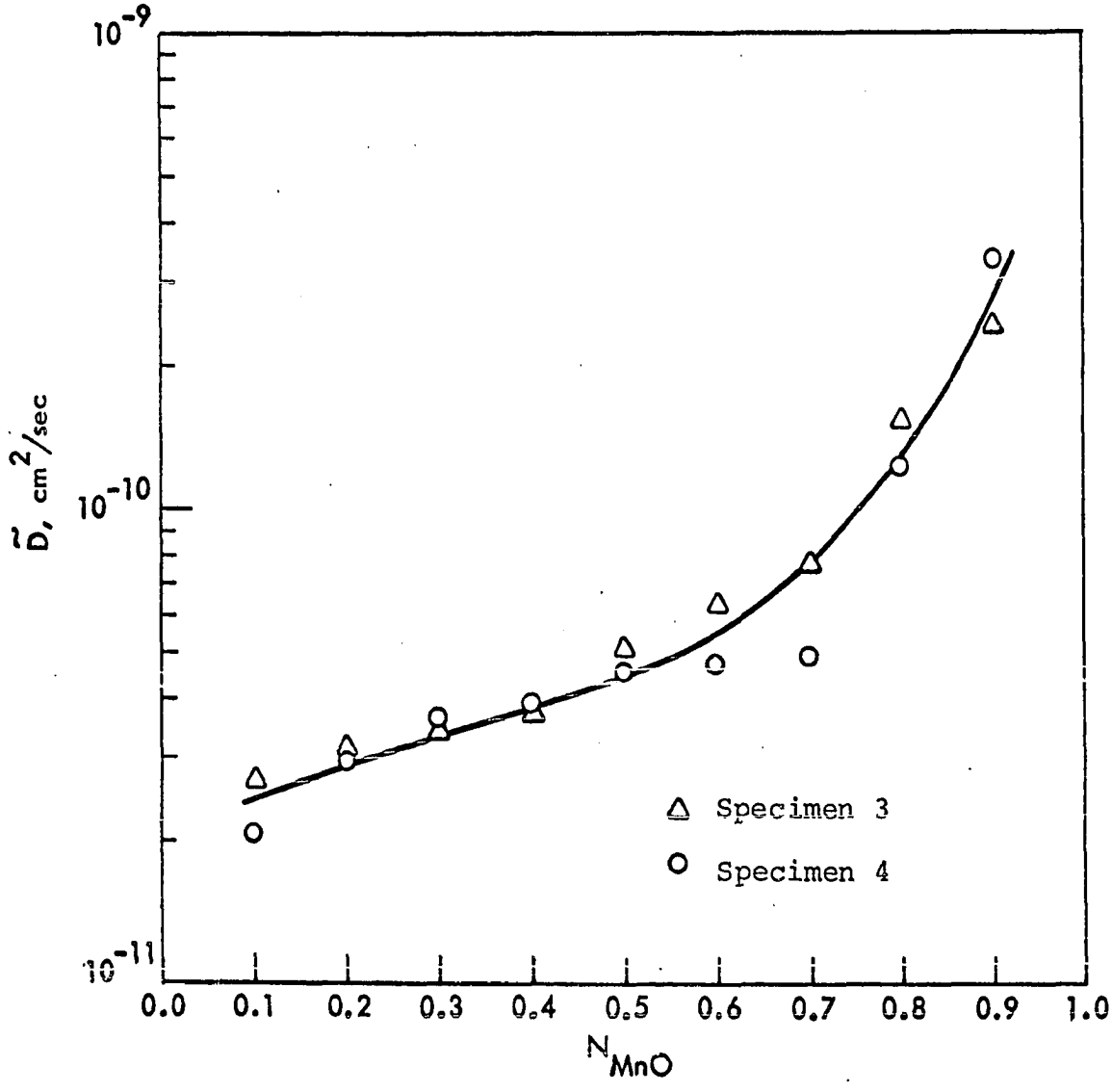

Figure 37. Comparison of simultaneously annealed specimens in the Mn_xO-MgO system

Table 9. Comparison of $\tilde{D}$ obtained from specimens 8 and 9

N_{CoO}	$\tilde{D}$ (Specimen 8)	$\tilde{D}$ (Specimen 9)
0.3	8.66×10^{-10}	1.16×10^{-9}
0.4	1.31×10^{-9}	1.33×10^{-9}
0.5	1.36×10^{-9}	1.76×10^{-9}
0.6	1.58×10^{-9}	2.12×10^{-9}
0.7	1.88×10^{-9}	3.71×10^{-9}
0.8	3.50×10^{-9}	5.45×10^{-9}
0.9	4.29×10^{-9}	8.19×10^{-9}

Representative results for the calculation of D in the system Mn_xO-MgO are shown in Figures 38 and 39. In Figure 38 the expression for $\tilde{D}$ at 1529±4°C and $p_{O_2} = 10^{-9}$ is given as

$$\tilde{D} = 3.83\times10^{-8}\ cm^2/s)\ \exp(-3.53\ N_{MgO}). \qquad (102)$$

Figure 39 shows that the data at 1348±4°C and $p_{O_2} = 10^{-9}$ atm can be represented by two slopes as follows:

$$\tilde{D}(N_{MnO} = 0.1\text{-}0.4) = (1.43\times10^{-9}\ cm^2/s)\ \exp(-0.46\ N_{MgO}) \qquad (103)$$

$$\tilde{D}(N_{MnO} = 0.6\text{-}0.9) = (2.54\times10^{-8}\ cm^2/s)\ \exp(-2.04\ N_{MgO}). \qquad (104)$$

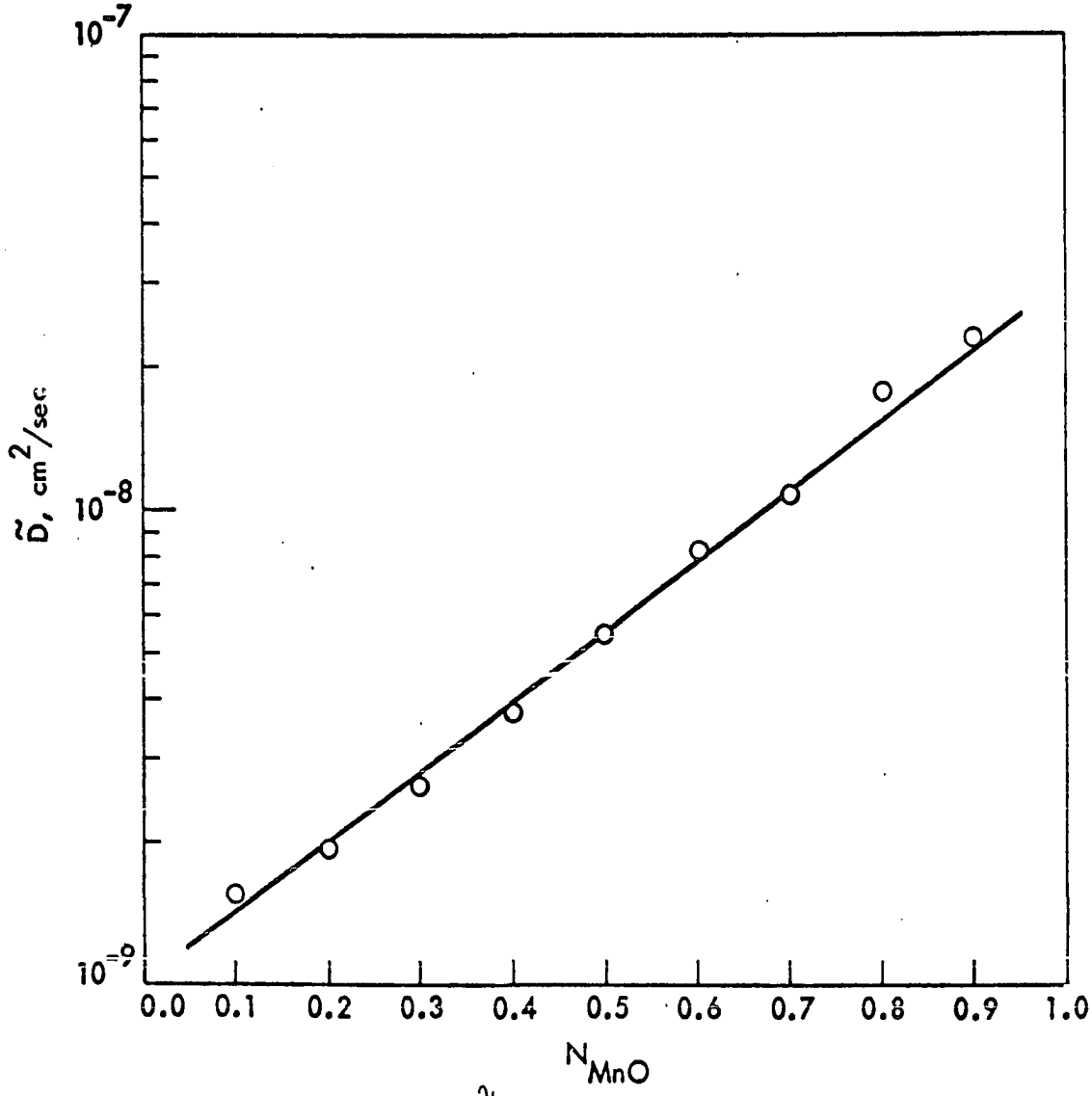

Figure 38. Variation of $\tilde{D}$ with N_{MnO} at 1529±4°C and $p_{O_2} = 10^{-9}$ atm

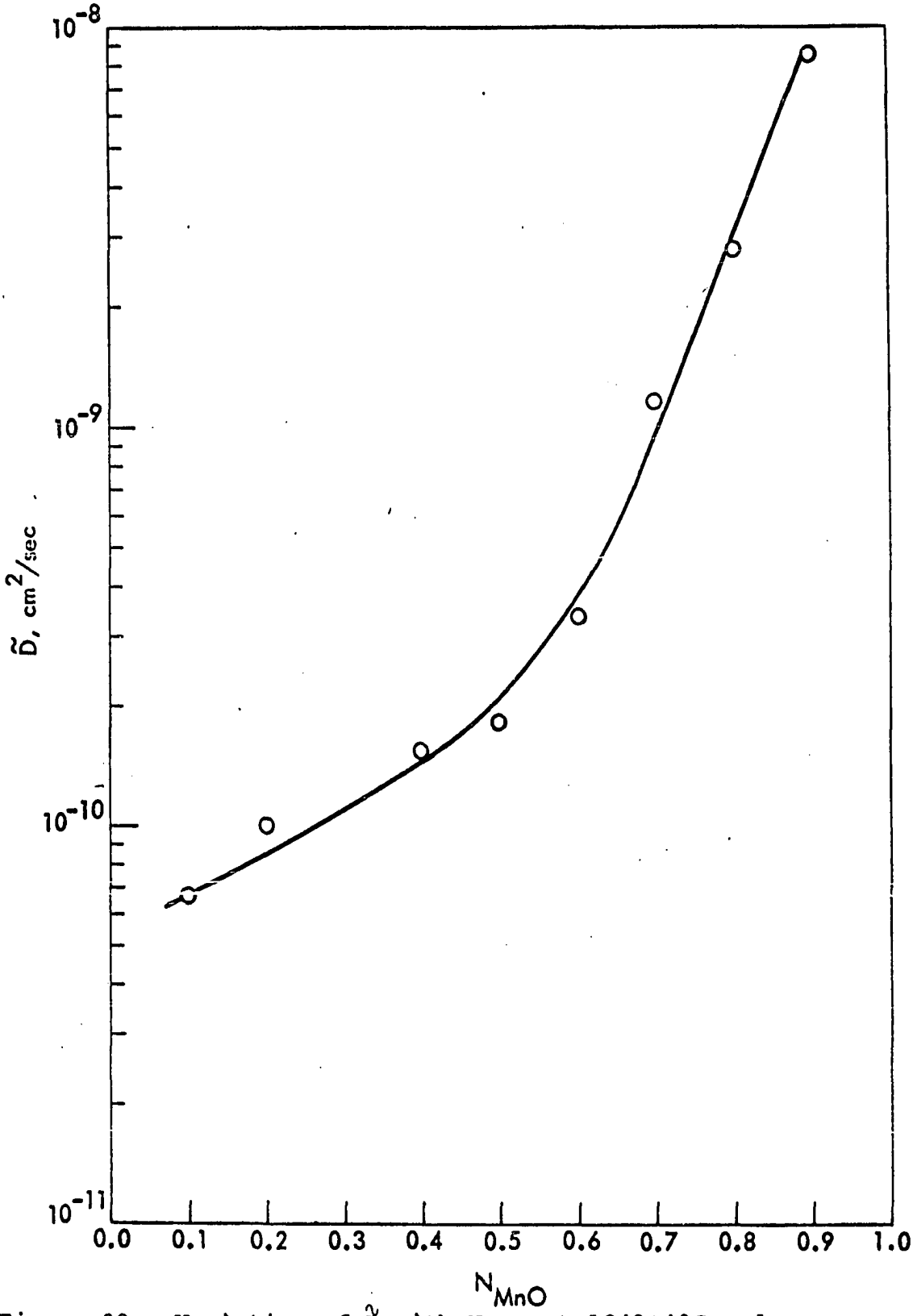

Figure 39. Variation of $\tilde{D}$ with N_{MnO} at 1348±4°C and p_{O_2} = 10^{-9} atm

Representative results for the calculation of $\tilde{D}$ in the system Ni_xO-Co_xO are shown in Figures 40 and 41. In Figure 40 the results at 1367±4°C and p_{O_2} = 0.21 atm can be represented by

$$\tilde{D} = (1.39\times10^{-8}\ cm^2/s)\ \exp(-3.42\ N_{NiO}). \qquad (105)$$

The data in Figure 41 for 1145±1°C at p_{O_2} = 0.21 atm can be represented by

$$\tilde{D}(N_{CoO} = 0.4\text{-}0.9) = (2.14\times10^{-9}\ cm^2/s)\ \exp(-3.58\ N_{NiO}). \qquad (106)$$

The data for $p_{O_2} = 9\times10^{-5}$ atm for the system Ni_xO-Co_xO is shown in Figures 42 and 43. The data at 1410±3°C can be represented by the expression

$$\tilde{D} = (1.82\times10^{-9}\ cm^2/s)\ \exp(-2.01\ N_{NiO}). \qquad (107)$$

The data at 1268±2°C shown in Figure 43 may be represented by the following:

$$\tilde{D}(N_{CoO} = 0.1\text{-}0.6) = (7.26\times10^{-11}\ cm^2/s)\ \exp(-0.66\ N_{NiO}) \qquad (108a)$$

$$\tilde{D}(N_{CoO} = 0.7\text{-}0.9) = (3.11\times10^{-10}\ cm^2/s)\ \exp(-5.49\ N_{NiO}). \qquad (108b)$$

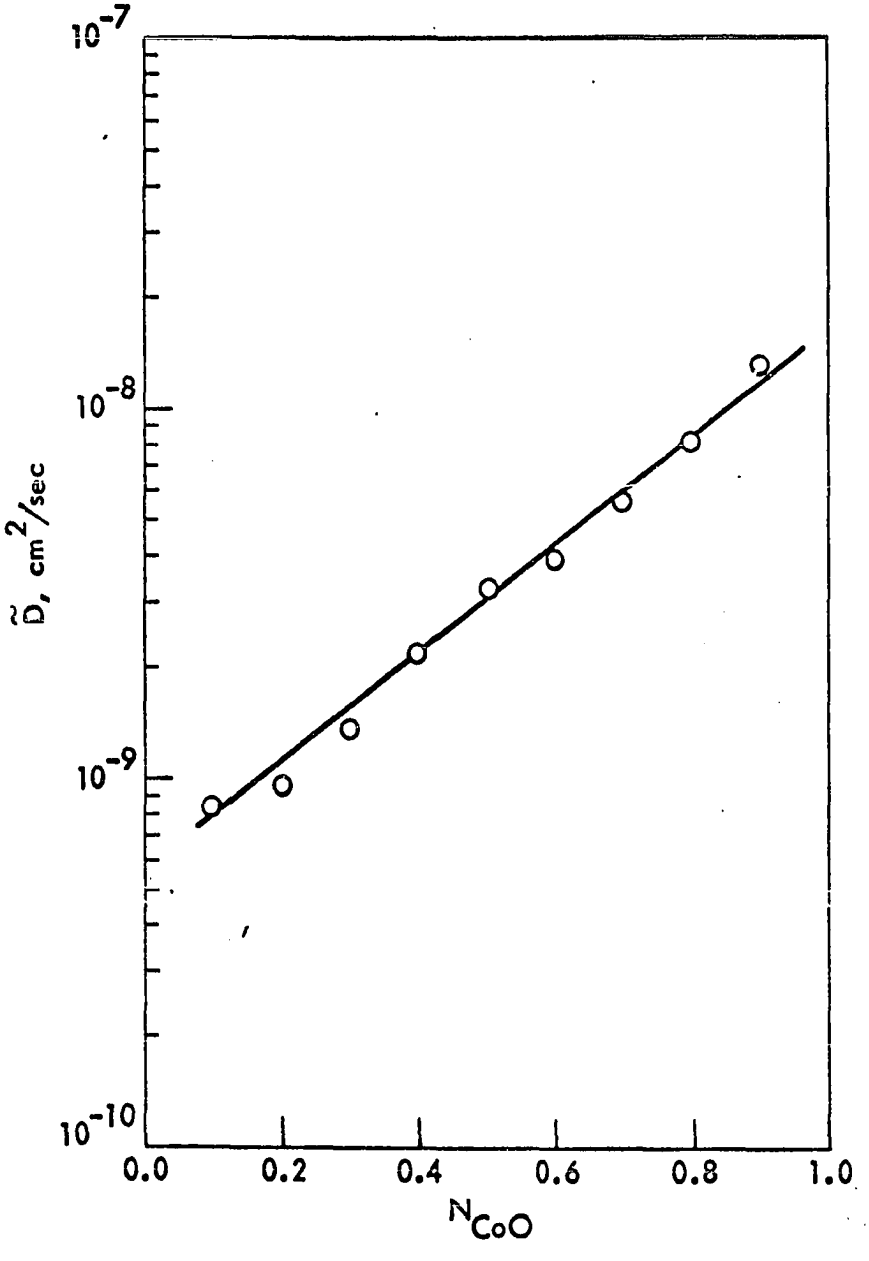

Figure 40. Variation of $\tilde{D}$ with N_{CoO} at 1367±4°C at p_{O_2} = 0.21 atm

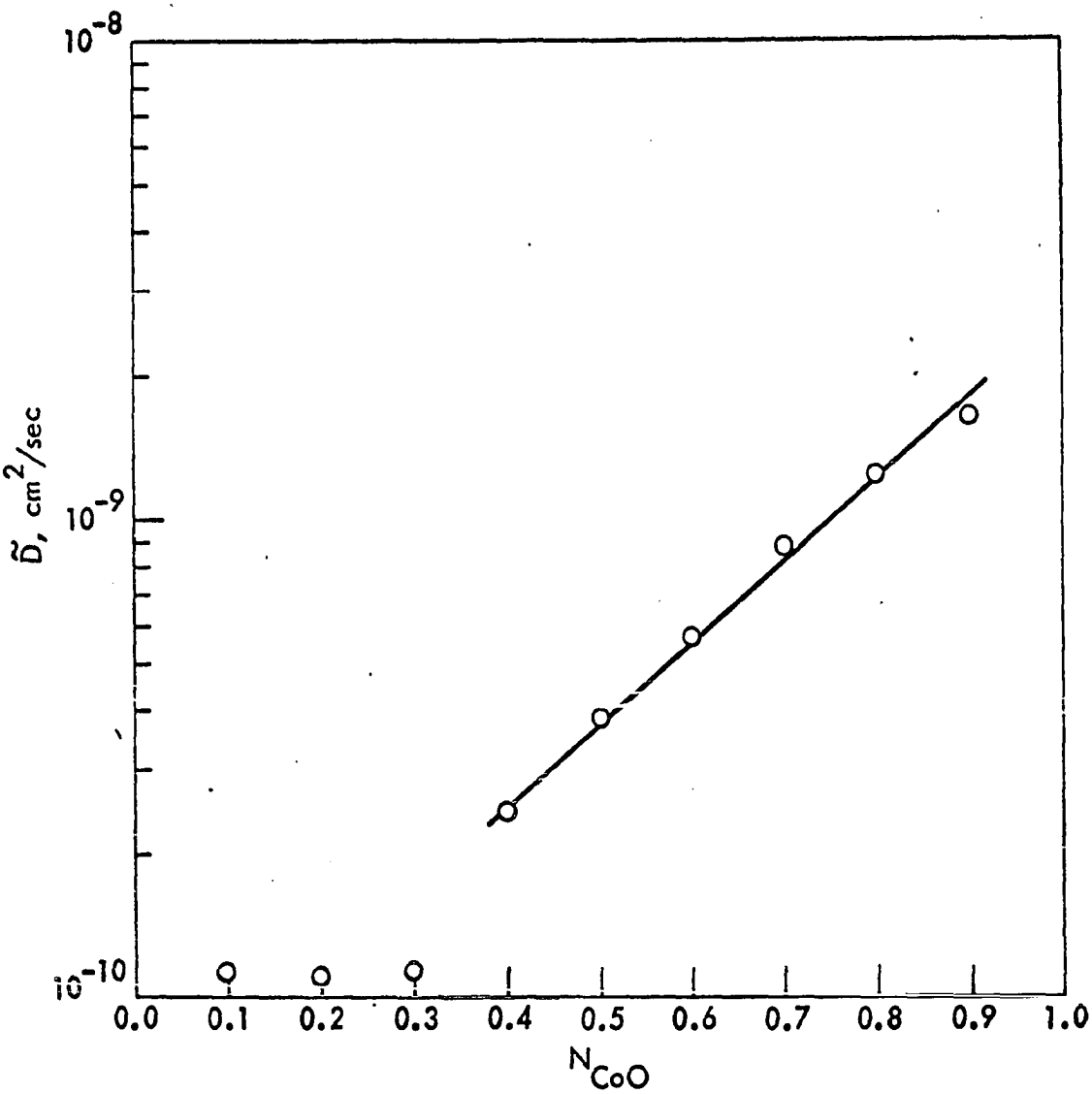

Figure 41. Variation of $\tilde{D}$ with N_{CoO} at 1145±1°C at p_{O_2} = 0.21 atm

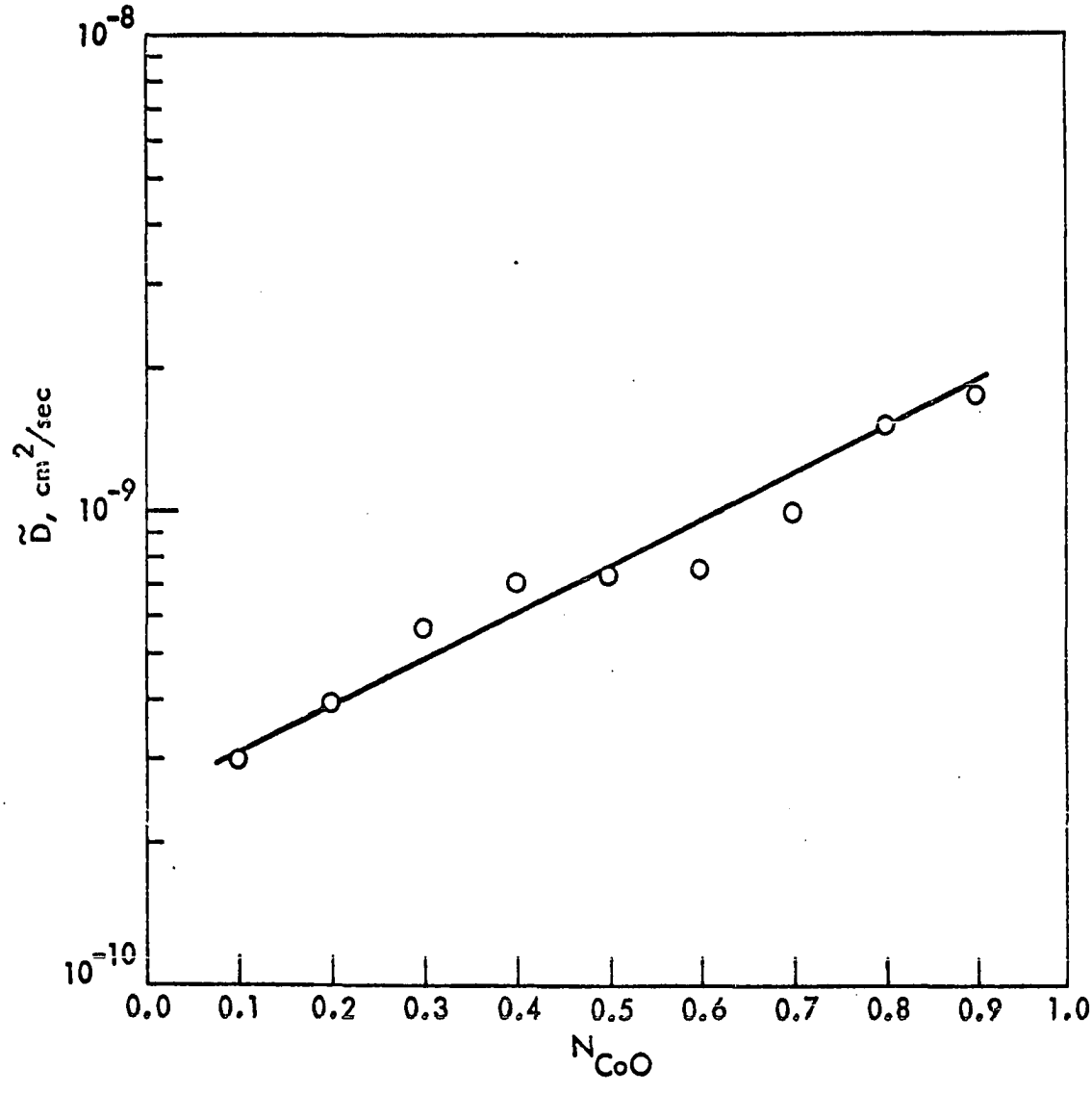

Figure 42. Variation of $\tilde{D}$ with N_{CoO} at 1410±3°C at p_{O_2} = 9×10^{-5} atm

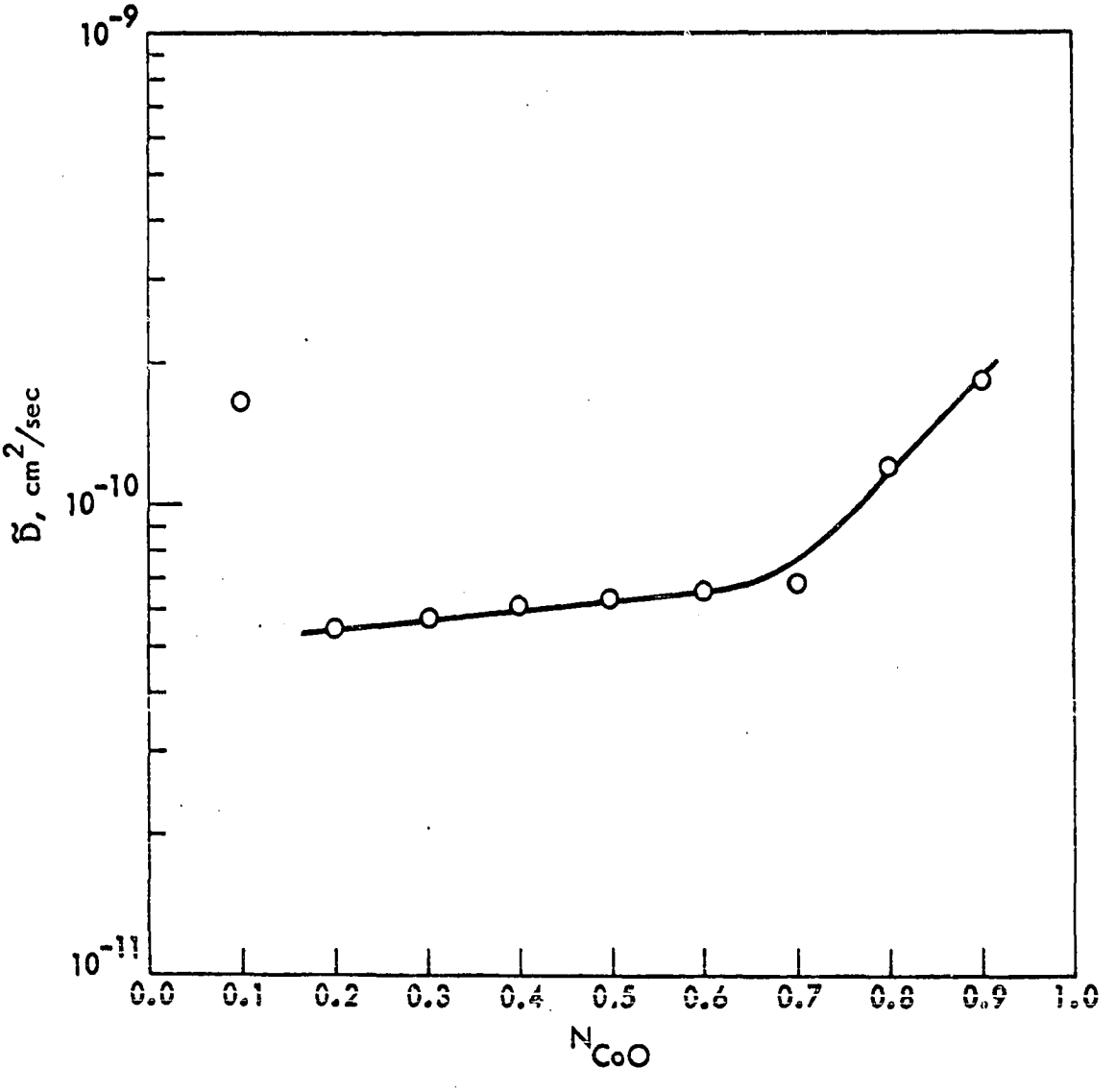

Figure 43. Variation of $\tilde{D}$ with N_{CoO} at 1268±2°C at p_{O_2} = 9×10^{-5} atm

The high value of $\tilde{D}$ at $N_{CoO} = 0.1$ shown in Figure 43 suggests that the nonlinear relation between D and concentration actually assumes the configuration of a dip at intermediate concentrations. A comparison between low concentration values of D for diffusion couples annealed under similar conditions is given in Table 10. Since crystals used in the construction of specimen 8 were of the same purity as those utilized in construction of specimen 9, it is improbable that differences in defect concentrations were important if in fact the dip for specimen 8 was the result of some physical phenomena.

Table 10. Comparison of low concentration $\tilde{D}$ values for diffusion specimens 8 and 9

N_{CoO}	$\tilde{D}$ (Specimen 8)	$\tilde{D}$ (Specimen 9)
0.1	2.67×10^{-9}	8.59×10^{-10}
0.2	8.97×10^{-10}	1.02×10^{-9}
0.3	8.66×10^{-10}	1.16×10^{-9}
0.4	1.31×10^{-9}	1.33×10^{-9}

Barr and Lidiard (83) have observed a dip in the electrical conductivity of AgCl with increasing defect concentration. In this system silver interstitials, $Ag_i^{\cdot}$, are considered the dominant mobile defect species. Upon the addition of silver interstitials to AgCl, the conductivity

increases linearly with concentration. The addition of silver vacancies, V'_{Ag}, causes the conductivity to pass through a minimum and then to increase to a final value. These considerations suggest that a similar situation could have influenced the results in the Ni_xO-Co_xO system.

Although Stiglich (10) and Hed (66) suggest the possibility of interstitial occupation in the Ni_xO-Co_xO system, it is improbable that this phenomena could have contributed to the formation of the dip. If interstitial occupation did significantly influence the diffusion mechanism then the dip would be expected to disappear at higher temperatures where interstitials could overshadow vacancies. Then at lower temperatures where vacancies might predominate such a dip might appear. The data, i.e. Figures 42 and 43, does show the dip disappears at high temperatures; however, the data in Table 10 shows the dip to appear and disappear in the same experiment.

Another explanation for a dip in $\tilde{D}$ could be a nonlinear variation in the activity coefficient of one component with increasing concentration in the solid solution. Such an effect has been discussed by Jost (13) for metallic systems. Evidence indicates, however, that Ni_xO and Co_xO form an ideal solution. Sakata and Sakata (84) have observed the lattice parameter to vary linearly with composition in Ni_xO and Co_xO solid solutions above 850°C indicating that the

change in volume on mixing is zero. Stiglich (10) points out that it is not unlikely that the enthalpy of mixing of Ni_xO and Co_xO is zero because of their adjacent position on the periodic table of elements. These factors imply that the activity coefficient should be unity thereby eliminating any thermodynamic contribution to the dip in $\tilde{D}$.

Recent isotope effect measurements in Co_xO, Ni_xO, and Co_xO-Ni_xO systems suggest that no change in diffusion mechanism exists over the range of temperature and oxygen partial pressure of interest. For example, Chen, Peterson, and Reeves (85) found the isotope effect to be constant with temperature for Ni_xO in the range 1081-1411°C. These authors attributed their results to the existence of a cation vacancy mechanism. Volpe, Peterson, and Reddy (86) have found the isotope effect to be constant for Co_xO in the range 1201-1678°C at p_{O_2} = 1 atm. These results were also held consistent with a cation vacancy mechanism. Chen and Peterson (87) indicate no change in the isotope effect with temperature for the system Co_xO-Ni_xO.

Based on the evidence presented above it is likely that the dip is due to inaccuracy of slope measurement with the resulting error appearing in the calculation of $\tilde{D}$. It is also likely that this error should be more pronounced for experiments at low temperatures, i.e. where steeper slopes exist in the concentration profiles.

Extrapolation of Equations 105-108 allows comparison of $\tilde{D}$ at $N_{CoO} = 0$ and $N_{CoO} = 1$ with measurements of tracer diffusion coefficients in Ni_xO and Co_xO. Whitney and Stubican (88) have recently shown for diffusion of a trivalent cation in a dilute solid solution in MgO, $\tilde{D}$ may be related to the self diffusion coefficient, D_{self}, of the trivalent cation through

$$\tilde{D} \simeq \frac{3}{2} D_{self} \cdot \tag{109}$$

If $\partial \ell n \gamma^* / \partial \ell n N^* = 0$, $D_{self} = D^*$, therefore

$$\tilde{D} \simeq \frac{3}{2} D^*. \tag{110}$$

Results of the extrapolation are given in Table 11 where appropriate values of D^* are given from the work of Crow (7) Shim and Moore (49). The values of $\tilde{D}$ in Table 11 are comparable to or slightly less than those of D^*. One possible explanation for the apparent low values of $\tilde{D}$ is that at low impurity concentrations the relation between $\tilde{D}$ and concentration may be parabolic, etc., rather than exponential. Jones and Cutler (65) found $\tilde{D}$ to increase linearly with mole percent Mn in the system Mn_xO-MgO at 1500°C and $p_{O_2} = 10^{-9}$ atm at low Mn concentrations.

The activation energy for the diffusion process may be calculated through consideration of the variation of $\tilde{D}$ with both impurity concentration and temperature. The relation

Table 11. Comparison of $\tilde{D}(N_{CoO} = 0)$ and $\tilde{D}(N_{CoO} = 1)$ to D^*_{Ni} and D^*_{Co}

p_{O_2} Reference	T (°C)	$D(N_{CoO} = 0)$ This work	$D(N_{CoO} = 1)$ This work	D^*_{Ni} Crow (7)	D^*_{Co} Crow (7)	D^*_{Ni} Shim and Moore (49)
10^{-5}	1268	3.7×10^{-11}	3.1×10^{-9}	6×10^{-11}[a]	8×10^{-9}[a]	-
0.21	1145	5.8×10^{-11}	2.1×10^{-9}	5.3×10^{-11}[b]	1.8×10^{-8}[b]	8.1×10^{-11}
	1367	4.6×10^{-10}	1.4×10^{-8}	6.7×10^{-10}[b]	9.3×10^{-8}[b]	6.9×10^{-10}

[a] $p_{O_2} = 5\times10^{-5}$ atm.

[b] $p_{O_2} = 1.0$ atm.

between $\tilde{D}$ and concentration is, as before,

$$\tilde{D} = C \exp(-\beta N). \tag{111}$$

The interdiffusion coefficient also obeys the Arrhenius relation

$$\tilde{D} = D_o \exp(-Q/RT) \tag{112}$$

where D_o is a constant called the frequency factor, Q is the diffusion activation energy, R is the gas constant, and T is absolute temperature. Combining Equations 111 and 112, the expression for $\tilde{D}$ becomes

$$\tilde{D} = D_o' \exp(-\beta N) \exp(-Q/RT). \tag{113}$$

The quantity Q may then be obtained from the slope of a plot of $\log_e[\tilde{D}/\exp(-\beta N)]$ versus 1/T. These plots for the systems Mn_xO-MgO and Ni_xO-Co_xO are shown in Figures 44-46.

The activation energy for the system Mn_xO-MgO was found to be 2.8 ev. This value is higher than that of about two ev reported by Jones and Cutler (65) for the same system (and same temperature range) at $p_{O_2} = 0.21$. Consideration, however, must be given to the fact that at about 10^{-9} atm the stoichiometric compound MnO exists (at the temperatures of interest), i.e. the induced cation vacancy concentration in MgO is very low. Therefore the diffusion activation energy would approximate the activation energy of motion of the divalent cations

Figure 44. Arrhenius plot for the system Mn_xO-MgO at $p_{O_2} = 10^{-9}$ atm

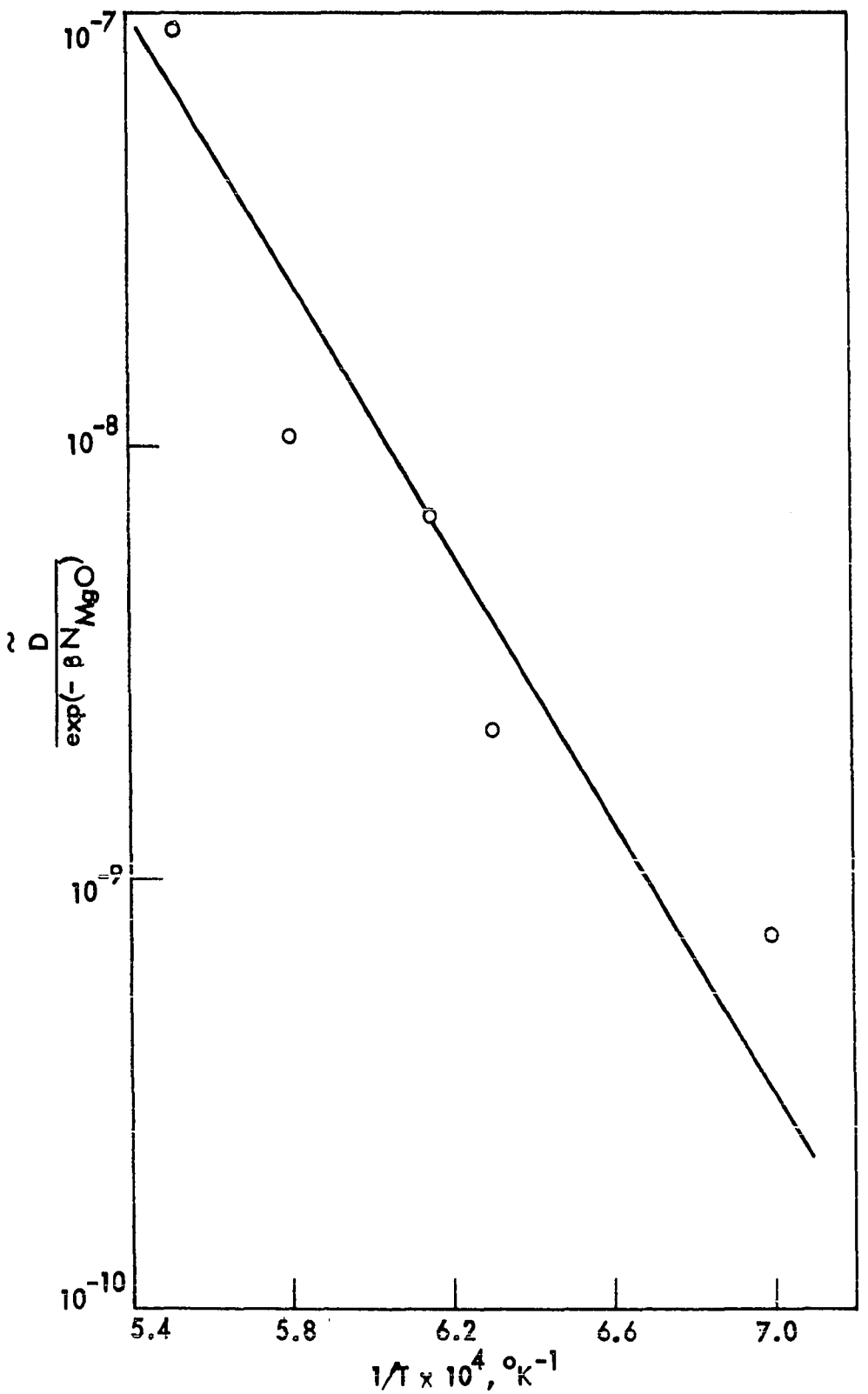
10^{-7}
10^{-8}
10^{-9}
10^{-10}
$\frac{D}{\exp(-\beta N_{MgO})}$
5.4
5.8
6.2
6.6
7.0
$1/T \times 10^4$, $^oK^{-1}$

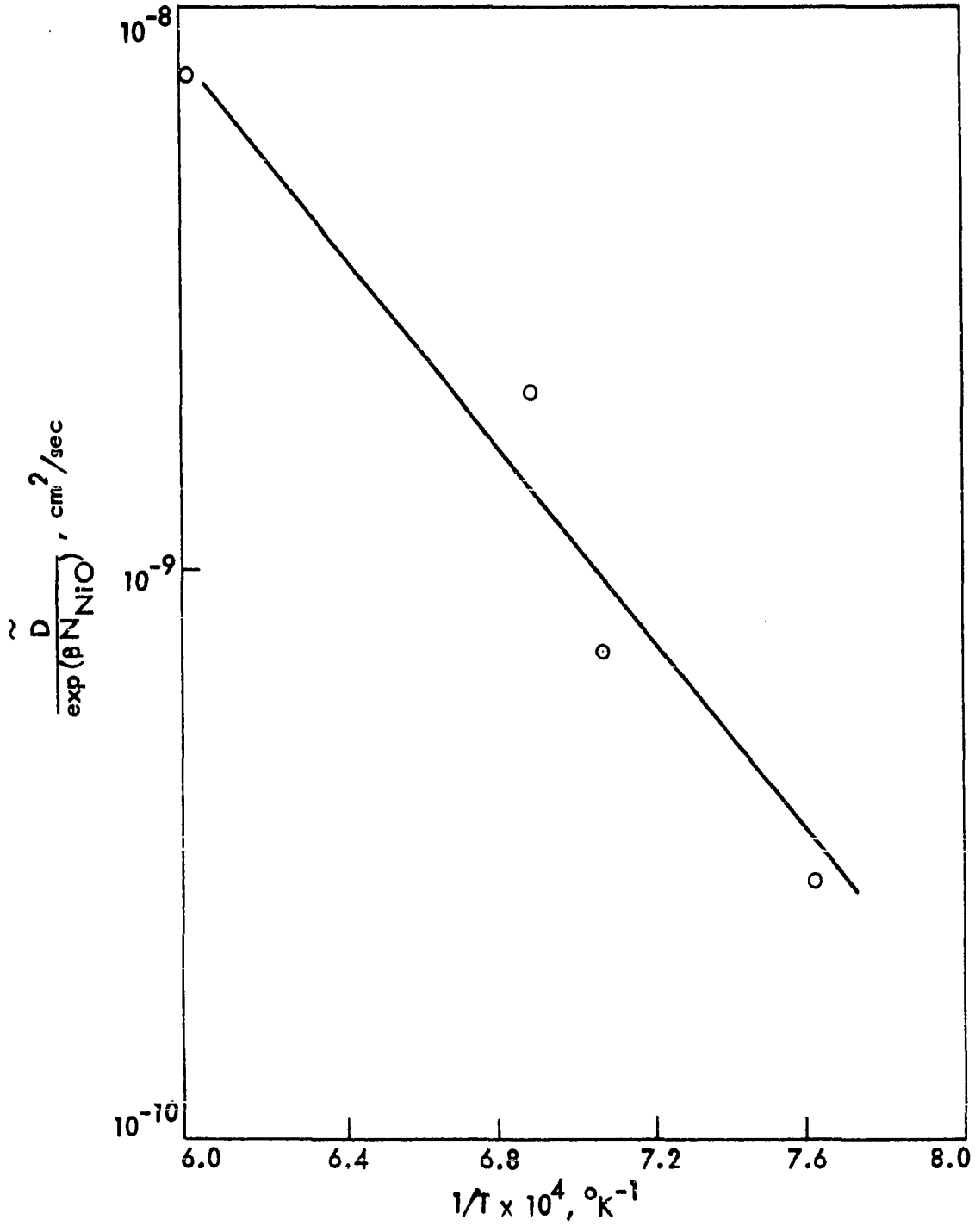

Figure 45. Arrhenius plot for the system Ni_xO-Co_xO at p_{O_2} = 0.21 atm

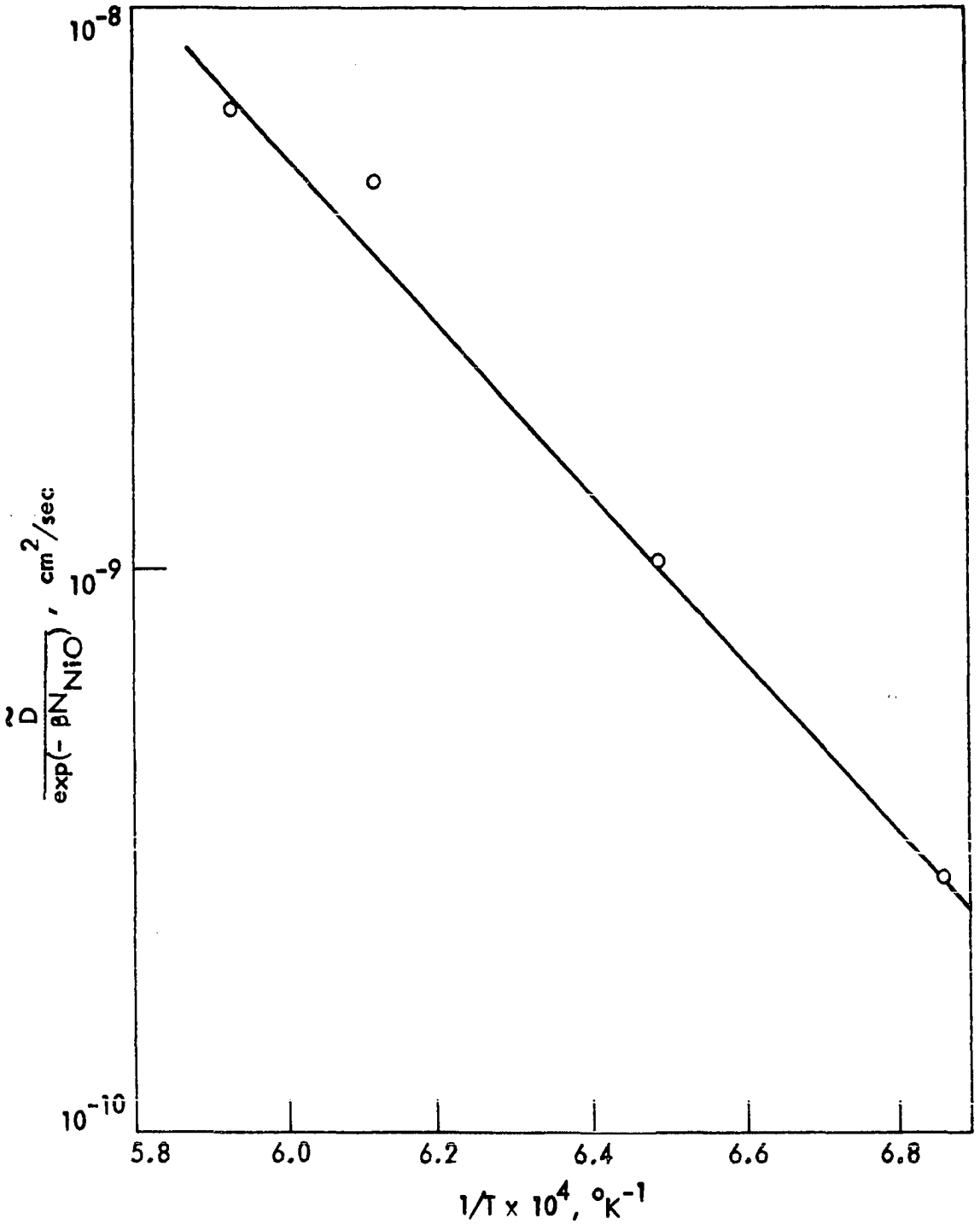

Figure 46. Arrhenius plot for the system Ni_xO-Co_xO at $p_{O_2} = 9 \times 10^{-5}$ atm

Mg^{2+} and Mn^{2+}. The value of Q = 2.8 ev at $p_{O_2} = 10^{-9}$ atm is of the same magnitude expected of the diffusion of divalent cations in MgO of about two to four ev (89).

The activation energies for the system Ni_xO-Co_xO at p_{O_2} = 0.21 atm and at $p_{O_2} = 9x10^{-5}$ atm were found to be 1.9 ev and about 3 ev respectively. The value of Q for diffusion in air is comparable to the results of Stiglich (10) who found Q for $1/T \times 10^4 < 6.4$ of about 2.3 ev and for $1/T \times 10^4 > 6.4$ of about 1.8 ev. The value of about 3 ev for the Ni_xO-Co_xO system at $p_{O_2} = 9x10^{-5}$ atm appears anomalously high in relation to the results of Stiglich (10) who found Q for $1/T \times 10^4 < 6.5$ of about 2 ev and for $1/T \times 10^4 > 6.5$ about 1.5 ev.

A possible explanation of this high value of Q at $9x10^{-5}$ atm p_{O_2} is error in the actual p_{O_2} experienced by diffusion specimens. It has been recently disclosed that premixed commercial gases may segregate upon standing due to the different densities of the gases (Berard, 90). In such a case a premixed cylinder containing argon and oxygen would produce a mixture relatively enriched in oxygen during the early stage of consumption of the cylinder contents and relatively enriched in argon during the later stage of consumption. This phenomena is indicated by the experimental data wherein if

$$\tilde{D} \propto p_{O_2}^{1/x} \tag{114}$$

at $1/T \times 10^4 = 6.4$, from Figures 45 and 46, $\tilde{D} \propto p_{O_2}^{0.049}$ and at $1/T \times 10^4 = 6.8$, $D \propto p_{O_2}^{0.34}$. The dependence of $\tilde{D}$ on p_{O_2} appears to increase as temperature is decreased. Since this order is the same as the order of processing experimental specimens using the same cylinder of premixed gas, i.e. processing high temperature diffusion anneals first, it is probable that the data for Ni_xO-Co_xO at "9×10^{-5} atm p_{O_2}" represents a series of experiments with continuously decreasing p_{O_2}.

CONCLUSIONS

(1) There is no obvious Kirkendall effect upon interdiffusion in the system Mn_xO-MgO. A Kirkendall effect is seen upon interdiffusion in the system Ni_xO-Co_xO as revealed by the movement of a line of pores which apparently act as inert markers indicating the magnitude of net material movement out of the Co_xO member of the diffusion specimen.

(2) Surface preparation and the resulting fit between members of the experimental diffusion specimens have been found to affect the results of diffusion experiments. The effect of poor contact at the interface between interdiffusing specimens is to lower values of the interdiffusion coefficient.

(3) The interdiffusion coefficient $\tilde{D}$ in the systems Mn_xO-MgO and Ni_xO-Co_xO was found to obey the relationship

$$\tilde{D} = \tilde{D}_o \exp(-\beta N_i) \exp(-Q/RT)$$

where $\tilde{D}_o$ is a constant, β is a constant for the given experimental conditions, N_i (i = MgO or i = NiO) is the mole fraction of constituent, Q is the diffusion activation energy, and T is absolute temperature. For the system Mn_xO-MgO at 1529 ± 4°C and $p_{O_2} = 10^{-9}$ atm, $\tilde{D}$ is represented by

$$\tilde{D} = (3.83 \times 10^{-8}\ cm^2/s) \exp(-3.53\ N_{MgO}).$$

For the system Ni_xO-Co_xO at p_{O_2} = 0.21 atm $\tilde{D}$ is represented by

$$\tilde{D} = (1.39 \times 10^{-8}\ cm^2/s)\ \exp(-\ 3.42\ N_{NiO}).$$

(4) The diffusion activation energy for the system Mn_xO-MgO in the range 1150 to 1529°C at $p_{O_2} = 10^{-9}$ atm was found to be 2.8 ± 0.7 ev. This value is of comparable magnitude to the diffusion of various divalent cations in MgO. There was no indication of a change in diffusion mechanism over the range of temperature investigated; however, considering the magnitude of experimental error involved in this determination, such a change in mechanism could have been masked by experimental error.

(5) The diffusion activation energy for the system Ni_xO-Co_xO in the range 1043 to 1367°C at p_{O_2} = 0.21 atm was found to be 1.9 ± 0.8 ev. There was no indication of a change in diffusion mechanism over the range of temperature investigated; however, considering the magnitude of experimental error involved in this determination, such a change in mechanism could have been masked by experimental error.

LITERATURE CITED

1. J. Crank, "Diffusion Coefficients in Solids, Their Measurement and Significance," Discuss. Faraday Soc., 23, 99-104 (1957).

2. P. G. Shewmon, Diffusion in Solids. McGraw-Hill Book Co., New York, 1963.

3. John R. Manning, Diffusion Kinetics for Atoms in Crystals. D. Van Nostrand Co., Inc., Princeton, New Jersey, 1968.

4. R. J. Friauf, "Correlation Effects for Diffusion in Ionic Crystals," J. Appl. Phys. Supp., 33 [1] 494-505 (1962).

5. Leonid V. Azàroff, "Role of Crystal Structure in Diffusion. I. Diffusion Paths in Closest-packed Crystals," J. Appl. Phys., 32 [9] 1658-62 (1961).

6. Leonid V. Azàroff, "Role of Crystal Structure in Diffusion. II. Activation Energies for Diffusion in Closest-packed Structures," J. Appl. Phys., 32 [9] 1663-65 (1961).

7. W. B. Crow, "Diffusion of Cobalt, Nickel, and Iron in Cobalt Oxide and Nickel Oxide," Tech. Rept. ARL-70-0090, Aerospace Research Laboratories, June 1970.

8. W. L. Roth, "On the Nature of Defects in the Magnetic Structure of Wüstite," J. Appl. Phys., 30 303S-04S (1960).

9. W. L. Roth, "Defects in the Crystal and Magnetic Structure of Ferrous Oxide," Acta Crystallogr., 13 [Part 2] 140-49 (1960).

10. J. J. Stiglich, "Interdiffusion and Defect Structure in NiO + CoO Solid Solutions"; Ph.D. Thesis, Northwestern University, Evanston, Illinois, 1970.

11. A. Fick, "Uber Diffusion," Progg. Ann., 94, 59, (1855). Original not available; cited in L. S. Darken, "Formal Basis of Diffusion Theory"; p. 1 in Atom Movements, American Society for Metals, Metals Park, Ohio, 1951.

12. L. S. Darken, "Diffusion, Mobility, and Their Interrelations Through Free Energy in Binary Metallic Systems," Trans. AIME, 175, 184-201 (1948).

13. W. Jost, Diffusion in Solids, Liquids, and Gases, Vol. I, 3rd printing (with Addendum). Academic Press, New York. 1960.

14. A. R. Cooper, Jr., and J. H. Heasley, "Extension of Darken's Equation to Binary Diffusion in Ceramics," J. Amer. Ceram. Soc., 49 [5] 280-84 (1966).

15. R. Lindström, "Chemical Diffusion in Alkali Halides," J. Phys. Chem. Solids, 30 [2] 401-05 (1969).

16. F. A. Kröger, The Chemistry of Imperfect Crystals. North-Holland Publishing Co., Amsterdam, 1964.

17. F. A. Kröger and H. J. Vink; pp. 307-435 in Solid State Phys. Edited by F. Seitz, and D. Turnbull. Academic Press, Inc., New York, 1956.

18. N. M. Tallan, R. W. Vest, and H. C. Graham, "Defect Structure and Electrical Properties of Some Refractory Metal Oxides," Mater. Sci. Res., 2 33-67 (1965).

19. A. J. Dekker, Solid State Physics. Prentice-Hall, Inc., New Jersey, 1965.

20. N. F. Mott and R. W. Gurney, Electronic Processes in Ionic Crystals, 2d. Clarendon Press, Oxford, 1948.

21. H. Bakker, "A Simple Straight-forward Method to Calculate the Correlation Factor and its Relation to the Isotope Effect for Impurity Diffusion," Phys. Status Solidi, 38 167-76 (1970).

22. N. N. Greenwood, Ionic Crystals, Lattice Defects and Nonstoichiometry. Butterworth and Co., London, 1954.

23. J. Yamashita and Tatsumi Kurosawa, "Formation Energy of Lattice Defects in Simple Oxide Crystals," J. Phys. Soc. Jap., 9, 944-53 (1954).

24. B. C. Harding, D. M. Price, and A. J. Mattlock, "Cation Self-diffusion in Single Crystal MgO," Phil. Mag., 23 [182] 399-08 (1971)

25. L. H. Rovner, "Diffusion of Oxygen in Magnesium Oxide," Naval Research Technical Report No. 10, March 1, 1971.

26. A. Z. Hed and D. S. Tannhauser, "Contribution to the Mn-O Phase Diagram at High Temperature," J. Electrochem. Soc., 114 [4] 314-18 (1967).

27. M. W. Davies and R. D. Richardson, "Nonstoichiometry of Manganous Oxide," Trans. Faraday Soc., 55, 604-10 (1959).

28. N. G. Eror, "Electrical Conductivity and Thermogravimetric Studies on CoO, NiO, and MnO"; Ph.D. Thesis, Northwestern University, Evanston, Illinois, 1965.

29. D. M. Smyth, "Deviations from Stoichiometry in MnO and FeO," Phys. Chem. Solids, 19 [1/2] 167-69 (1961).

30. C. E. Birchenall, "Ionic Disorder in Manganous Oxide," Trans. AIME, 218 [12] 1134-35 (1960).

31. C. J. Kevane, "Oxygen Vacancies and Electrical Conduction in Metal Oxides," Phys. Rev., 133 [5A] A1431-36 (1964).

32. A. Z. Hed and D. S. Tannhauser, "High Temperature Electrical Properties of Manganese Monoxide," J. Chem. Phys., 47 [6] 2090-2103 (1967).

33. M. Gvishi, N. M. Tallan, and D. S. Tannhauser, "The Hall Mobility of Electrons and Holes in MnO at High Temperature," Solid State Com., 6 [3] 135-37 (1968).

34. J. B. Price and J. B. Wagner, "Diffusion of Manganese in Single Crystal Manganous Oxide," J. Electrochem. Soc., 117 [2] 242-47 (1970)

35. J. P. Boquet, M. Kawahara, and P. Lacombe, "Conductibilite Electronique, Conductibilite Ionique, et Diffusion Thermique dans MnO a haute temperature (de 900 a 1150° C). Academie des Sciences Comptes Rendus, 265 [23] 1318-21 (1967).

36. I. Bransky and N. M. Tallan, "High-temperature Defect Structure and Electrical Properties of NiO," J. Chem. Phys., 49 [3] 1243-49 (1968).

37. C. Wagner and H. H. Baumback, "Die elektrische Leitfähigkeit von Nickeloxyd," Z. Phys. Chem. (Abteilung B) 24 59-67 (1934).

38. S. P. Mitoff, "Electrical Conductivity and Thermodynamic Equilibrium in Nickel Oxide," J. Chem. Phys., 35 [3] 882-89 (1961).

39. Gerhart Zintl, "Metal Deficit in Cobalt Oxide-Magnesium Oxide and Cobalt Oxide-Nickel Oxide Systems," Z. Phys. Chem. (Frankfurt am Main), 48 [5-6] 340-58 (1966).

40. H. G. Sockel and H. Schmalzried, "Coulometric titration in Nonstoichiometric Metal Oxides," Ber. Bunsenges. Physik. Chem., 72 745-754 (1968).

41. Y. D. Tretyakov and R. A. Rapp, "Nonstoichiometries and Defect Structures in Pure Nickel Oxide and Lithium Ferrite," Trans. AIME, 245 [6] 1235-41 (1969).

42. C. Wagner and E. Koch, "Electrical Conductivity of Oxides of Cobalt and Iron," Z. Phys. Chem (Abteilung B), 6 439-46 (1936).

43. A Duquesnoy and F. Marion, "On the Variations of the Electrical Conductivity of the Oxides CoO, NiO, and MnO as a Function of Equilibrium Oxygen Partial Pressure at High Temperature," C. R. H. Acad. Sci., 256 [13] 2862-65 (1963).

44. R. E. Carter and F. D. Richardson, "An Examination of the Decrease of Surface Activity Method of Measuring Self-diffusion Coefficients in Wustite and Cobaltous Oxide," J. Metals, 200 [11] 1244-57 (1954).

45. R. E. Carter and F. D. Richardson, "Oxidation of Cobalt Metal," Trans. AIME, 203 [2] 336-43 (1955).

46. A. I. Shelykh, K. S. Artemov, and V. E. Shvaiko-Shvaikovskii, "Electrical Properties of Cobaltous Oxide Single Crystals at High Temperature and Their Dependence on the Partial Pressure of Oxygen," Sov. Phys.-Solid State, 8 [3] 706-09 (1966).

47. N. G. Eror and J. B. Wagner, "Electrical Conductivity and Thermogravimetric Studies of Single Crystalline Cobaltous Oxide," J. Phys. Chem. Solids, 29 [9] 1597-1611 (1968).

48. B. Fisher and D. S. Tannhauser, "Electrical Properties of Cobalt Monoxide," J. Chem. Phys., 44 [4] 1663-72 (1966).

49. T. T. Shim and W. J. Moore, "Diffusion of Nickel in Nickel Oxide," J. Chem. Phys., 26 [4] 802-04 (1957).

50. R. Lindner and A. Akerström, "Diffusion of Nickel-63 in Nickel Oxide (NiO)," Disc. Faraday Soc., 23 133-36 (1957).

51. J. S. Choi and W. J. Moore, "Diffusion of Nickel in Single Crystals of Nickel Oxide," J. Phys. Chem., 66 [7] 1308-11 (1962).

52. Michael O'Keefe and W. J. Moore, "Diffusion of Oxygen in Single Crystals of Nickel Oxide," J. Phys. Chem., 65 [8] 1438-39 (1961).

53. K. Fueki and J. B. Wagner, "Studies on the Oxidation of Nickel in the Temperature Range 900 to 1400°C.," J. Electrochem. Soc., 112 [4] 384-88 (1965).

54. J. B. Price and J. B. Wagner, "Determination of the Chemical Diffusion Coefficients in Single Crystals of CoO and NiO," Z. Phys. Chem. (Frankfurt), 49S, 257-70 (1966).

55. M. L. Volpe and J. Reddy, "Cation Self-diffusion and Semiconductivity in NiO," J. Chem. Phys., 53 [3] 1117-25 (1970).

56. B. J. Wuensch and T. Vasilos, "Diffusion of Transition Metal Ions in Single-Crystal MgO," J. Chem. Phys., 36 [11] 2917-22 (1962).

57. E. B. Rigby and I. B. Cutler, "Interdiffusion Studies in the System Fe_xO-MgO," J. Amer. Ceram. Soc., 48 [1] 95-99 (1965).

58. S. L. Blank and J. A. Pask, "Diffusion of Iron and Nickel in Magnesium Oxide Single Crystals," J. Amer. Ceram. Soc., 52 [12] 669-75 (1969).

59. H. Tagai, S. Iwai, T. Iseki, and M. S. Tokio, "Diffusion of Iron, Manganese, and Chromium Oxides into Single Crystal Magnesia," Radex Rundsch., 4 577-83 (1965).

60. J. Brynestad and H. Flood, "Redox Equilibrium in Wustite and Solid Solutions of Wustite and Magnesium Oxide," Z. Elektrochem., 62 [9] 953-58 (1958).

61. F. Koch and J. B. Cohen, "Defect Structure of Fe_xO"; to be published in Acta Crystallogr.

62. M. Appel and J. A. Pask, "Interdiffusion and Moving Boundaries in NiO-CaO and NiO-MgO Single Crystal Couples," J. Amer. Ceram. Soc. 54 [3] 152-58 (1971).

63. H. Schmalzried and J. B. Holt, "Interdiffusion in Mixed Crystal NiO-MgO," Z. Phys. Chem. (Frankfurt am Main), 60 [1-4] 220-22 (1968).

64. W. C. Hahn, Jr., and A. Muan, "Activity Measurements in Oxide Solid Solutions: The System NiO-MgO and NiO-MnO in the Temperature Interval 1100°-1300°C," J. Phys. Chem. Solids, 19 [3-4] 338-48 (1961).

65. J. T. Jones and I. B. Cutler, "Interdiffusion in the System Mn_xO-MgO," J. Amer. Ceram. Soc., 54 [7] 335-338 (1971).

66. A. Z. Hed, "Complex Defects in CoO," J. Chem. Phys., 50 [7] 2935-37 (1969).

67. J. R. Drabble and A. W. Palmer, "Arc-transfer Method of Crystal Growth," J. Appl. Phys. 37 [4] 1778-80 (1966).

68. B. A. Smith and I. G. Austin, "Growth of Single Crystals of Transition Metal Oxides by Arc-transfer Method," J. Crystal Growth, 1, 79-87 (1967).

69. J. R. Drabble, "The Arc-transfer Process of Crystal Growth," J. Crystal Growth 3,4, 804-807 (1968).

70. T. K. Ghosh and F. J. P. Clarke, "Etching and Polishing Studies on Magnesium Oxide Single Crystals," Brit. J. Appl. Phys., 12 [1] 44-50 (1961).

71. T. Vasilos, B. J. Wuensch, P. E. Gruba, and W. H. Rhodes, "Transport Processes in Ceramic Oxides," Tech. Rept. AD-709975, 1970.

72. T. Takeda and H. Kondoh, "Chemical Etch Pits of NiO Crystal Annealed at High Temperature," J. Phys. Soc. Jap., 17 [8] 1315-16 (1962).

73. A. Levy, "The Accuracy of the Bubble Meter Method for Gas Flow Measurements," J. Scientific Instr., 41 [7] 449-53 (1964).

74. L. S. Darken and R. W. Gurry, "The System Iron-oxygen. I. The Wustite Field and Related Equilibria," J. Amer. Chem. Soc., 67 [8] 1398-12 (1945).

75. C. E. Wicks and F. E. Block, "Thermodynamic Properties of 65 Elements--Their Oxides, Halides, Carbides, and Nitrides," Bur. Mines Bull. 605, Dept. of Interior, United States Gov. Print. Office, 1963.

76. R. D. Dewey, R. S. Mapes, and T. W. Reynolds; pp. 205-280 in Progress in Nuclear Energy, Series IX, Analytical Chemistry. Edited by D. C. Stewart and H. A. Elion. Pergamon Press, New York, N.Y. 1970.

77. K. F. J. Heinrich, Editor. Quantitative Electron Probe Microanalysis. Nat. Bur. Stand. U.S. Spec. Publ. 298, 1968.

78. D. M. Poole and P. M. Martin, "Electron-probe Micro-analysis: Instrumental and Experimental Aspects," Met. Reviews, 3 61-84, 1969

79. D. R. Beaman and J. A. Isasi, "A Critical Examination of Computer Programs Used in Quantitative Electron Microprobe Analysis"; presented at the Fourth National Conference on Electron Microprobe Analysis, Pasadena, California, July 16-18, 1969.

80. A. L. Albee and A. A. Chodos, "Semiquantitative Electron Microprobe Determination of Fe^{2+}/Fe^{3+} and Mn^{2+}/Mn^{3+} in Oxides and Silicates and its Application to Petrologic Problems," Amer. Mineral., 55 [3-4] 491-501 (1970).

81. L. G. Parratt, "Electronic Band Structure of Solids by X-ray Spectroscopy," Rev. Modern Phys., 31 [3] 616-45 (1959).

82. A. Z. Menshikov, I. A. Brytov, and E. Z. Kurmaev, "Crystal-field Splitting of Levels and X-ray Spectra of Transition Metal Monoxides," Phys. Status Solidi, 35 [1] 89-93 (1969).

83. L. W. Barr and A. B. Lidiard, Defects in Ionic Crystals Physical Chemistry--An Advanced Treatise, Vol. X, Solid State. Edited by W. Jost. Academic Press, New York, 1970.

84. T. Sakata and K. Sakata, "Change of Oxygen Concentration with Temperature of the Nickel and Cobalt Oxide Solid Solutions," J. Phys. Soc. Jap., 13 [7] 675-83 (1958).

85. W. K. Chen, N. L. Peterson, and W. T. Reeves, "Isotope Effect for Cation Self-diffusion in CoO Crystals," Phys. Rev., 186 [3] 887-91 (1969).

86. M. L. Volpe, N. L. Peterson, and J. Reddy, "Isotope Effect for Cation Self-diffusion in Single Crystals of NiO," Phys. Rev. B, 3 [4] 1417-21 (1971).

87. W. K. Chen and N. L. Peterson, "Cation Diffusivities in CoO-NiO Mixed Oxides: Effect of Composition on Stoichiometry," paper 2-JIV-71 presented at 73rd Annual Meeting of the American Ceramic Society, April 27, 1971. [Cited in Bull. Amer. Ceram. Soc., 50 [4] 467 (1971).]

88. W. P. Whitney and V. S. Stubican, "Interdiffusion in the System MgO-$MgAl_2O_4$," J. Amer. Ceram. Soc., 54 [7] 349-52 (1971).

89. B. C. Harding, "The Diffusion of Barium in Magnesium Oxide," Phil. Mag., 15 [11] 1039-48 (1967).

90. M. F. Berard, Iowa State University, Personal Communication to D. A. Brosnan, March 1, 1972.

91. Bevington, Philip R., Data Reduction and Error Analysis for the Physical Sciences. McGraw-Hill Book Company, New York, 1969.

92. Colby, J. W., Private Communication of Unpublished Results to C. D. Wirkus, Iowa State University, Ames, Iowa, 1970.

93. C. Wagner, "Evaluation of Data Obtained with Diffusion Couples of Binary Single-Phase and Multiphase Systems," Acta Met., 17 [2] 99-107 (1969).

94. L. Boltzmann, "Integration of Diffusion Equations by Variable Coefficients," Ann. Phys., 53, 959-64 (1894).

95. C. Greskovich and V. S. Stubican, "Interdiffusion Studies in the System MgO-Cr_2O_3," J. Phys. Chem. Solids, 30 [4] 909-17 (1969).

ACKNOWLEDGEMENTS

I wish to gratefully acknowledge the assistance and leadership of my graduate committee consisting of Drs. T. D. McGee (Chairman), J. T. Jones, M. F. Berard, D. M. Roberts, and P. Chiotti. I wish to particularly thank Drs. J. T. Jones and M. F. Berard for their assistance in the preparation of this thesis.

I wish to express my appreciation for the opportunity provided me by the Ceramic Engineering Department at Iowa State University and to its Chairman, Dr. D. R. Wilder. The counsel and teachings of Dr. O. Hunter, Jr. have been particularly helpful during the course of my graduate work.

I wish to thank Mr. J. L. Stein and Mr. W. S. Treffner of the General Refractories Company, Philadelphia, Pa., for their support leading to the completion of this work.

I wish to thank Mrs. Mary E. Brown for her diligent efforts in typing and processing of thesis material, and in the final stages, for making the completion of this work possible.

This research was sponsored by the Engineering Research Institute at Iowa State University through funds provided by the Aerospace Research Laboratories, Office of Aerospace Research, United States Air Force, under Contract No. F33615-68-C-1034.

APPENDIX A

Error Analysis

An analysis of the source and propagation of errors in this work and the effect on experimental results is given in this Appendix. The objective of this analysis is to obtain values for the uncertainties $\Delta\tilde{D}$ and ΔQ in the values of the interdiffusion coefficient $\tilde{D}$ and the diffusion activation energy Q respectively. The method of analysis is the propagation of errors theory as presented by Bevington (91). According to this theory the uncertainty is a quantity similar to the standard deviation; however, the uncertainty is only an approximation of the standard deviation due to approximations made in the error analysis when applying Taylor's expansion to the functional relationship between experimental variables.

The propagation of errors theory may be applied to the Wagner equation for $\tilde{D}$ as follows. The Wagner equation is given as follows:

$$\tilde{D}(N_2) = \frac{V_M(N_2^*)}{2t(\partial N_2/\partial x)_{x^*}} \left[(1-N_2)\int_{-\alpha}^{x^*} \frac{N_2}{V_M}\,dx + N_2\int_{x^*}^{\alpha} \frac{(1-N_2)}{V_M}\,dx\right]. \qquad (114)$$

For convenience we define

$$A = \int_{-\alpha}^{x^*} \frac{N_2}{V_m}\, dx \tag{115}$$

$$B = \int_{x^*}^{\alpha} \frac{(1-N_2)}{V_m}\, . \tag{116}$$

Then according to the propagation of errors theory

$$\frac{\Delta\tilde{D}}{\tilde{D}} \simeq \Big[\Big(\frac{\Delta V_m}{V_m}\Big)^2 \Big(\frac{\Delta t}{t}\Big)^2 + \Big\{\frac{\Delta(\partial N_2/\partial x)_{x^*}}{(\partial N_2/\partial x)_{x^*}}\Big\}^2 + \frac{A^2(\Delta N_2)^2 + (1-N_2)^2(\Delta A)^2 + B^2(\Delta N_2)^2 + N_2^2(\Delta B)^2}{\{(1-N_2)A + N_2B\}^2}\Big]^{1/2} \tag{117}$$

The uncertainty $\Delta Q/Q$ in the diffusion activation energy may be deduced through similar considerations. Consider the Arrhenius equation

$$\tilde{D} = \tilde{D}_o \exp(-Q/RT)\,. \tag{118}$$

If Q is calculated on the basis of two experimental values, i.e. $(\tilde{D}_1, T_1)$ and $(\tilde{D}_2, T_2)$, then

$$Q = R\, \ell n\Big(\frac{\tilde{D}_1}{\tilde{D}_2}\Big)\Big\{\frac{T_1T_2}{T_1 - T_2}\Big\}. \tag{119}$$

Applying the propagation of errors theory

$$\left(\frac{\Delta Q}{Q}\right) = \frac{\left(\frac{\Delta D_1}{D_1}\right)^2 + \left(\frac{\Delta D_2}{D_2}\right)^2}{\left(\ln\frac{D_1}{D_2}\right)^2} + \left(\frac{\Delta T_1}{T_1}\right)^2 + \left(\frac{\Delta T_2}{T_2}\right)^2$$

$$+ \frac{\left[(\Delta T_1)^2 + (\Delta T_2)^2\right]}{(T_1 - T_2)^2} . \qquad (120)$$

Sources of errors include those involved with the physical performance of experiments and those involved with the generation and analysis of experimental data. The following errors are considered in this Appendix.

(1) Errors in experimental procedure

a) temperature measurement
b) time measurement

(2) Errors in electron microprobe analysis

a) spectrometer adjustment
b) specimen height and tilt
c) short term instrument stability
d) contamination (during analysis)
e) counting statistics
f) operator error

(3) Error in computer analysis

a) author estimate

(4) Error in data analysis

a) slope measurement
b) area measurement
c) calculation error.

The following errors were not considered in this Appendix:

a) chemical contamination during fabrication

of diffusion couples

b) error in atmosphere control

c) heating and cooling of diffusion couple

d) error in surface condition at joint between interdiffusing substances in diffusion couple.

The error in temperature measurement was assumed equal to the spread of observed temperature values. The time measurement error of diffusion anneal duration was assumed to be about 0.5%.

Errors (2)a through (2)f above were termed "Instrumental Error" and was assigned a value of 3% at N_{NiO} or N_{MnO} of 0.5 and 8% at N_{NiO} or N_{MnO} of 0.2. The error due to counting statistics, i.e. the count variance ΔC, was calculated according to

$$\Delta C = \frac{10^2 \sqrt{C}}{C} \quad (\%). \tag{121}$$

This ΔC was converted to an appropriate concentration variance ΔN using the actual computer analysis of the diffusion profile. The error in the computer analysis of raw microprobe data was chosen as 2% at N_{NiO} or N_{MgO} of 0.5 and as 4% at N_{NiO} or N_{MnO} of 0.2. A total error in the concentration was then calculated according to

$$\Delta N \text{ (Total)} = \{N^2 \text{ (Computer program)} + \Delta N^2 \text{ (Counting statistics)} + \Delta N^2 \text{ (Instrumental)}\}^{1/2}. \quad (122)$$

Error in manual slope measurement was based on measurement of the slope ten times and observing the range of values obtained. The magnitude of this error was from 12% to 25% depending on the magnitude of the slope. Error in manual area measurement in graphical integration was measured in a similar manner and ranged from 7% to 16%. All calculations were performed twice, and no calculation error was assumed.

The calculation of the quantities $\Delta\tilde{D}/\tilde{D}$ and $\Delta Q/Q$ was based on factors contained in Tables 12 and 13. Results are presented in Tables 12-14.

Table 12. Error analysis of couples in Ni_xO-Co_xO system

Specimen	13	14	13	14	12
T (°C)	1283	1367	1283	1367	1043
ΔT	6	8	6	8	4
t(s)	9.60×10^4	8.50×10^4	9.60×10^4	8.508×10^4	4.68×10^4
Δt	580	520	580	520	285
N	0.5	0.5	0.2	0.2	0.5
ΔN (Computer)	0.02	0.02	0.016	0.016	0.02
ΔN (Instrument)	0.015	0.015	0.015	0.015	0.015
C/10 s	33,418	37,258	15,087	17,384	47,944
ΔC/10 s	0.5	0.5	0.8	0.8	0.4
ΔN (Counting)	0.0027	0.0020	0.010	0.010	0.030
ΔN (Total)	0.0248	0.0250	0.0238	0.0238	0.0387
V_m	11.394	11.394	11.200	11.200	11.394
ΔV_m	0.002	0.002	0.0035	0.0035	0.0052
$(\partial N_2/\partial x)_x$*	0.0023	0.0015	0.0040	0.0030	0.0130
$\Delta(\partial N_2/\partial x)_x$*	0.00035	0.00018	0.00056	0.00036	0.0026

Table 12 (Continued)

Specimen	13	14	13	14	12
A	4.360	5.590	1.431	1.410	1.552
B	0.542	0.662	9.645	16.282	1.700
ΔA	0.446	0.391	0.143	0.141	0.186
ΔB	0.054	0.066	0.964	1.628	0.204
$\tilde{D}$	1.23×10^{-9}	3.36×10^{-9}	4.45×10^{-10}	9.62×10^{-10}	2.38×10^{-10}
$\frac{\Delta \tilde{D}}{\tilde{D}}$	0.26	0.21	0.18	0.27	0.24

Table 13. Error analysis of couples in Mn_xO-MgO system

Specimen	5	6	5	6
T (°C)	1449	1529	1449	1529
ΔT	8	8	8	8
t (s)	6.78×10^4	4.17×10^4	6.78×10^4	4.17×10^4
Δt	414	254	414	254
N	0.5	0.5	0.2	0.2
ΔN (Computer)	0.02	0.02	0.016	0.016
ΔN (Instrument)	0.015	0.015	0.015	0.015
C/10 s	24,168	26,234	13,013	24,521
ΔC/10 s	0.6	0.6	0.8	0.6
ΔN (Counting)	0.040	0.006	0.01	0.005
ΔN (Total)	0.042	0.024	0.022	0.020
V_m	12.200	12.200	11.564	11.564
ΔV_m	0.003	0.002	0.002	0.002
$(\partial N/\partial x)_x$*	0.004	0.004	0.010	0.003
$\Delta(\partial N/\partial x)_x$*	0.0006	0.0005	0.0016	0.00096
A	1.482	4.776	0.563	1.792
B	7.195	10.312	9.057	15.041
ΔA	0.207	0.621	0.084	0.251
ΔB	1.110	1.315	1.360	2.261
$\tilde{D}$	9.75×10^{-10}	5.51×10^{-9}	1.93×10^{-10}	1.95×10^{-9}
$\Delta\tilde{D}/\tilde{D}$	0.38	0.33	0.22	0.43

Table 13 (Continued)

Specimen	2	3	2	3
T (°C)	1348	1150	1348	1150
ΔT	8	4	8	4
t (s)	6.14×10^4	8.67×10^4	6.14×10^4	8.67×10^4
Δt	371	524	371	524
N	0.5	0.5	0.2	0.2
ΔN (Computer)	0.015	0.015	0.016	0.016
ΔN (Instrument)	0.015	0.015	0.015	0.015
C/10 s	6,721	2,844	3,211	1,250
ΔC/10 s	1.2	1.9	1.8	2.8
ΔN (Counting)	0.026	0.004	0.038	0.005
ΔN (Total)	0.033	0.020	0.059	0.020
V_m	12.200	12.200	11.564	11.564
ΔV_m	0.004	0.004	0.003	0.003
$(\partial N/\partial x)_x$*	0.018	0.020	0.017	0.026
$\Delta(\partial N/\partial x)_x$*	0.0036	0.004	0.0039	0.0054
A	1.301	1.445	0.816	0.955
B	5.296	1.420	6.345	2.176
ΔA	0.182	0.202	0.130	0.172
ΔB	0.740	0.199	1.015	0.391
$\tilde{D}$	1.82×10^{-10}	4.60×10^{-10}	1.00×10^{-10}	2.99×10^{-11}
$\Delta\tilde{D}/\tilde{D}$	0.31	0.25	0.39	0.26

Table 14. Uncertainty in diffusion activation energy

Specimens	13, 14	13, 14	5, 6	5, 6	2, 3	2, 3
N	N_{NiO}= 0.5	N_{NiO}= 0.2	N_{MnO}= 0.5	N_{MnO}= 0.2	N_{MnO}= 0.5	N_{MnO}= 0.2
$\Delta Q/Q$	0.36	0.44	0.30	0.25	0.34	0.30

The following conclusions are evident from Tables 1-3:

(1) The error in D ranged from 21 to 43%;

(2) The error in Q ranged from 25 to 44%;

(3) The error in D was generally lower in the system Ni_xO-Co_xO than in the system Mn_xO-MgO probably due to better experimental procedure (surface preparation, fit at diffusion interface, etc.);

(4) The error in Q was generally higher for the system Ni_xO-Co_xO than for the system Mn_xO-MgO possibly because of the narrow temperature range of measurements;

(5) The major sources of predicted uncertainty are as follows:

   a) measurement of slope

   b) measurement of area

   c) measurement of temperature difference (Improvements in these determinations will lead to more accurate results.).

APPENDIX B

Mathematical Analysis of Diffusion Data

Concentration data as output from the Magic III program (92) were plotted as a function of penetration distance to yield the diffusion profile. The diffusion profiles were then analyzed to reveal $\tilde{D}$ using Wagner's treatment (93) for diffusion in one dimension. Wagner's solution to Fick's Second Law includes provision for the change in molar volume with concentration during the interdiffusion process. Additionally a coordinate x = 0, the so called Matano interface, need not be determined in Wagner's analysis. Terminology pertinent to the Wagner analysis is given in Table 15.

Wagner defines the Matano interface for a binary system in terms of N_2^- and N_2^+ as follows:

$$\int_{-\alpha}^{x_m} \frac{N_2 - N_2^-}{V_m}\, dx + \int_{x_m}^{\alpha} \frac{N_2^+ - N_2}{V_m}\, dx = 0. \qquad (122)$$

The rate of change in concentration of each component for a given position along the coordinate system is equal to the negative divergence of the flux of the component with the origin of the coordinate system fixed at the Matano interface.

$$\frac{\partial}{\partial t}\left(\frac{N_1}{V_m}\right) = \frac{\partial}{\partial t}\left(\frac{1 - N_2}{V_m}\right)_{x-x_m} = - \frac{\partial J_1}{\partial (x-x_m)}. \qquad (123)$$

Table 15. Terminology for the Wagner analysis

Term	Description
J_i	particle flux for component i, i = 1, 2
N_i	mole fraction for component i, i = 1, 2
N_i^+	initial concentration of component i on the "+" side of the diffusion couple, i = 1, 2
N_i^-	initial concentration of component i on the "-" side of the diffusion couple, i = 1, 2
v_i	velocity of component i, i = 1, 2
x	coordinate position along the diffusion profile
x_m	coordinate position of the Matano interface
V_m	molar volume
* (superscript)	denotes the value of a variable quantity at any specific location x^* in the diffusion profile

$$\frac{\partial}{\partial t}\left(\frac{N_2}{V_m}\right) = -\frac{\partial J_2}{\partial (x-x_m)} . \tag{124}$$

An auxiliary variable, Y, is defined as

$$Y = \frac{N_2 - N_2^-}{N_2^+ - N_2^-} \tag{125}$$

whereas

$$N_1 = (1 - N_2^+)\ Y + (1 - N_2^-)(1 - Y) \qquad (126a)$$

$$N_2 = N_2^+\ Y + N_2^-(1 - Y)\,. \qquad (126b)$$

Wagner adopts the technique of Boltzmann (94) by expressing the initial conditions in terms of a single variable, i.e.

$$\lambda = \frac{x - x_m}{t^{1/2}}\,. \qquad (127)$$

Substitution of Equations 125, 126a, 126b, and 127 into Equations 122 and 123 yields

$$\frac{\lambda}{2t}\left[(1 - N_2^+)\ \frac{d}{d\lambda}\left(\frac{Y}{V_m}\right) + (1 - N_2^-)\ \frac{d}{d\lambda}\left(\frac{1-Y}{V_m}\right)\right] = \frac{\partial J_1}{\partial x} \qquad (128)$$

and

$$\frac{\lambda}{2t}\left[N_2^+\ \frac{d}{d\lambda}\left(\frac{Y}{V_m}\right) + N_2^-\ \frac{d}{d\lambda}\left(\frac{1 - Y}{V_m}\right)\right] = \frac{\partial J_2}{\partial x} \qquad (129)$$

multiplying Equation 128 by N_2^- and Equation 129 by $(1-N_2^-)$ and subtracting the results

$$-\frac{\lambda}{2t}\ (N_2^+ - N_2^-)\ \frac{d}{d\lambda}\left(\frac{Y}{V_m}\right) = N_2^-\ \frac{\partial J_1}{\partial x} - (1 - N_2^-)\ \frac{\partial J_2}{\partial x}\,. \qquad (130)$$

Multiplying Equation 128 by N_2^+ and Equation 129 by $(1-N_2^+)$ and subtracting the results

$$\frac{\lambda}{2t}\ (N_2^+ - N_2^-)\ \frac{d}{d\lambda}\left(\frac{1 - Y}{V_m}\right) = N_2^+\ \frac{\partial J_1}{\partial x} - (1-N_2^+)\ \frac{\partial J_2}{\partial x}\,. \qquad (131)$$

Multiplying Equations 130 and 131 by $d\lambda = dx/t^{1/2}$ and integrating between $\lambda = -\alpha$ and $\lambda = \lambda^*$ for Equation 131 leads to Equations 132 and 133 below. In arriving at Equations 132 and 133 several simplifying assumptions have been made. At large absolute values of λ the rate of change in composition is small resulting in approximately constant values of $\tilde{D}$. At this extreme, values of N_2 and Y can be expressed in terms of an error function. Also at large $|\lambda|$, Y and (1-Y) tend quasi-exponentially to approach zero. Thus $\partial N_2/\partial x$ approaches zero and

$$\frac{1}{2t}\,(N_2^+ - N_2^-)\,\left[-\frac{\lambda^* Y^*}{V_m^*} + \int_{-\alpha}^{\lambda^*} Y\frac{d\lambda}{V_m}\right] = \frac{1}{t^{1/2}}\,[N_2^-\,J_1^* - (1 - N_2^-)\,J_2^*] \qquad (132)$$

$$\frac{1}{2t}\,(N_2^+ - N_2^-)\,\left[-\frac{\lambda^*(1 - Y^*)}{V_m^*} - \int_{\lambda^*}^{\alpha} \frac{(1 - Y)\,d\lambda}{V_m}\right]$$

$$= \frac{1}{t^{1/2}}\,[-N_2^+\,J_1^* + (1 - N_2^+)\,J_2^*] \qquad (133)$$

where J_1^* and J_2^* are the fluxes at $\lambda = \lambda^*$. Multiplying Equation 132 by $(1-Y^*)$ and Equation 133 by Y^* and subtracting yields

$$\frac{1}{2t}\,(N_2^+ - N_2^-)\,\left[(1 - Y^*)\int_{-\alpha}^{\lambda}\frac{Y\,d\lambda}{V_m} + Y^*\int_{\lambda}^{\alpha}\frac{(1 - Y)\,d\lambda}{V_m}\right]$$

$$= \frac{1}{t^{1/2}}\,[N_2^*\,J_1^* - (1 - N_2^*)\,J_2^*]. \qquad (134)$$

Writing Fick's First Law in terms of Wagner variables

$$\tilde{D} = \frac{J}{\partial c/\partial x} = \frac{N_2\,N_1(v_1 - v_2)}{\partial N_2/\partial x} = \frac{V_m\,(N_2 J_1 - N_1 J_2)}{\partial N_2/\partial x} \qquad (135)$$

or

$$\tilde{D} = \frac{(N_2^+ - N_2^-)\,V_m\,(N_2^*)}{2t\,(\partial N_2/\partial x)_{x=x^*}}. \qquad (136)$$

Substituting Equation 136 into Equation 134, setting $d\lambda = dx/t^{1/2}$ (appropriately changing limits of integration), and solving for $\tilde{D}$

$$\tilde{D}\,(N_2^*) = \frac{(N_2^+ - N_2^-)\,V_m\,(N_2^*)}{2t\,(\partial N_2/\partial x)}\left[(1 - Y)\int_{-\alpha}^{x^*}\frac{Y}{V_m}\,dx + Y^*\int_{x^*}^{\alpha}\frac{(1 - Y)}{V_m}\,dx\right]. \qquad (137)$$

If $N_2^+ = 1$ and $N_2^- = 0$, $Y = N_2$ and Equation 137 becomes

$$\tilde{D}\,(N_2^*) = \frac{V_m\,(N_2^*)}{2t\,(\partial N_2/\partial x)_{x^*}}\left[(1 - N_2)\int_{-\alpha}^{x^*}\frac{N_2}{V_m}\,dx + N_2\int_{x^*}^{\alpha}\frac{(1 - N_2)}{V_m}\,dx\right]. \qquad (138)$$

Equation 138 may be utilized if the total concentration profile is available and if the change in molar volume with concentration is known. The value $(\partial N_2/\partial x)_{x=x^*}$ may be taken directly from the concentration profile. The terms enclosed by brackets in Equation 138 may be deduced by graphical integration of a plot of N_2/V_m versus x as discussed by Greskovich and Stubican (95).